uc3m | Universidad Carlos III de Madrid

Degree in Biomedical Engineering

Academic Year (2017-2018)

Bachelor Thesis

SET UP OF A LIGHT SHEET FLUORESCENCE MICROSCOPE FOR CELLULAR STUDIES

Ignacio Albert Smet

Tutor: Jorge Ripoll Lorenzo

Co-Tutor: Arrate Muñoz Barrutia

Leganes, June 2018

ABSTRACT [1]

Light-sheet fluorescence microscopy (LSFM) has been present in cell biology laboratories for quite some time, mainly as custom-made systems, with imaging applications ranging from single cells (in the µm scale) to small organisms (mm). Such microscopes distinguish themselves for having very low phototoxicity levels and high spatial and temporal resolution, properties that render it ideal for 3D characterization of cell motility in migration and traction force studies.

Cellular motion has proven to be essential in biological processes such as tumor metastasis and tissue development. Experimental setups make extensive use of microdevices (bioMEMS) that are providing higher degrees of empirical complexity.

The following report details the process of setting-up a functional LSFM device for imaging cell motion in microfluidic devices. It begins with a brief summary of fluorescence imaging and current techniques, important to understand why single-plane illumination microscopy (SPIM) was chosen among other light-sheet methods.

Then, the whole SPIM set-up process is described, containing explanations about the physical and material properties of the hardware used, the intricacies of the control system, and important procedures. These procedures include: calibration of the microscope, sample preparation in microdevices, and image acquisition from the software provided.

Real fluorescence images acquired serve as evidence of the functionality of the instrument. The current limitations are highlighted, and pointers on how to improve or enhance the device are given.

The report contains many diagrams, tables and pictures to aid in the understanding of important concepts. In the Annex, a comprehensive table listing the project costs by category is attached. This table includes links to the manufacturers and providers. The aim of this writing is to serve as an exhaustive guideline and be of reproducible use for researchers aiming to build SPIM systems for similar applications.

[1] Parts of this abstract are shared with the article “Applications of LSFM in microdevices: cell motility and tracking” which will be published within the collection “Light Sheet Microscopy: from Technological Developments to Prospective Applications”, *Frontiers in Neuroanatomy* (Frontiers Media S.A.).

ACKNOWLEDGEMENTS

To Guillermo Vizcaino, through whom I have seen the art of clock-work perfectionism.

To David Gil, the Head of International Mobility programs at UC3M, who gave me, my brother, my friends, and many others life-changing opportunities that were unthinkable to us.

To the Georgia Institute of Technology and Nanyang Technological University for hosting me and educating me as their own.

And to all the great historical scientists, namely:

- Johannes Kepler for initiating the field of modern optics.
- Willebrord Snellius for Snell's Law of refraction.
- Isaac Newton for discovering spectral decomposition of white light.
- James Maxwell for his *Dynamical Theory of the Electromagnetic Field*.
- Frederick Kipping for pioneering in the development of silicon polymers.
- Theodore Maiman for inventing LASER devices.
- Arrate Muñoz for trusting me with the responsibility of seeing this project through, and her constant guidance and support.
- Jorge Ripoll, for being a cool guy and helpful genius.

And finally, to my parents, who have made this project possible by having spent almost their entire income in our education.

Table of Contents

Blank Page

List of Figures

List of Tables

List of Equations

Acronyms

TABLE I. ACRONYMS (ALPHABETICAL)

Letter	Acronym	Meaning
#	2PE	2-Photon Excitation Fluorescence Microscopy
A	ADC	Analog-to-Digital Converter
	AI	Analog Input
	AO	Analog Output
	AR	Anti-Reflective
B	bioMEMS	bio-Micro Electro-Mechanical Systems
C	CAD	Computer-Aided Design
	CCD	Charge-Coupled Device
	CMOS	Complementary Metal-Oxide-Semiconductor
	CNR	Contrast-to-Noise Ratio
	CTE	Coefficient of Thermal Expansion
	DAC	Digital-to-Analog converter
	DAQ	Data Acquisition device
	DMEM	Dulbecco's Modified Eagle Medium
	DOF	Depth of Focus
	DR	Dynamic Range
	DSLM	Digital Scanned Laser Light-Sheet Microscopy
E	ECM	Extracellular Matrix
	ETL	Electrically Tunable Lens
	FBS	Fetal Bovine Serum
	FLIM	Fluorescence Lifetime Imaging
	FOV	Field Of View
	FPGA	Field-Programmable Gate Array
	FPS	Frames Per Second
	FRAP	Fluorescence Recovery After Photobleaching
	FRET	Fluorescence Resonance Energy Transfer
	FWHM	Full Width at Half Maximum
G	GFP	Green Fluorescent Protein
	GND	Ground
	GPU	Graphics Processing Unit
H	H&E	Hematoxylin and Eosin
I	I/O	Input / Output
	iSPIM	Inverted SPIM
L	LASER	Light Amplification by Stimulated Emission of Radiation
	LED	Light-Emitting Diode
	LSFM	Light-Sheet Fluorescence Microscopy
	LUT	Look-Up Table
M	MIP	Maximum Intensity Projection

	MS/s	Mega Samples per Second
N	NA	Numerical Aperture
P	PALM	Photoactivated Localization Microscopy
	PBS	Phosphate-Buffered Saline
	PDMS	Polydimethylsiloxane
	PSF	Point-Spread Function
R	RGB	Red-Green-Blue
	RMS	Root-Mean Squared
	RoHS	Restriction of Hazardous Substances Directive
	ROI	Region of Interest
S	sCMOS	Scientific CMOS
	SIM	Structured Illumination Microscopy
	SNR	Signal-to-Noise Ratio
	SPIM	Single Plane Illumination Microscopy
	STD	Standard Deviation
	STED	Stimulated Emission Depletion
	STORM	Stochastic Optical Reconstruction Microscopy
	SSD	Solid-State Drive
T	TFM	Traction Force Microscopy
	TIRF	Total Internal Reflection Fluorescence Microscopy
	TPI	Threads Per Inch
U	USAF	U. S. Air Force
W	WD	Working Distance
	WF	Wide-field Fluorescence Microscopy

1. Introduction

1.1. Motivation

Cellular motion is a crucial phenomenon in many physiological processes and diseases (see *2.1. Cell motility and tracking*). The essential tool in modelling and quantification of moving cells is image processing, which allows researchers to program algorithms that extract significant information from large amounts of data.

To continue the development of algorithms in the field of cellular motion, the Biomedical Imaging and Instrumentation Group at Universidad Carlos III de Madrid requires an imaging workstation capable of acquiring sequences of volumetric scans (image stacks) of live cells embedded in a gel matrix.

Currently, the experiments being performed suffer from two limitations. In first place, cells are seeded on planar substrates which only allows for 2D and thin-volume (2.5D) tests; conditions which do not mimic the real 3D mechanical environment in which cells are found naturally. Secondly, the fluorescence microscopes available cannot capture images fast enough to track certain aspects of the cell's motion and, even if they could, high phototoxicity levels would prevent high-frequency imaging over extended periods of time.

An additional requirement of this optical microscopy workstation is to perform imaging in microdevices. The increasingly-relevant field of biomedical microdevices (bioMEMS) has allowed finer control of experiments and reduced reagent costs. The tendency of *in vitro* cell culturing in microfluidic devices pushes for systems that can integrate with them.

With this in mind, a light-sheet fluorescent microscopy (LSFM) system (see *1.3.2. LSFM techniques*) was proposed; more concretely, a single-plane illumination microscopy (SPIM) device. With other simpler microscopes already available at the laboratories, SPIM will offer needed advantages to help the research group advance in their work.

1.2. Fluorescence Imaging

This section discusses briefly the physical principles that make fluorescence and how these can be exploited to perform optical imaging.

1.2.1. Light and Matter

Interactions between light and matter can be summarized into three wide concepts: emission, absorption, and deflection. These behaviors have been extensively studied and described in literature within the following topics: scattering, diffraction, polarization, refraction, reflection, absorption, emission, and heat [1].

Most optical systems, including the human eye, rely on these principles to resolve images. Microscopes mainly employ refraction and reflection for image capturing and formation. Fluorescence systems, like the one described in this report, are named after fluorescence: selective emission and absorption of light.

1.2.2. Fluorescence: Physical Principle

> "The finer crystals are perfectly transparent. Their colour by transmitted light is an intense emerald green; but by reflected light, the colour is a deep sapphire blue."
>
> Edward Daniel Clarke (1819)

Discovered in 1819 [2] and coined in 1852 [3], fluorescence is the physical principle by which a substance absorbs and emits light almost immediately. It differs from phosphorescence in the time scale of the event. The energy transitions involved are best illustrated by a Perrin-Jablonski diagram (Figure 1).

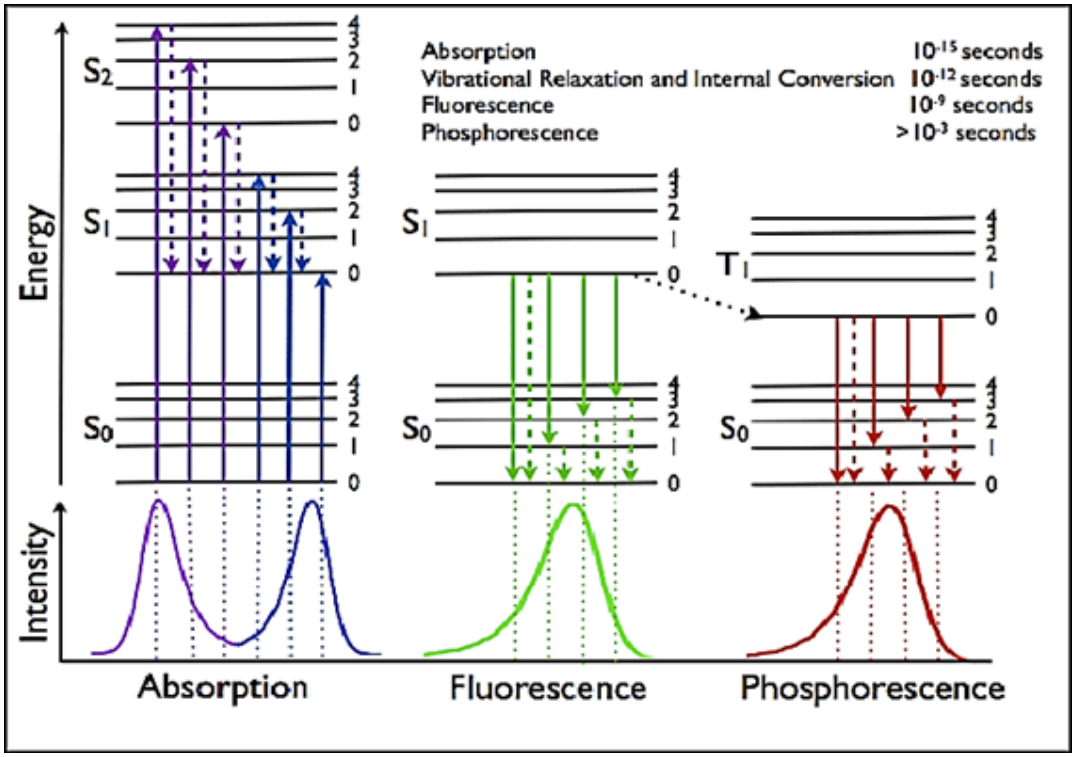

FIGURE 1. PERRIN-JABLONSKI DIAGRAM [4]

Generally, the energy of the photon absorbed by the fluorophore (fluorescent molecule) is higher than the emitted. This increase in wavelength is described as “Stokes shift”. The exception to this rule is two and three photon fluorescence, which involves the absorption of several lower-energy photons and emission at higher energies.

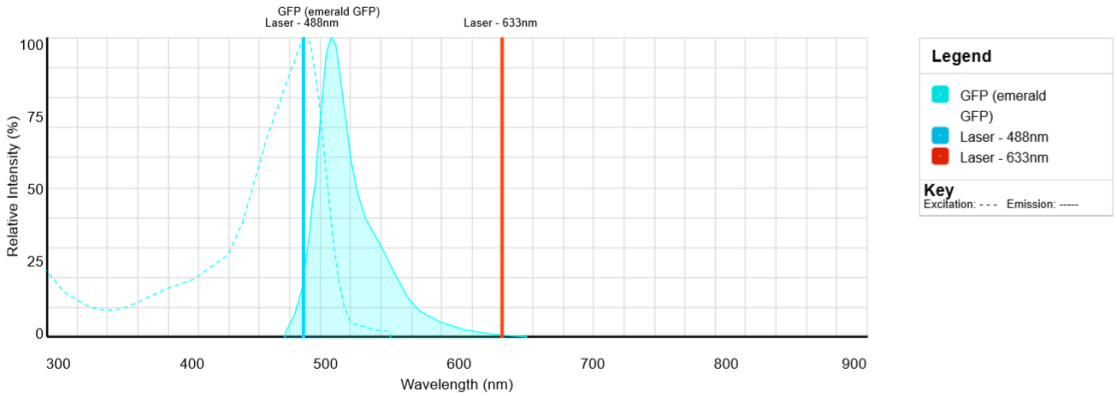

FIGURE 2. ABSORPTION AND EMISSION SPECTRA OF GFP [5]

Cyan: spectra of green fluorescent protein, GFP, for absorption (discontinuous line) and emission (highlighted area). *Light blue*: 488nm excitation laser. *Red*: 633nm excitation laser.

Following Figure 2, the blue laser emits photons at the energy of maximal absorption of GFP causing intense fluorescence. The energy of the red laser is too low to cause fluorescence. With an absorption maximum of 488nm and an emission maximum of 510nm, the Stokes shift of GFP is 22nm.

1.2.3. Fluorescent Imaging

Fluorescent imaging exploits the absorption and emission properties above described to form images. A biological sample is first tagged with fluorescent molecules; for example, genetically modified cells that express GFP or antibodies bound to a fluorescent marker. This implies fluorophore labelling is highly specific to the structure being imaged, for instance: a given membrane protein, actin filaments in the cytoskeleton, or distinct metabolic products.

When the sample is illuminated with a laser or a lamp at energies within the excitation spectrum of the fluorophore, the incoming photons are absorbed and light is emitted at the emission spectrum. Since the energies are different, an optical filter can be used to block the excitation light and transmit the emission light. The light given off by the fluorophore forms an image that is magnified and captured by the microscope.

A fluorescent image shows brightness proportional to the concentration of fluorophore, which is quantitatively related to the molecule being marked. Fluorescence imaging can help determined not only physical structures but also chemical functions within cells.

The main limitation of fluorescence imaging is that every structure / molecule has to be tagged with a different fluorophore, sometimes requiring several excitation sources and optical filters. In comparison to, for example, regular hematoxylin and eosin (H&E) microscopy which stained with two dyes and only requires white light illumination.

1.3. State of the Art

1.3.1. Fluorescent Imaging Techniques

There are a variety of imaging techniques which differ in terms of resolution, costs, speed, and the size of the specimen being imaged. For this thesis, the focus will be on those methods that can image on a cellular scale. The following table summarizes the fluorescent imaging techniques currently used in biomedical research and briefly states the physical basis, the average resolution, and limitations and uses [6] – [9].

TABLE II. LIST OF FLUORESCENCE MICROSCOPY TECHNIQUES

Technique	Basis	Applications	Resolution
Wide-Field Fluorescence (WF)	Accepts all emitted light (in and out of focus).	General purpose. Very high photobleaching.	250nm
Deconvolution	WF acquisition in all focal planes. Deconvolution algorithm to restore voxel intensity values.	Small and dimly fluorescent samples (<5µm). Optical sectioning. Decreased photobleaching.	200nm
Confocal laser-scanning	A pinhole rejects out-of-focus light.	Optical sectioning. Thin samples (<200µm). High photobleaching.	200nm
2-Photon (2PE) "Confocal"	Excitation only at objective focal point.	Optical sectioning. Thick tissues (<500µm). Infrared thermal damage. Low photobleaching.	300nm
Spinning Disk Confocal	Rejects out-of-focus light via a spiral array of pinholes that sweeps across the sample.	Optical sectioning. Thin samples (<200µm). High photobleaching.	250nm High speed.
Light-sheet fluorescence microscopy (LSFM)	WF imaging of a thin sheet of excitation light.	Optical sectioning. Transparent samples. Very low photobleaching.	1µm Very high speed.
Total Internal Reflection (TIRF)	Light strikes at the critical angle (or greater). No propagation of excitation light into the sample.	Surface imaging (<100nm). E.g.: plasma membranes.	100nm
Fluorescence Recovery After Photobleaching (FRAP)	An area is purposely photobleached and the restoration of fluorescence is followed.	Living cells. Cell dynamics and diffusion.	WF or confocal.

Technique	Basis	Applications	Resolution
Fluorescence Resonance Energy Transfer (FRET)	Donor-Acceptor pair of fluorescent molecules such that: Donor is excited, the emission of Donor excites Acceptor if close (<10nm), Acceptor emission is detected.	Donor-acceptor probes. Functional imaging (e.g.: signaling pathways).	WF or confocal.
Fluorescence Lifetime Imaging (FLIM)	Measures fluorescence decay time (~50ns) of a population of fluorophores after excitation.	Living systems. Kinetics and localization of fluorophores.	WF, confocal or 2PE. Highest speed.
Stimulated Emission Depletion (STED)	Confocal technique. "Depletion" laser excites fluorophore to red instead of green producing a red doughnut with green sub-resolution spot in the middle.	Low background noise. Super-resolution. Very high photobleaching.	50nm
Stochastic Optical Reconstruction Microscopy (STORM) & Photoactivated Localization Microscopy (PALM)	WF technique. Stochastic "activation" (emission) of specialized fluorophores. Excitation of a small subset of single fluorophores while the majority remain "dark", then calculate the center of the fluorescence (Airy disc).	Super-resolution. Specialized fluorophores. Very high photobleaching.	20nm
Structured Illumination Microscopy (SIM)	WF technique. Superimposes an optical pattern over the fluorescence of the sample.	Super-resolution. Super-stable environment.	100nm

From the techniques listed above, laser-scanning confocal microscopy is the main competitor of light-sheet fluorescence microscopy (LSFM). Confocal microscopy is more widespread and simple in terms of optics and control software but suffers from high phototoxicity and slow acquisition speeds.

Its superior analogue, the spinning disk microscope, can mitigate these two problems [10] while taking advantage of the technologies developed for confocal systems, such as the bioMEMS (bio-micro electro-mechanical systems) designed for sample preparation. The cost of spinning disk systems, however, is far superior to those of confocal microscopes and can become a limiting factor.

Even if ignoring the equipment cost, spinning disk microscopy cannot, at present, provide the sectioning speed and imaging depth of a light-sheet system, nor its low photobleaching [11]. Beyond neurodevelopment, these properties are essential to image cell protrusions during traction, and to investigate prolonged migration phenomena more frequently on a wider scale. For these reasons, a LSFM device is ideal for three-dimensional cell motility and tracking research.

1.3.2. LSFM techniques

There are several imaging methods within the category of light-sheet fluorescence microscopy [6], [12] – [16]. All of them have in common some form of lightsheet as the excitation source, and a detector placed at 90º from the illumination plane. The differences arise mainly from the shape of the lightsheet (see Figure 3), which changes the properties of the excitation.

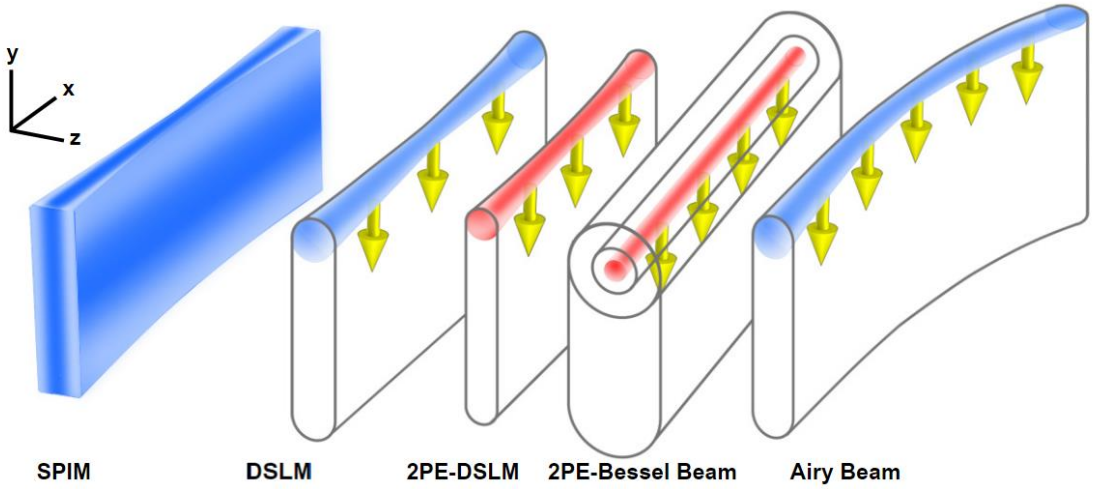

FIGURE 3. DIFFERENT KINDS OF LIGHT SHEETS [17]

1. SPIM: Single Plane Illumination Microscopy

This is the technique implemented in this project and will be thoroughly explained during the report. The physical lightsheet in SPIM is created by a laser beam traversing a cylindrical lens, after which it emerges with planar shape.

Compared to other light-sheet approaches, SPIM offers reduced photobleaching, highly efficient image recording, and significant depth penetration. It offers the highest temporal resolution of all sectioning fluorescence techniques.

2. DSLM: Digital Scanned Laser Light-Sheet Microscopy

The system built for this project may also implement DSLM. A virtual light-sheet is produced by laterally scanning a beam. With respect to SPIM, temporal resolution decreases and phototoxicity is increased (the two main advantages of LSFM). Also, stitching and registration of DSLM images is not straightforward. On the up side, it solves some distortions regarding beam waist.

3. Scanned Bessel Beam

Bessel beams are generated via projection of an annular pattern and, like DSLM, a virtual lightsheet is created by digitally scanning the beam.

Compared to Gaussian beams, Bessel beams have high energy side lobes. These side lobes thicken the beam waist but grant the beam “self-healing” properties: when

obstructed, it may reform later in the optical path. Thanks to being propagation-invariant, deeper imaging is possible.

Additionally, the core (center) of the Bessel beam can be much thinner that the diameter of a Gaussian beam, resulting in narrower slices. The effects of the side lobes can be counteracted if Bessel beams are coupled to multiphoton excitation [18].

4. Scanned Airy Beam

Airy beams are formed by modulation of a Gaussian beam using a spatial light modulator and, like Bessel beam, have “self-healing” properties. Airy beams may image deeper than any other through thick scattering media.

Generally, digital laser scanning is used to create a virtual Airy lightsheet. Research is being conducted to generate a physical excitation plane with tilted cylindrical lens (similar to SPIM), something that cannot be done with Bessel beams [19]. This could allow for even deeper imaging with the temporal resolution of SPIM.

5. Multiphoton Excitation Lightsheets

Any of the previous LSFM techniques can be used together with multiphoton excitation. This is a rare physical phenomenon and most commonly appears as two-photon excitation (2PE).

The longer wavelength (infrared) of the excitation photons offers deeper sample penetration because of decreased scatter and absorption but suffers from a reduced focal spot. Multiphoton relies on a large photon fluxes which causes the sample to be heated.

6. iSPIM: Inverted SPIM

iSPIM [20], and other similar techniques, attempt to adapt LSFM for widespread use by enabling conventional sample preparation techniques.

1.3.3. Novel SPIM approaches

As research moves forward new technologies and methods appear. SPIM gained popularity relatively recently (2004) [21]. Since, SPIM technology has advanced significantly in the following areas:

1. Algorithms

Image processing and reconstruction research is extensive in SPIM, especially in systems that implement rotation platforms. Conveniently enough, many algorithms have been developed for other tomographic imaging modalities (e.g.: Computed tomography) so there are well-established and experienced research groups that can face these challenges.

Since SPIM became popular, algorithms are becoming more efficient at handling the huge amount of data acquired in systems with multiple cameras (multi-view, multi-color), high-resolution and high-speed microscopy [22-24].

2. Laser surgery and SPIM

SPIM enables three-dimensional imaging of cultures, which better resembles physiologically and clinically relevant conditions [25]. As a result of SPIM, research groups have been able to execute plasma-induced laser ablation on arbitrarily-shaped three-dimensional patterns preventing damage to surrounding tissues.

3. Cytometry

Cytometry involves the measurements of certain characteristics of cells like number, size, phase, or shape. It is named flow cytometry when performed in a fluid stream. In many cases, cytometry involves lasers and fluorescence, which opens the possibility of using SPIM for cytometric experiments as shown in [26-28].

4. Spheroid cultures

Cultures in three dimensions simulate *in vivo* conditions better than flat Petri dishes. When allowed to grow in a volume, cultures will take a spheroid shape. LSFM techniques offer fast sectioning and low photodamage useful to track the development of spheroids over time [29]. Spheroids may combine different cell types to form organoids, employed for drug test [30], regenerative medicine [31] and oncology research [32].

5. Automation

Biology laboratory equipment trends towards automation of cell culturing and testing [33], processes which are frequently monotonous and consume large amounts of human resources. The appearance of bioMEMS, integrated with LSFM, investigates high-throughput and low-consumption devices that can increase production and lower costs [34].

6. Open source SPIM

Groups of optical system developers have gotten together to promote and create open-source websites with information about SPIM microscopes. It includes understandable CAD (computer-aided design) models on how to build such device, lists of the necessary equipment, and an elementary control software. This initiative is carried out by two main sites: OpenSPIM [35] and Open SPIN Microscopy [36].

1.4. Legal Framework

The laboratory and equipment set-up conditions must meet legal requirements for prevention of health-associated risks and work-related accidents, environmental protection, and appropriate use of the university's resources.

1. Restriction of Hazardous Substances Directive (RoHS)

The European Union's Directive 2015/863 [37] regulates the amount of hazardous materials in electronic products for environmental waste control. The hardware acquired for this system is RoHS compliant.

2. Warranty

Preserving the warranty of the equipment is important to benefit from refund and return policies of the manufacturers. Care must be taken when manipulating electronic devices because static electricity discharges may fry an integrated circuit. Dropping and improperly disassembling parts of the hardware will void the warranty.

3. Laser protection

The use of lasers was done according to laser safety manuals [38], [39]. A warning sign was place to indicate the use of laser equipment within the room and glasses were worn during the alignment and calibration stages to prevent eye damage. A methacrylate box and tube system cover the beam throughout the optical path. The optical working plane is set parallel to the ground and at a height lower than the hip.

4. Electricity supply

Connecting several devices through power strips at a single mains socket can be hazardous as it increases the risks of fire, electrocution and damage to the equipment. The current output of the sockets in the laboratory is limited for safety. Additionally, fuses and emergency buttons are implemented that may off the current in case of an accident.

All the electronic equipment is held above the ground to safeguard it from water leaks or unforeseen spilling of liquids. Insulation of soldered parts such as cables and breadboards is compulsory.

5. CO_2 control

Required because the microscope is designed for live imaging. Luckily, cell cultures in microdevices produce negligible quantities of CO_2, so a ventilation pump is not needed. Just in case, the lab is equipped with carbon dioxide sensors.

2. Objectives

2.1. Cell motility and tracking

The goal of this project is to set up a device capable of imaging processes related to cellular motion. Fluorescence imaging of such experiments requires high time resolution and low phototoxicity to make fast recordings over prolonged periods of time. From *1.3.1. Fluorescent Imaging Techniques*, the most adequate to fulfil these two purposes is SPIM.

The Biomedical Imaging and Instrumentation Group at Universidad Carlos III de Madrid has been performing image acquisition and processing in two main areas within this field: cell migration and traction force calculations.

2.1.1. Cell migration

Cell migration takes place in core physiological processes, namely: embryonic development, wound healing and immune response. It is also a principal driver of tumor metastasis.

So far, the dominance of flat cultures for cell migration studies has made them unable, in many cases, to mimic real biochemical environments [40], [41]. The microscope developed for this thesis will allow recording cell migration in a volume. The growing and processing of two-dimensional cultures has been extensively studied and 3D have become the state of the art. The images acquired will be used to continue research on the line of [42] – [45].

2.1.2. Traction Force Microscopy (TFM)

Apart from tracking cells in space to characterize migration, research has also been conducted in measuring static or dynamic forces exerted by the cell on the extracellular matrix (ECM) [46]. These forces are related to differentiation and gene expression, playing a central role in migration processes and structural behavior.

Measuring these forces optically is known as *traction force microscopy* (TFM). Gel matrices (e.g.: collagen, hyaluronic acid, Matrigel) are synthesized with embedded fluorescent beads, and then fluorescently-labeled cells are seeded into the gel. Optical fluorescence microscopy is used to image a cell and its surrounding beads. The deformation of the matrix is measured by tracking the movement of the beads in space with respect to the cell. Knowing the mechanical properties of the cell (the Young modulus), the forces (stress) can be estimated from the measured deformations.

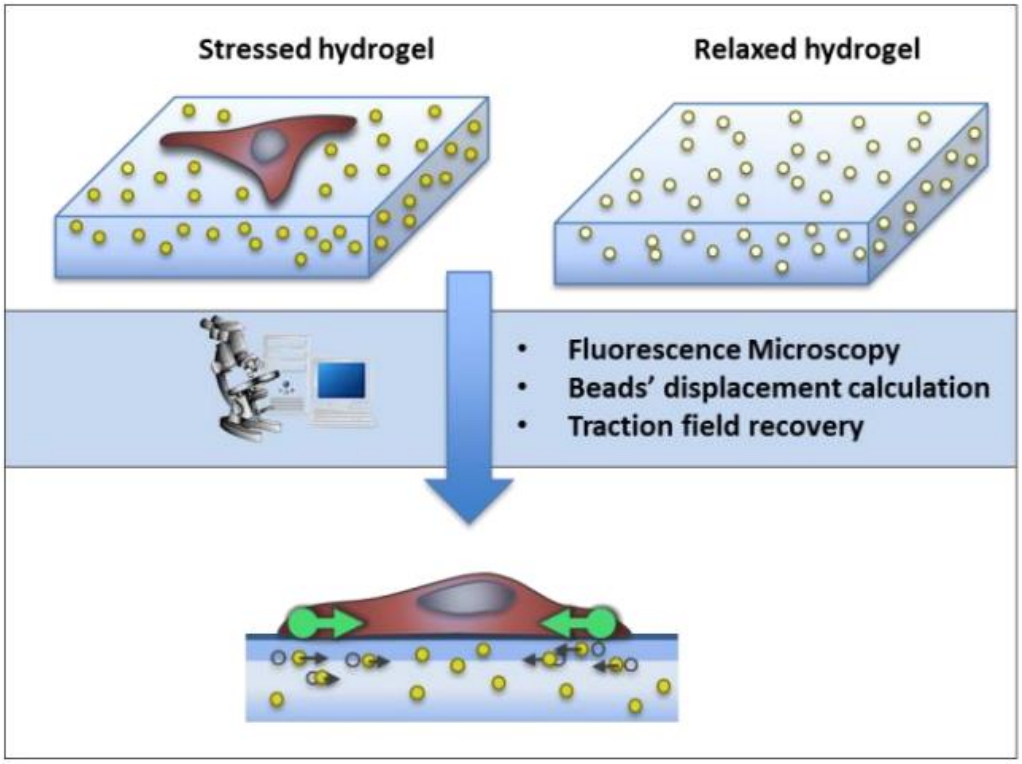

FIGURE 4. SCHEMATIC REPRESENTATION OF TFM [47]

Most groups, including the one at Universidad Carlos III de Madrid, have been conducting most image processing research in 2D and 2.5D TFM [47] – [50]. In 2.5D, three-dimensional images are acquired with a confocal microscope from cells seeded on a very thin layers of gel. The SPIM station should be able to take full 3D images from single cells allowing researchers at the university to publish work on the line of [51] – [54].

2.2. Experiments in microdevices

Microfluidic devices serve as cell-culturing platforms that allow medium to be changed continuously instead of periodically. Most are made of PDMS (polydimethylsiloxane) cast from a microfabricated silicon mold. For instance, the images acquired for [47] – [50] above came from cells seeded in microdevices.

So far, there have been many publications that study 3D cell motion in microfluidic platforms taking advantage of the optical transparency of PDMS. Examples of these can be found in [55] – [57]. The report will discuss the current limitations of lightsheet methods when performing scans on confocal-designed microdevices and the need to reinvent some designs to maximize the potential of SPIM for cell motility imaging.

2.3. Objectives' conclusion

In line with the objectives set, the next chapters of the thesis will describe the fundamentals and the process of setting-up a SPIM microscope capable of performing three-dimensional TFM and cell migration imaging in PDMS microfluidic devices.

3. Materials and Methods

3.1. SYSTEM COMPONENTS

In this section, the physical and material properties of the hardware used for building the SPIM device are described.

3.1.1. Illumination Components

These are components that shine some form of light into the sample so it can be imaged by the camera.

3.1.1.1. Lasers:

Lasers (light amplification by stimulated emission of radiation) are light sources capable of emitting coherent light: electromagnetic waves with a constant phase and same frequency. Spatial coherence allows focusing of the beam and collimation, while temporal coherence grants lasers the ability to function as monochromatic and pulsatile light sources.

Laser diodes come in a variety of prices so there must be a good reason to explain why a laser pointer costs a few euros and fluorescence microscopy lasers costs thousands. The optical lasers supplied by high-end manufacturers offer the following advantages:

- Well defined beam diameter (1 mm): allows for precise control over the beam size during beam expansion and focusing, relevant to calculate the focal spot diameter and the depth of focus (DOF).
- Circular beam shape (ellipticity <10%): symmetry of the beam is important when characterizing spatial resolution in every direction.
- Power stability (< 0.5 %): stable power output is desired to obtain quantitative data from our measurements with a constant SNR. If power emission is unstable over time, then the recorded fluorescence signal will also be, rendering the system unable to quantify with precision the amount of fluorophore at a given point in the image.
- Pointing stability (< 5µrad/K): important for collimation of the 488nm (blue) and 633nm (red) lasers. Ensures both lasers are focusing on the same spot and the image captured for blue and red fluorescence represents the same spatial plane.
- RMS noise (< 0.2 % for 10Hz - 10MHz): power stability is maintained when the laser is activated on pulsatile mode across a range of pulse frequencies.
- Operating environment temperature (15 - 40°C): outside this range of temperatures the laser quality decreases as the beam becomes more unstable. The temperature range of these lasers has been designed to be optimal for room temperature, like in a biology lab.

- Power output (100mW): high power output and fine control with a step size of 0.1mW, although usually steps of 1mW are used. Important to optimize the amount of signal with phototoxicity.
- Narrow bandwidth (±1nm): ensures a single wavelength of light is emitted. Highly specific excitation illumination.
- Polarization: sometimes essential to characterize optical systems but not relevant for our current application.

More specifications and infographics are available from the manufacturer in [58].

3.1.1.2. LED:

Like lasers, LEDs (light emitting diodes) are also diodes that emit light, but the emission mechanism is different: LEDs emit incoherent and non-monochromatic light by electroluminescence. Their emission spectrum is narrow and sometimes considered monochromatic with regards to human eye vision. For example, white colored light on a laptop screen is actually a combination of tightly packed RGB (red-green-blue) LED pixels that stack-up and appear white.

For this system, the quality of the LED does not have to be as good as that of the laser because it is not used for quantification of any sort, but rather to navigate through and focus the sample. Qualitatively, it is also used to see the contour of cells and microchannel walls.

3.1.2. Optical Components

Optical material like mirrors and lenses must be handled with care. Special tissues sold by the manufacturer must be used to avoid scratching and permanent damage when cleaning dust or fingerprints.

3.1.2.1. Mirrors

Mirrors come in a variety of shapes and materials. The shape (Ø1 inch round) has to match that of the mirror holder. The material of the mirror will determine its reflectance at given wavelengths and incident angles. For our lasers, more economical aluminum-surface mirrors are used with reflectance values of $R_{488nm,\ 45^o} \approx 91.8\%$ and $R_{633nm,\ 45^o} \approx 86.3\%$. The material also determines the damage threshold of an incident beam, and the mirror's resistance to scratching.

Fun fact! One fascinating thing about working with mirrors is that you don't actually see the object itself because of their unusually high reflectance. It will be confusing to see yourself, your surroundings and *maybe* some specks of dust on the surface; rest assured you will never be seeing the same mirror twice!

3.1.2.2. Filters

Optical filters are characterized by their transmittance spectrum, which is analogous to an electronic filter transfer function. It effectively allows some frequencies (or wavelengths) of light to pass through it while blocking the rest (see Figure 5).

1. Dichroic

Dichroic filters are a special kind of optical filter which reflects certain wavelengths of light (like a mirror) and transmits others. The reflected wavelengths belong to the stopband, and the transmitted wavelengths to the passband. Alternating layers of material of different refractive indices causes phased reflections that interfere constructively at certain wavelengths, and destructively at other wavelengths.

Fun fact! Compared to conventional filters, dichroics reflect unwanted wavelengths instead of absorbing them. This results in negligible heating and very large laser beam damage thresholds. They are more selective optical filters (sharper cutoff) but the reflected light has to be dealt with somehow.

2. Bandpass Emission (or Barrier)

Bandpass filters selectively transmit a band of wavelengths while attenuating (stopping) all others. It can be created by having a long-pass and a short-pass filter in sequence.

Emission filters effectively reject wavelengths other than those corresponding to fluorescence emission from the sample. This is very important because the CMOS digital camera produces grayscale images: it detects the intensity of the photon flux but not its energy (color). The spectrum of light reaching the detector must correspond to that which we aim to measure, making narrow bandwidths desirable. Narrow bandwidths play a major role when imaging several fluorophores, as it is essential to reject cross-talk between their emission spectra. A narrow bandwidth also helps reduce light-scatter and background noise.

Fun fact! Optical bandpass filters are angular sensitive, so they must be mounted perpendicular to the direction of light. In certain angles, they can actually serve as a poor dichroic filter.

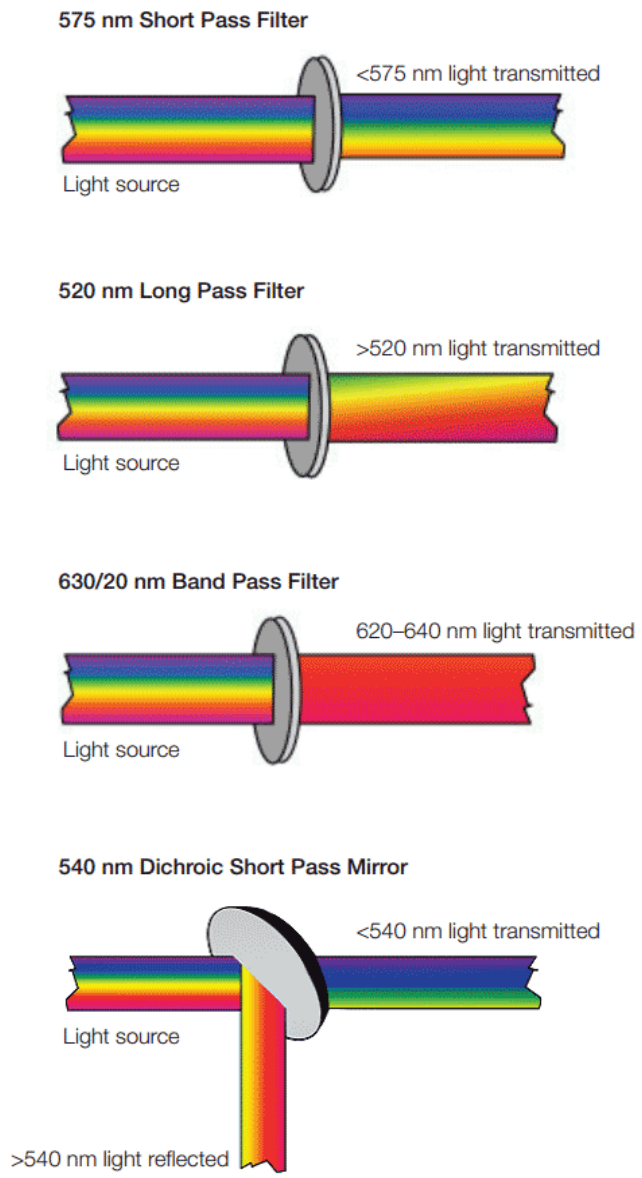

FIGURE 5. TYPES OF OPTICAL FILTERS [59]

3.1.2.3. Lenses

Lenses use the physical principle of refraction to focus or disperse light. They are the core of any microscopy system. In SPIM, several types of lenses are used. Their distinct shape, material and size are what makes them suitable for their function.

Fun fact! Lenses date back several millennia, to ancient Egypt and Mesopotamia. The first documented book on optics was written in 2nd century AD in the Roman Empire, and rediscovered and rewritten during the Islamic Golden Age (11th century). “Classical optics” spans from this age up to the Industrial Revolution, while “modern optics” refers to discoveries from the 20th century onwards.

1. Spherical

Lens are generally spherical because it is an easy shape to make. The surface of spherical lens corresponds to the surface of a sphere, which can be concave or convex on either side. Our system employs plano-convex lens which, as their name suggests, are planar on one side and convex on the other side. The radius of the convex side determines the focal distance.

Plano-convex lens are non-symmetrical and have directionality: if the beam enters through the convex side, it will be focused, while entering through the planar side will cause it to be dispersed.

Spherical lenses suffer from two aberrations [60]: spherical aberration and chromatic aberration. These two are explained in the table below.

TABLE III. ABERRATIONS IN SPHERICAL LENSES

Spherical Aberration	Chromatic Aberration
Blurring caused because the rays that pass through the outer side of the lens will focus at a different point from rays that pass through the center.	Lens cannot focus all colors on the same convergence point because light of different wavelengths has different refractive indices, just how a prism divides white light into its components based on wavelength.
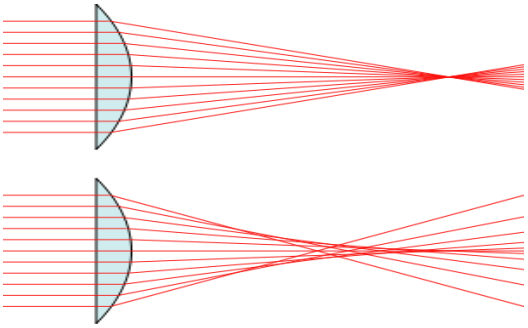	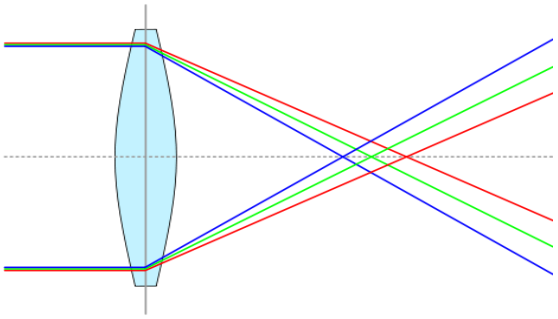
FIGURE 6. SPHERICAL ABERRATION [61]	**FIGURE 7. CHROMATIC ABERRATION [62]**

But not all spherical lenses are the same. Like with other optical components, high-end manufacturers offer higher quality products. The lenses used for this system have anti-reflective (AR) coating which makes the glass surface non-reflective. The surface is also smoother and of accurate shape. Using achromatic doublet lenses yields superior optical performance (see table below with data provided by Thorlabs) and offers better broadband and off-axis performance than aspheric lenses.

TABLE IV. ADVANTAGES OF ACHROMATIC DOUBLET LENS VS. REGULAR PLANO-CONVEX LENS [63]

1. Achieve a tighter focus

When focusing a laser beam, the spot (circle of least confusion) from the doublet lens is significantly smaller.

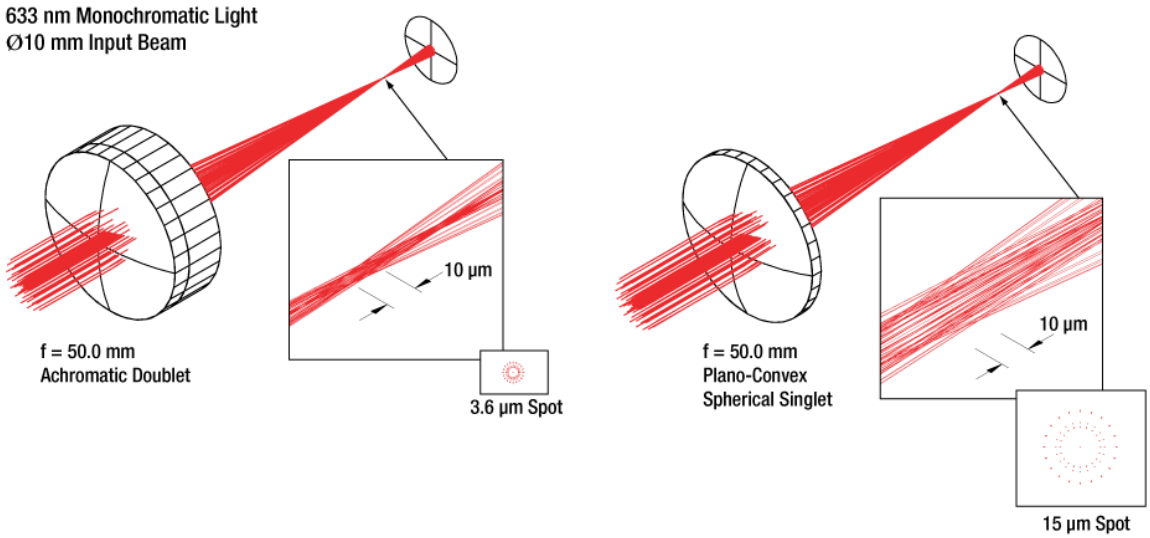

2. Superior off-axis performance

Compared to spherical singlets and aspheric lenses, achromatic doublet lenses have reduced sensitivity to centration on the beam axis which greatly reduces lateral and transverse aberrations.

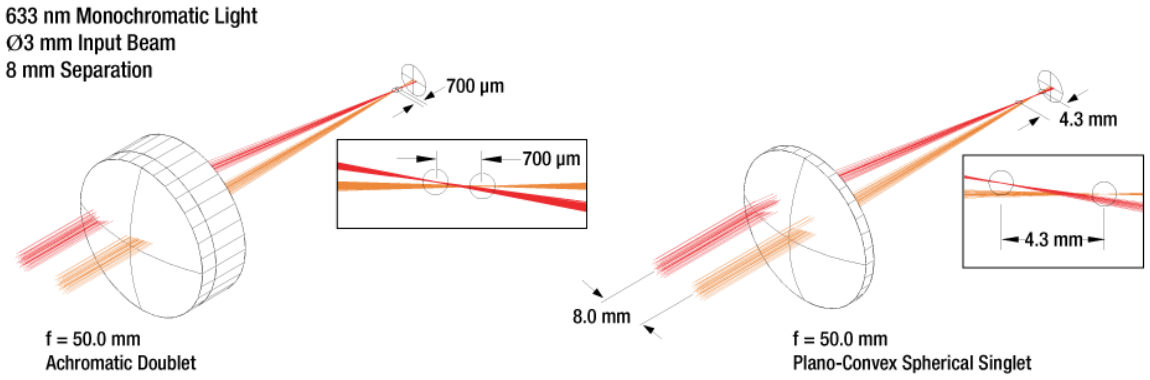

3. Nearly constant focal length across a wide range of wavelengths

Achromatic doublet lenses use glasses of two different refractive indexes that cancel chromatic aberration. The circle of least confusion for white light is therefore reduced.

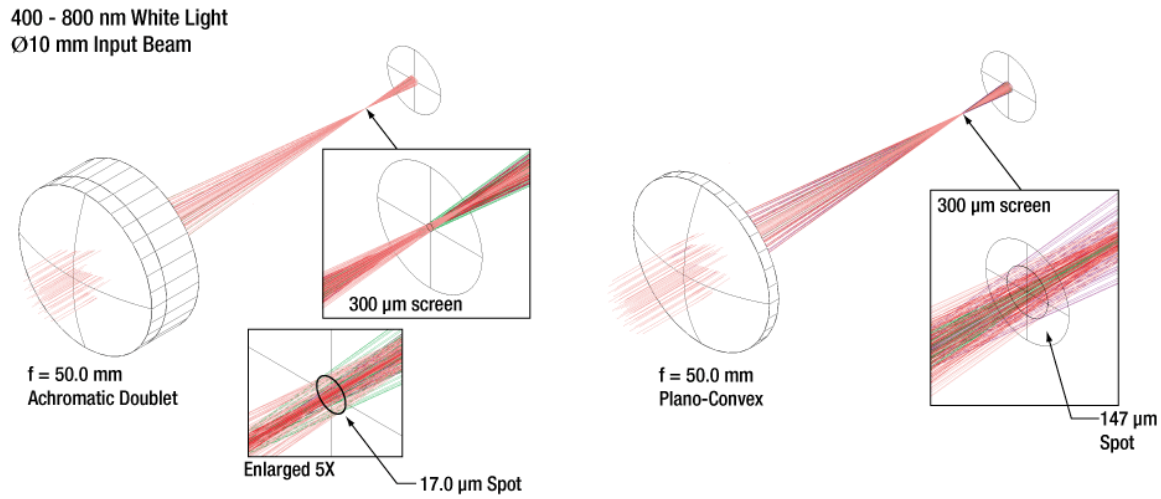

2. Cylindrical

The surface of a cylindrical lens corresponds to the surface of a cylinder. This is the essential lens that defines SPIM with respect to other LSFM techniques. A cylindrical lens is responsible for creating a light-sheet from an incident laser beam (see Figure 8 below). The cylindrical lenses used in our system are plano-convex with AR coating.

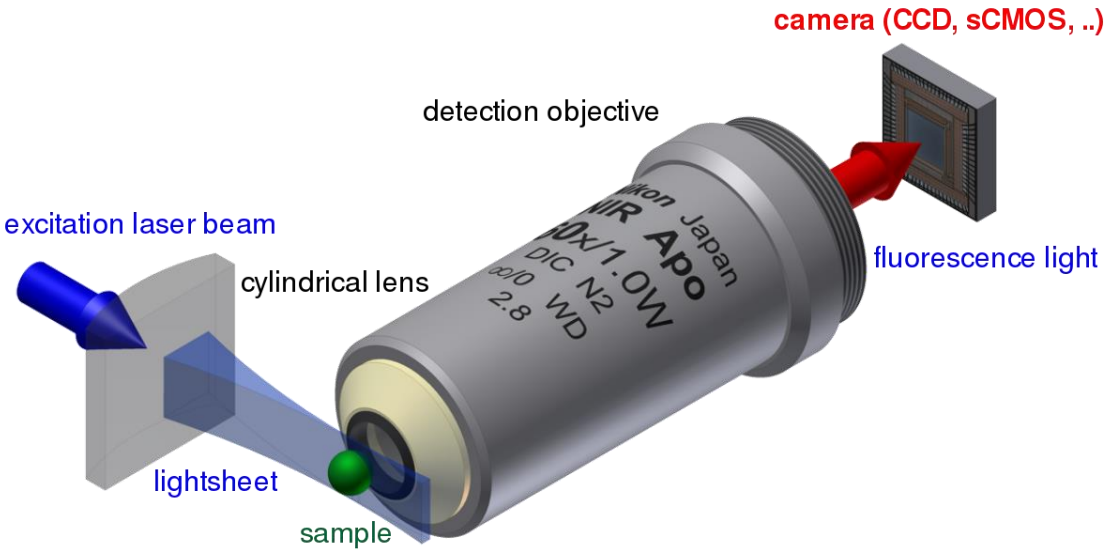

FIGURE 8. CYLINDRICAL LENS CREATING A LIGHTSHEET IN SPIM [64]

3. Tunable Lens

Electrically tunable lens (ETL) are plano-convex lenses that change their radius when a current is applied: the change in radius changes the focal length. This allows focusing to be controlled from the computer and eliminates the need for optomechanical focusing. ETLs are essential for rapid synchronized changes of the focal spot when capturing images in the z-direction.

Fun fact! These are the only lens in our system not made of glass. In fact, tunable lenses are not even solid! They are made of a liquid which functions as a lens because of its electrowetting properties.

4. Objective Lens

A microscope cannot be understood without its objective. It is responsible for primary image formation and plays a determinant role on the quality of the image in terms of magnification and resolution.

Different objectives offer various degrees of correction for the primary optical aberrations and are categorized into the following: achromats, fluorites (or semi-apochromats) and apochromats.

- Achromatic objectives (cheapest and most common) correct for chromatic aberration by focusing blue and red at the same spot. Spherical aberration is corrected for in the color green.
- Fluorites or semi-apochromats are superior to achromats, offering spherical correction of more than one color. This provides higher numerical aperture and therefore brighter images with better contrast.
- Apochromats are corrected spherically for two or three wavelengths and chromatically for red, green and blue. They provide the highest levels of correction (almost eliminating chromatic aberration) and are, of course, the most expensive and difficult to manufacture.

However, all three types of objectives project images that are curved rather than flat. This inherent condition of curved lens surfaces is aggravated by increased magnification. Objectives can implement flat-field correction to give images with common focus throughout the view field. Low-distortion flat-field correction makes an objective more expensive but is essential for digital imaging. Objectives of this kind are preceded by the term “plan”: plan achromats, plan fluorites, or plan apochromats.

Numerical Aperture

The numerical aperture (NA), or object-side aperture, is a dimensionless number that characterizes the range of angles over which the objective can accept light:

EQ. 1: NUMERICAL APERTURE

$$NA = n \cdot \sin(\alpha)$$

n: index of refraction of the medium (air, water, oil).

α: maximal half-angle of the cone of light that can enter the lens.

The numerical aperture of a microscope objective measures its ability to gather light and its resolution at a given distance from the sample.

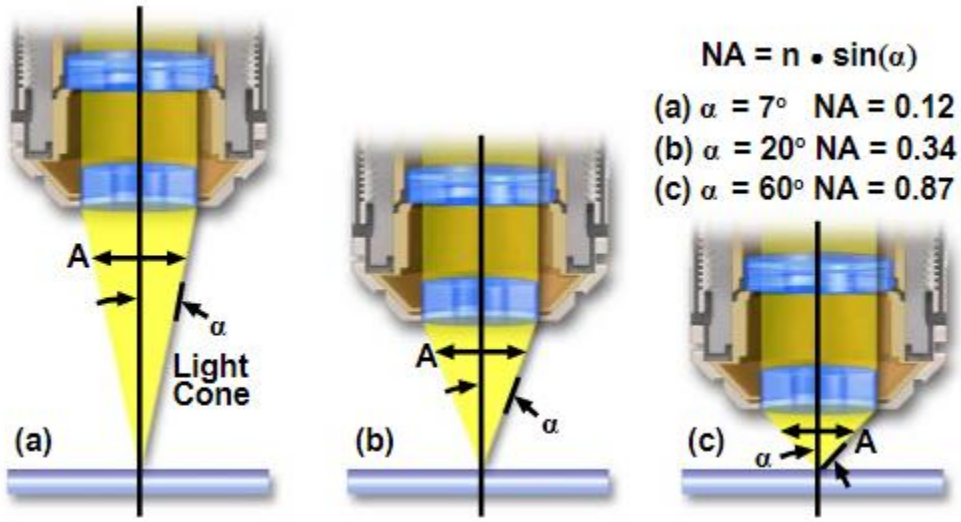

FIGURE 9. NUMERICAL APERTURE [65]

The NA can be increased by using an immersion medium with a refractive index similar to the one where the sample is placed. In our SPIM system, this would be glass or PDMS from the microdevices where cells are seeded. Objectives are specific for the immersion medium where they are to be used:

1) Air (Dry)

The refractive index of air (n = 1.00) implies that, in theory, air objectives can have a maximum NA of 1, but this is practically impossible. The maximum NA that can be obtained with air objectives is around 0.95.

Although the maximum numerical aperture is lower than for water or oil, dry objectives have a lower risk of damaging the front lens by crushing it against the sample. Using the

microscope is also easier because it saves having to prepare the sample for immersion in a medium.

2) Oil

Oils have a refractive index of around 1.5, which is close to the refractive indices of glass (n = 1.6) and PDMS (n = 1.4). This reduces refraction of light travelling from the medium to the objective. With a higher refractive index than air, oil objectives also have a higher NA.

Using these objectives without oil or immersing them in some different medium results in spherical aberration due to refraction at the surface of the front lens that cannot be corrected. It is possible to image the sample but at the expense of a defective image.

3) Water

Water (or PBS) is preferred as an immersion medium for applications with cells or cultures. The refractive index of pure water (n = 1.33) is lower than that of oil, resulting in slightly lower numerical aperture. High numerical aperture water immersion lenses are excellent for live imaging but cost tens of thousands of euros. Like oil objectives, using them with the wrong medium will negatively affect image quality.

Water and oil immersion objectives can be assembled with a spring-loaded retractable nose-cone that protects the front lens elements and the specimen from collision damage.

Fun fact! The objective is the first element that light encounters as it proceeds from the specimen to the image plane. Objectives derive their name from the fact that they are, by proximity, the closest component to the object (specimen) being imaged [66].

5. Tube Lens

These are spherical lens like the ones discussed at the beginning of this section but, as their function in a microscopy system is different, they will be considered separately. Contrary to the plano-convex lens mentioned earlier, tube lenses are biconcave and therefore non-directional (can be oriented in any direction).

Tube lens are relevant in infinity-corrected optical systems which have an image distance that is set to infinity. The tube lens is in charge of refocusing the parallel rays that exit the objective into an eyepiece or digital sensor.

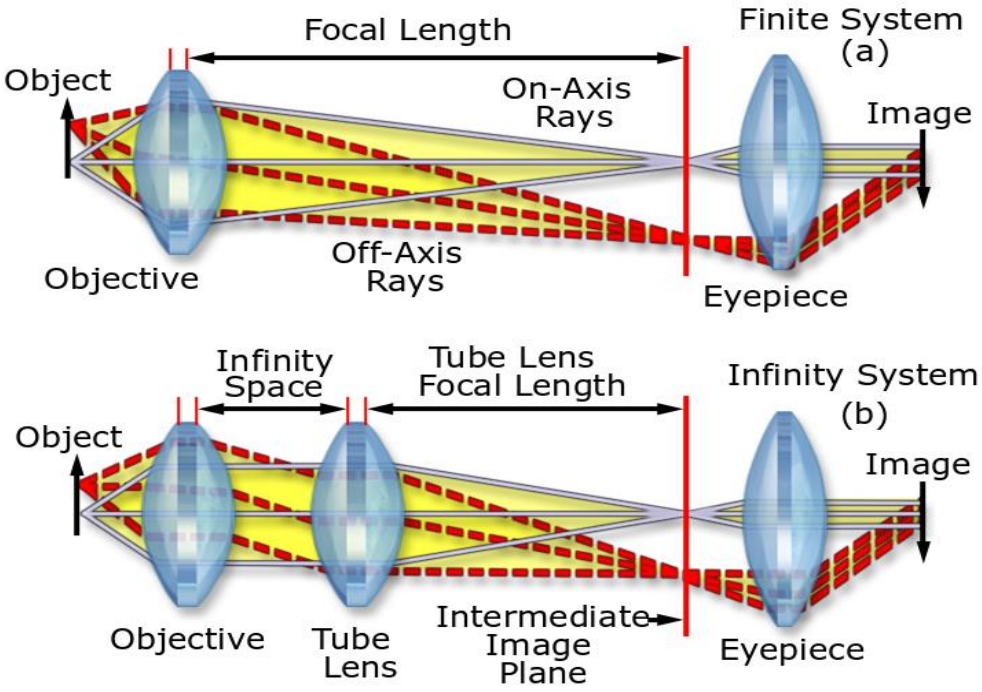

FIGURE 10. TUBE LENS AND INFINITY SPACE [67]

The figure above compares a finite microscopy system with an infinite one. The infinite system requires the use of tube lens to refocus the parallel rays. Note that the distance between the tube lens and the sensor is still a fixed one. In a SPIM system, there is no eyepiece lens, but rather a CMOS sensor of a digital camera that captures the images.

Between the objective and tube lens there is a region called “infinity space” (see Figure 10) where light rays are parallel. Within this region, optical components such as ETLs or filters can be placed avoiding spherical aberrations or changes to the working distance. This is an advancement with respect to traditional microscopes that had a fixed tube length of 160mm which imposed a space limitation to the number of components between the acquired light and the sensor.

However, there still is an upper bound to the distance between the tube lens and the objective. If the tube lens is too far from the objective, there is a decrease in the number

of peripheral light rays collected by the lens, causing darkening and blurred edges in the image. As such, infinity optics refers to the parallel light rays that leave the objective focused towards infinity, but this does not mean that infinite space is available between the objective and the tube lens.

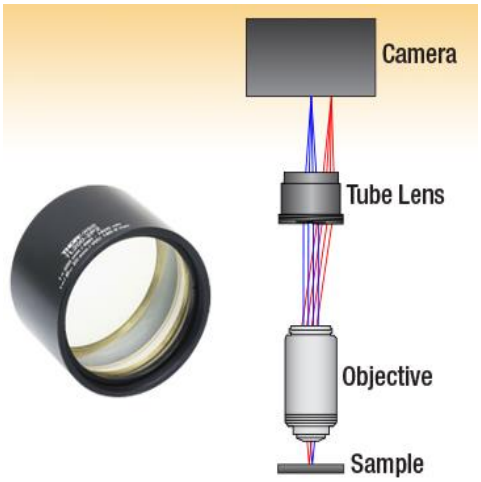

“An objective lens creates an image of an object at infinity; put another way, the objective collimates the light emitted from different positions at the object plane. These tube lenses are designed to refocus the collimated light rays into an image on the active area of a detector, as illustrated in the diagram to the left. In the diagram, the blue rays originate from the object plane at the center of the optical axis, while the red rays originate off-axis. If the tube lens is too close, the image may suffer from aberrations; if it is too far, vignetting will occur.”

FIGURE 11. TUBE LENS DIAGRAM AND EXPLANATION FROM MANUFACTURER [68]

3.1.3. Optomechanical Components

Optomechanics is a broad term that refers to the design and manufacture of precision mechanical components of optical devices which are generally machined from aluminum and steel.

3.1.3.1. Motors

Rigorous motion control is essential in light-sheet microscopy because it is a highly automatized and precise system: most of the control is micrometric and done from the computer.

1. Mirror Galvanometer (Galvo)

A mirror galvanometer, commonly referred to as galvo, consists of a motor and a mirror used to direct the incident beam of light. Galvos can have a single or dual axis. The dual-axis galvanometers employed in this system have two motor-mirror complexes placed at 90º of each other that can direct the beam in two independent directions (named X and Y).

The dual axis is essential for SPIM in many ways: it can create a virtual light-sheet, it allows to scan the sample in the z-direction, and it is responsible for pivoting the light-sheet to remove shadow artifacts. The uses of the galvo in the system are described in detail in *3.2.1.4 Entering the Galvo***.** Please note that the X-Y spatial directions of the galvo are different from the x-y-z axes of the sample and linear stages.

Galvos are not only defined by the number of axes. For this system, high speed, high precision and a large-beam diameter are required. The factors that determine the precision of the moving-magnet motor are: repeatability (15 µrad), linearity (99.9%), full scale bandwidth for square waves (65 Hz) and sine waves (130 Hz), and small angle (±0.2°) bandwidth (1 kHz) and step response (400 µs).

This system has a maximum beam diameter of 10mm and a maximum scan angle of ±20.0°. The electronics are essential to guarantee control over the mechanical movement, so low-noise linear power supplies and driver card heatsinks are implemented. Additionally, a capacitor is implemented to detect the mirror position with high-precision (15 µrad). The driver cards are connected to the data acquisition system (DAQ), which is in turn connected to the computer.

Fun fact! The mirror galvanometer was an invention of the early 1800s designed to measure electrical currents. Currents would cause a mirror to move and deflect a laser beam.

2. Linear or Translation stages

Linear stages exert precise motion control over one axis. To move the sample holder in the 3D space, three linear stages (x-y-z) must be combined to provide 3 translational degrees of freedom. There is a long list of parameters that characterize a linear stage motor. The most important to consider are the resolution (step size, accuracy, repeatability), the range, the speed resolution, and the load they can bear. The table below shows the corresponding values provided by the manufacturer for the x-y motors and the z motor.

TABLE V. CHARACTERISTICS OF THE LINEAR STAGES

Parameter	Description	Value z	Value x, y
Microstep Size	Default resolution measure. The calculated linear distance traveled for each microstep of motor movement.	0.0476 µm	0.0992 µm
Accuracy	The maximum error possible when moving between any two positions.	20 µm	29 µm
Repeatability	The maximum deviation in actual position when repeatedly instructing a device to move to a target position 100 times.	3 µm	2 µm
Travel Range	The maximum physical range of travel of a motion control device.	50.8 mm	28 mm
Speed Resolution	The smallest incremental change in speed that can be achieved by the device.	0.00022 mm/s	0.0009302 mm/s
Maximum Centered Load	The maximum allowable force that can be applied at the center of the stage, perpendicular to the stage surface.	100 N	100 N
Maximum Cantilever Load	The maximum torque that may be applied about the axis of motion.	300 N · cm	125 N · cm
References to product:		[69]	[70]

Since the stages, the platform that holds the sample and the seeded microdevices are not heavy, the centered load and the cantilever load are way beyond the limits required. With respect to the resolution, the motor in the z direction has a lower microstep size than the horizontal x-y motors. The motion resolution in z is more important because it may also participate in shifting the sample in and out of focus when the user is searching for the focal plane, so higher precision is desirable in this direction.

Note that, unlike the galvo motors which include a capacitive sensor, these have no position memory when started. This is not a trivial drawback and requires a calibration step discussed in *3.2.3.3 Stage motor positions*.

3.1.3.2. Support Components

Play a major role in positioning the optical elements aligned with each other and stable over time. The following components are made mainly from aluminum but also steel or plastics.

1. Optical breadboard

Like an electronic breadboard, optical breadboards and tables hold the optical components of the device. Optical breadboards are designed with mechanical properties that make them ideal for their function.

A rigid and even surface can maintain the system stable and aligned over time. The table frame (workstation) of this equipment has sorbothane pads that provide damping, serving as a low-pass mechanical filter that can isolate the table from vibrational effects from the floor.

The stiffness of a table determines how much weight it can hold. For our current application, portability and dynamic rigidity was more important than sustaining heavy weight, so an ultralight aluminum breadboard - more lightweight than solid aluminum, steel or granite - was selected instead.

The breadboard is entirely made of aluminum which makes it non-magnetic and minimizes thermal instabilities by having a homogeneous coefficient of thermal expansion (CTE). Its black anodized surface reduces reflectivity and backscatter of light which helps constrain light outside its optical path, thus minimizing the chances of eye damage and noise coming from reflected beams.

Fun fact! Ultralight aluminum tables have an internal honeycomb structure which, like the hollow bones of birds, makes it more lightweight.

2. Mounts

A large variety of optomechanical mounts are available from manufacturers and are used to hold optical components such as mirrors, lens and filters. They can be broadly classified into kinematic and fixed, where kinematic mounts can either be manually adjusted or motorized. The latter are much more expensive and should only be considered if necessary for the application. Four examples of the most important mounts in this SPIM system are highlighted below.

i. Mirror mounts

Fixed mirror mounts hold a mirror accurately at a fixed position (e.g.: at a 45º angle). However, the *real deal* are kinematic mirror mounts. This microscope relies on low-profile compact kinematic mirror mounts for laser beam collimation and alignment. The compact profile of these mounts minimizes volume and reduces space requirements in the optical

breadboard. To reduce wear when adjusting the angles, hardened steel is inserted at kinematic contact points. Stiff springs provide increased stability by holding the mirror tightly against the screws.

Kinematic means it can move: the angle of the mirror is controlled by two fine adjustment screws with high threads per inch (TPI) that respectively rotate the mount in two independent and orthogonal angular directions. For very stable and controlled motion, the screws push the mirror holder outward while the springs pull back. These screws allow for a ±4º adjustment range.

ii. Mounting Cubes

Cage cubes are compatible with cage systems (see *3.i. Cage systems* below) and are usually employed to hold filters or lens. Black anodized surfaces reduce reflectivity and backscatter.

iii. Rotation Mounts

As the name indicates, these kinematic mounts allow for rotation. They differ from mirror mounts in that the rotation occurs around the z-axis (the normal vector to the surface of the circumference). A rotation mount is characterized by the precision of rotation and the angle range (360º). In this system, a rotation mount is used to orient the round cylindrical lens which creates the illumination plane.

iv. Microscope Objective Lens Turret (Objective wheel)

These are commonly seen in off-the-shelf microscopes and allow to easily change the objective without having to unscrew and screw a new one. Having several objectives is useful to change the magnification or the immersion medium. Caps are available to protect objective lens and to cover unused ports.

3. Optical Axis Systems

There are several ways to mount optical and optomechanical components along a common optical axis. This microscope employs cage systems, rails and lens tube systems. These three categories are not excluding but rather complementary to each other.

i. Cage Systems

An optical cage system uses up to four rigid steel rods. Manufacturers usually offer cage systems with different center-to-center rod distance, plus accessories and adapters that allow integration between the different cage standards.

In cage systems, long rods can be slightly unstable, so the cage system components are mounted into posts regularly for increased stability. Also, using the maximum number of rods (four) is recommended when joining components.

ii. Rails

Like cage systems, optical rails offer parallelism and rigidity which makes them well suited for building long linear beam paths. Compared to rods from cage systems, their increased strength makes them ideal as large-scale load-bearing structures as well. Rail clamps can be fixed to the rails to support posts or other optomechanical parts.

iii. Lens Tube Systems

Lens tubes can mount lenses and optical filters in a coincident optical axis. Matte-painted extension tubes and slip-on covers can protect the user from the laser going through the tube system and cover the signal from background illumination in the lab (noise).

4. Posts, Clamps and Spacers

Essential to support other optomechanical components in the optical table and rail systems.

Posts are rigid and stable, generally made from a homogeneous material for thermal stability (constant CTE). Depending on the post, its length can be fixed or adjustable. For fixed posts, different heights are achieved by stacking posts of shorter length and/or including spacers. Posts and spacers keep all the components at the same height, which reduced the optical pathway to two dimensions.

Spacers are thin metallic plates of very specific widths placed on top of poles for slight and precise height increments.

Clamps are used to hold posts tightly and ensure alignment over time. Clamps also allow to place posts at positions between optical breadboard screw-holes.

5. Adapters

Adapters allow combinations of different size standards (RMS, SM1, SM2, C-mount) of optical and optomechanical components. This is fundamental for integrating optical equipment from several manufacturers. Like every other mechanical component, the quality of the machining will determine the positioning and alignment accuracy which affects the overall performance of the system.

3.1.4. Digital sCMOS Camera

An sCMOS (scientific CMOS) detector implements a hybrid CCD/CMOS architecture, benefiting from the properties attributed to both designs. Although the two types accomplish the task of capturing light, converting it into electrical signals and creating a digital image, they offer distinct advantages:

- CMOS (complementary-symmetry metal–oxide–semiconductor) detectors are active-pixel sensors. Each pixel has a photodetector and an active amplifier. These detectors have lower power consumption which results in less heating and smaller sensor sizes. CMOS sensors are also less vulnerable to static electricity discharges and can provide faster readout because the digital output from each pixel is read line by line by a digital multiplexer.
- CCDs (charge-coupled detector) used to have lower noise and higher detection surface. Higher quantum efficiency makes them more sensitive.

sCMOS are now the best digital detectors available and offer extremely low noise, rapid frame rates, wide dynamic range, high resolution and a large field of view.

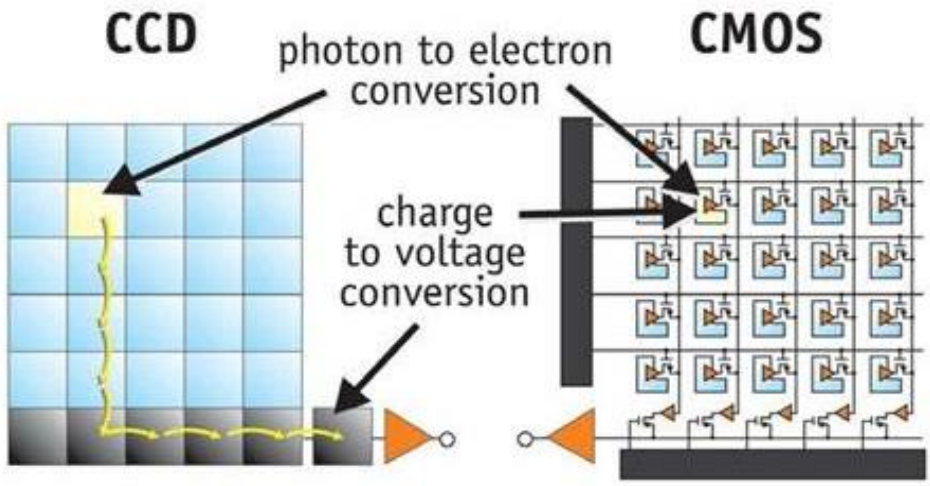

FIGURE 12. CCD VS CMOS READOUT [71]

Dynamic Range (DR) and Signal-to-Noise Ratio (SNR) are different parameters that determine the performance of a sensor. The DR is the maximum possible signal level divided by the noise level *when there is no light*. The SNR is the average signal divided by its RMS noise.

A 13.000€ camera offers more than just the sensor. An on-board field-programmable gate array (FPGA) processor enables highly tunable acquisition speeds and image data requirements.

This camera is capable of both USB 3.0 or Camera Link output. Camera Link has a faster readout (frames per second) because the CMOS sensor is actually composed of two adjacent sensors, each of them connected to its own Camera Link.

Furthermore, faster readout can be achieved by intelligent data reduction through lookup tables (LUT). Also, region of interest (ROI) selection within the pixels of the sensor reduces the need of reading every line of the pixel array.

To prevent overheating when the camera is intensively used, thermoelectric cooling (Peltier) with air and water can be implemented through refrigeration entries located on the case of the camera. Such cooling is not required for our imaging applications.

Another property of this camera is binning. Binning enhances low signals by integrating the signal received at several picture elements (pixels). For example, in a 2×2 binning the signal received will be 4 times higher (4-pixel area) but the spatial resolution in x and y will be halved. The memory space taken by the image will also be reduced, as the total number of pixels will be ¼ of the original.

The speed of this camera could be limited by the computer which is fed 2048-by-2048 16-bit images at 100 frames per second. The computer requirements for this data rate are discussed in *3.1.6. Computer*.

The table below contains the relevant specifications of the digital sensor camera provided by the manufacturer.

TABLE VI. CHARACTERISTICS OF DIGITAL CAMERA

Parameter	Value [72]
Quantum efficiency	82 % peak at 560 nm
Sensor	sCMOS
Number of pixels	2048 (H) × 2048 (V)
Cell size	6.5 µm × 6.5 µm
Effective area (sensor size)	13.312mm × 13.312mm
Maximum readout speed	100 frames/s
Maximum readout noise	1.6 electrons rms (1.0 median)
Dynamic range	37000:1
Binning	2×2, 4×4

3.1.5. Data Acquisition Device (DAQ)

It is the main interface between the digital and the analog world and enables the computer (digital) to interact with analog signals and devices. It serves simultaneously as an ADC (analog-to-digital converter) and a DAC (digital-to-analog converter). ADC is necessary to give feedback to the computer from the capacitive position sensors of the galvo, and DAC enables analog control of the galvo motors from a digital signal.

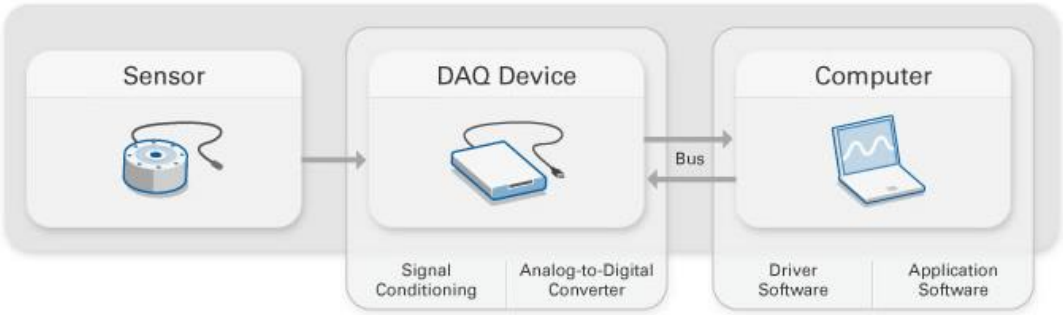

FIGURE 13. DAQ DEVICE INTERFACE DIAGRAM [73]

The DAQ bought for this system has the following analog channel specifications: 32 Analog Input (AI) channels of 16-Bit and 2MS/s (mega samples per second), and 4 Analog Output (AO) channels of 16-bit and 2.86 MS/s (single) or 1.25MS/s (multi). The sampling frequency (MS/s) of the DAQ has to be several orders of magnitude higher than the frequency of the device aimed to control.

For instance, if the required maximum oscillation frequency of the galvo is a sine wave of 100Hz with at angle of ±20.0° (40º range) and an angular step-size of 15 µrad:

$$40º = 0.70 \text{ rad} \rightarrow 0.70\text{rad} / 15\mu\text{rad/step} = 47\text{k steps} \rightarrow 100\text{Hz} \cdot 47\text{k} = 4.7\text{MHz}$$

In the example above, the DAQ should have an AO channel with 4.7MS/s to move with maximum precision the motors of the galvo at 100Hz. In practice, the galvo mirrors are not oscillating their entire angular range at maximum speed, so the DAQ can have a slower sampling speed.

Fun fact! The high sampling values is what requires the system to depend on an expensive 3000€ National Instruments DAQ and not a 40€ Raspberry Pi (no offense!).

3.1.6. Computer

The computer is the control center for the SPIM device. For it to interact with the rest of the components, drivers must be installed in the form of software and hardware.

The software Opt3D (programmed in LabVIEW) controls the operation of the DAQ and other devices. It is used for processing, visualizing, and storing measurement data and images.

Tunable lenses, camera, linear stages and lasers are connected through their drivers to the computer, so there must be enough ports for all of them. In general, these devices are designed to be connected to the computer via USB 2.0 or 3.0 ports (or allow for a USB adapter). The Camera Link feeds the computer at two SDR ports. If custom-building the computer, it is important not to forget other ports such as HDMI for the screen, ethernet for internet connection, and additional USB ports for the mouse, keyboard and other accessories.

For a system of this kind, there are important requirements beyond those of a standard desktop. At least 32GB of RAM memory (64GB recommended) is mandatory to deal with the volume of data incoming from the camera (2048×2048 16-bit 100 fps videos). A solid-state drive (SSD) is needed for longer studies because it enables the information from the RAM to be stored in the SSD and cleared.

A powerful CPU or graphics card (GPU) are only needed if image processing is going to be carried out at this station. It is advisable to separate computers dedicated to image acquisition (like this one) from the ones intended for image processing because of the differences in hardware, software and ergonomic needs of its users.

3.2. SYSTEM SETUP

In this section, the step-by-step process of setting up a functional SPIM system will be described. This process encompasses most of the hours dedicated to the thesis and explains how the *3.1 S* previously described are assembled into the final microscope. At the end of this section, a timeline (Figure 49) is included to summarize the whole process chronologically.

3.2.1. Hardware Assembly

Hardware assembly is analogous to building a device. The figure below shows the overall schematic of the microscope and is meant to be used as visual aid. The diagram will be referenced and shown in whole or in part during the hardware assembly steps together with images from the actual optical system.

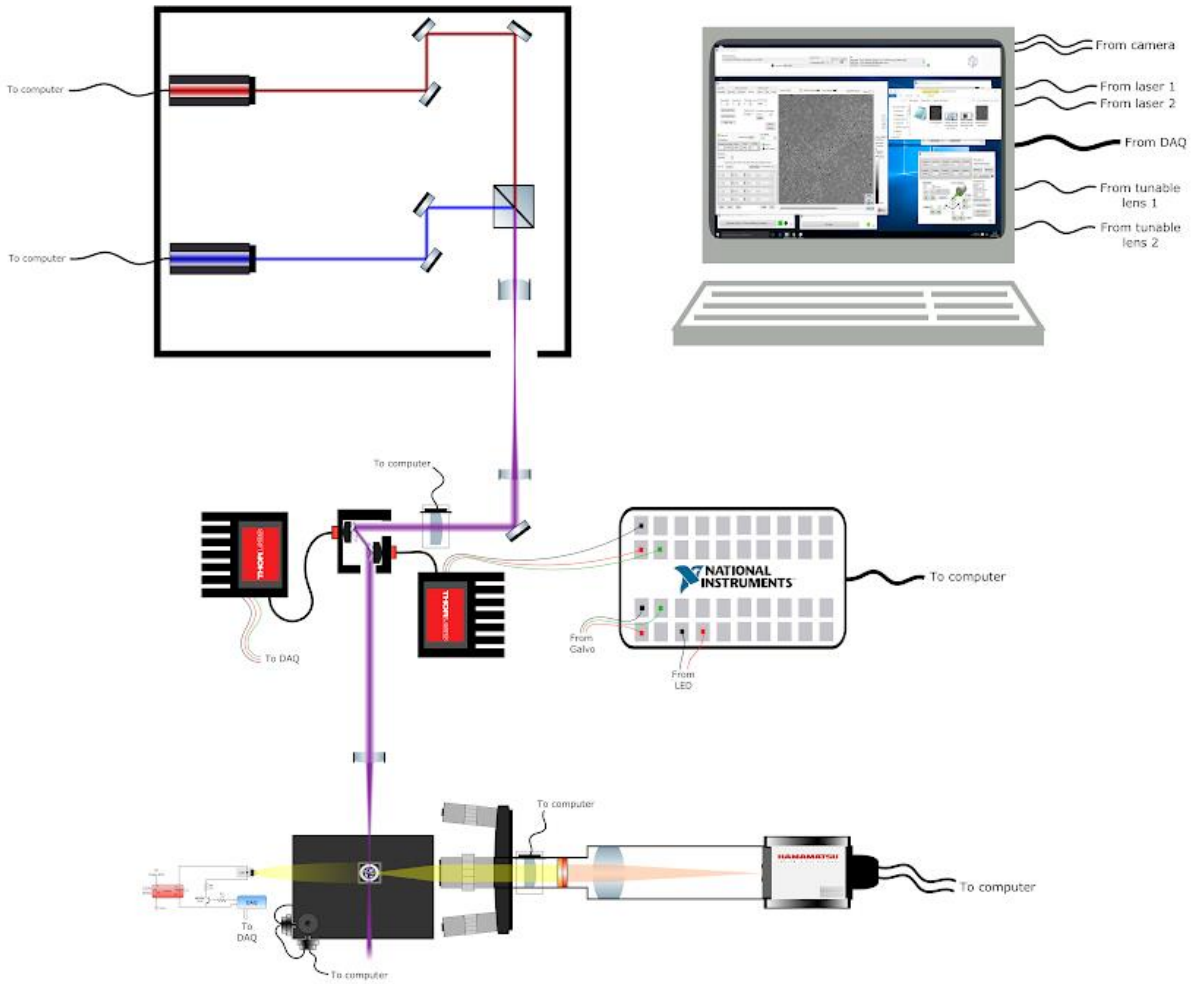

FIGURE 14. SPIM SET-UP DIAGRAM

3.2.1.1. Optical Table

The optical table is the base where all the optical components are mounted on. It is important that, before starting the project, the system's space requirements are estimated to ensure the table will be large enough to fit all of the components. For this project, the main ultralight breadboard mounted to the portable workstation has an area of 600 x 900 mm.

Since this board could not provide enough area by itself, another aluminum breadboard of 450 x 600 mm was mounted on top of the main breadboard. Three 25mm pedestal pillar posts arranged in a triangular fashion for stability secure the two breadboards together. This extended the useful area from 5400cm^2 to 6600cm^2 with a length increase of 30% (from 900mm to 1175mm). The remaining space (1450cm^2) between the breadboards is useful to pass and hide wires and cables of the system.

The main breadboard is now 37.7 mm (12.7 mm thickness of aluminum breadboard + 25mm pillar post height) lower than the extension breadboard. This height difference has to be considered when mounting optical components on the main breadboard so the optical plane remains at the same height.

3.2.1.2. Laser beam alignment and collimation

Consists of several steps that include mounting several components and calibration of these. This is a tedious and laborious process for someone inexperienced in optical hardware. The lasers will unalign with time and need to be recalibrated.

A. Mounting the lasers

Lasers are the first piece of equipment to be fixed onto the breadboard. As such, space considerations have to be accounted for: they must be mounted with enough separation to leave room for the kinematic mirrors but compact enough so there is space for the rest of the components.

The lasers should be close enough to the edges of the table to maximize the space for other components. A margin from the edge of the optical breadboard is needed to fit a covering methacrylate box for safety. This margin also minimizes the chances of the laser being hit by someone walking close to the optical table.

Short posts were used to mount the lasers because the beam emission height will mandate the heights for the rest of the components. Keeping a fixed height throughout the system is done to restrict the light path to an optical plane parallel to the breadboard.

The order of the lasers is important because of the stopband and passband wavelengths of the dichroic filter. In this setup, the "first" laser shines directly to a fixed mirror and should be that of longer wavelength. As the diagram in Figure 16 indicates, the red 633nm laser goes before the blue 488nm laser. At least two lasers are required for TFM: one to excite the cell fluorophores, and another to excite the fluorescent beads.

B. Mounting the kinematic mirrors

Posts and spacers bring the center of the mirrors, or any other piece of optical equipment, at the height of the laser beam. Pedestal pillar posts are held by clamps to the table. Clamps eliminate the need to restrict posts to the hole pattern of the breadboard. The clamp is screwed to the table, but it can slide (translate) and rotate before being tightly fixed. Additional clamps help secure the post to the table.

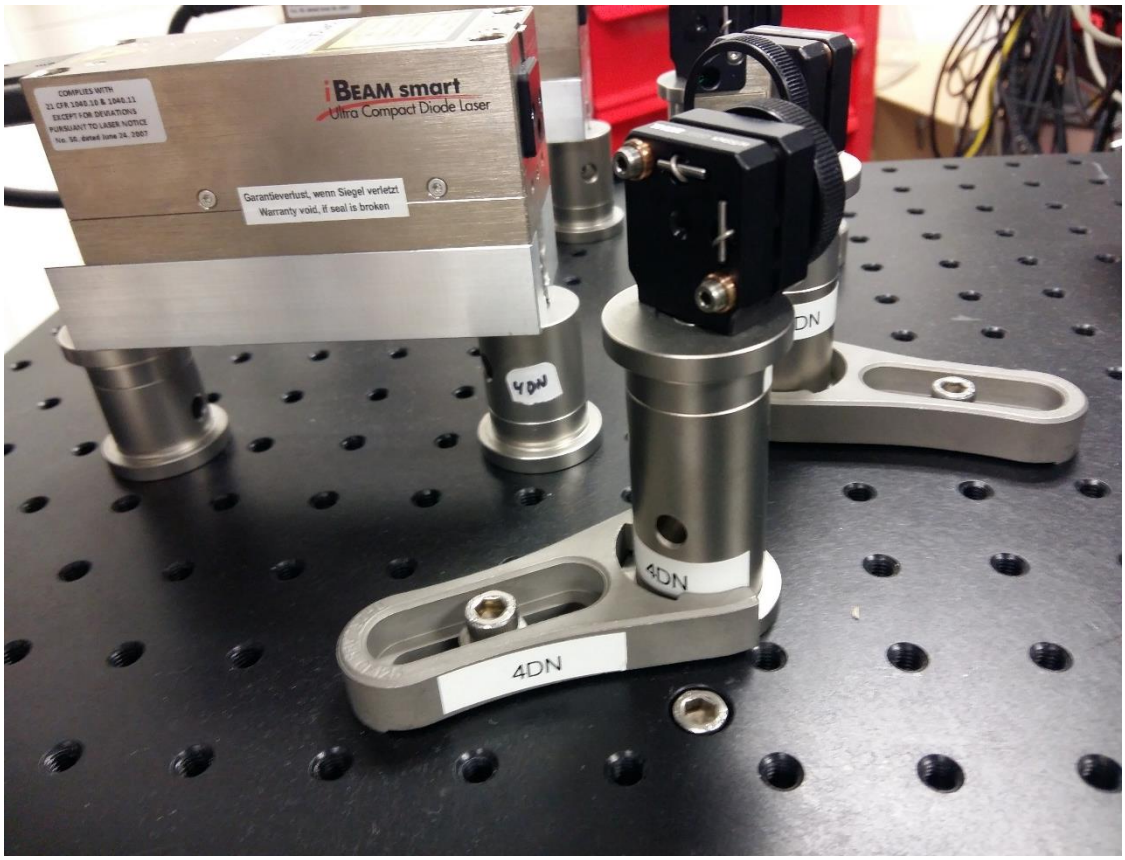

FIGURE 15. MOUNTED LASER AND KINEMATIC MIRRORS

The kinematic mirrors, mounted on top of the posts, allow for fine adjustment of the vertical and horizontal reflection angles which allows precise collimation of the beams. Compact kinematic mirror mounts are employed to minimize the space requirements providing room for beam expansion. Extra space potentially allows future insertion of another excitation laser.

C. Mounting the Cage System

The lasers face perpendicular to the cage system where collimation, alignment and beam expansion occur. A fixed 45º mirror reflects the 633nm (red) beam along the optical axis defined by the cage system, marking the beginning of it. Two long rods that start from the fixed mirror are regularly supported by posts screwed to the breadboard and cage mounts.

A cage cube supports the long-pass dichroic filter placed at an angle of about 45º. It receives the 488nm (blue) beam from the kinematic mirrors and reflects it along the optical axis of the cage system. The 633nm beam coming from the fixed mirror is transmitted (passes) through the dichroic. Care must be taken when placing the dichroic filter because it has directionality with respect to the incident beams.

D. Alignment and Collimation of the laser beams

Alignment and collimation of the laser beams are two terms frequently used throughout this section. Specifically, alignment refers to the process of aligning the beam with the optical axis of the cage system and the rest of the optical components. Collimation is the process of setting the two beams of light parallel and coincidental in space, resulting in a dichromatic beam of two wavelengths (488nm and 633nm).

As mentioned previously, doing this is not an effortless problem. It requires playing simultaneously with the positions of the mirror posts (using the clamps) and with the screws that control the angular orientation of the kinematic mirrors. Several tools such as pinholes and targets can be used to collimate the beams.

The laser beam should strike as close to the center of the mirrors as possible and at angle of about 45º. Of course, slight differences around these reference points are expected because the kinematic mirrors are selectively oriented for beam alignment.

To align the beams, switch both lasers on. Each ray should strike the kinematic mirrors and enter the cage system through a pinhole or target. The center of a second target behind the dichroic cage cube should also be hit. Pinholes and targets are designed so their opening is in line with the optical axis of the cage system.

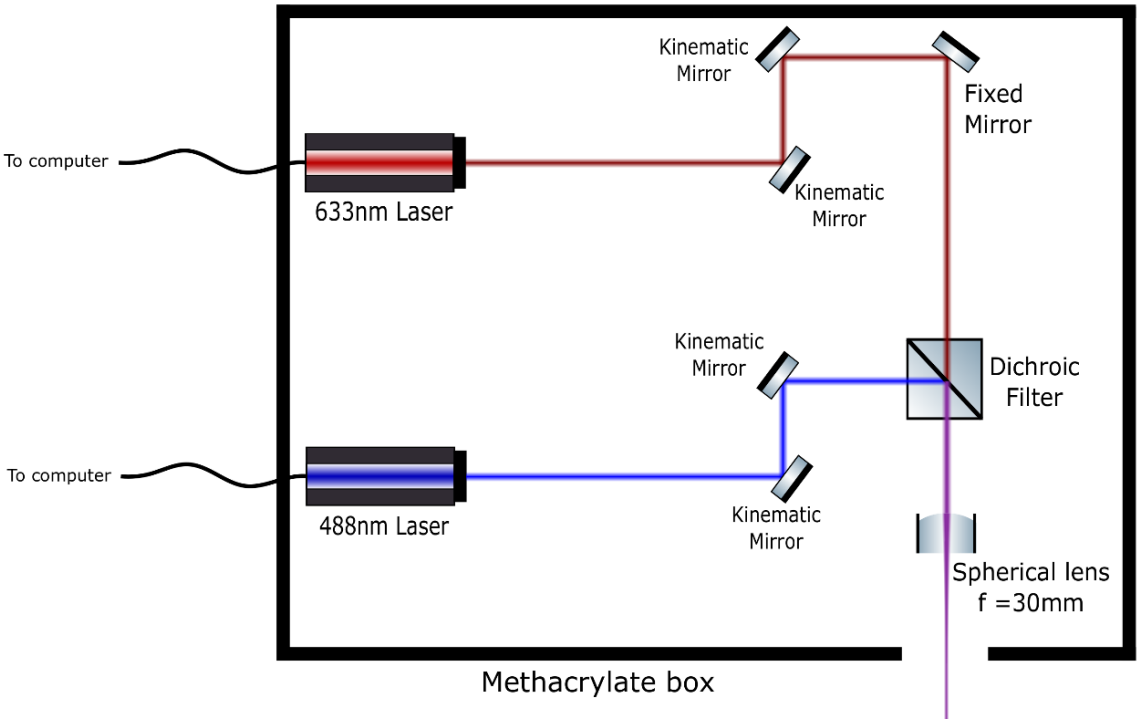

FIGURE 16. LASER ALIGNMENT SETUP (DIAGRAM)

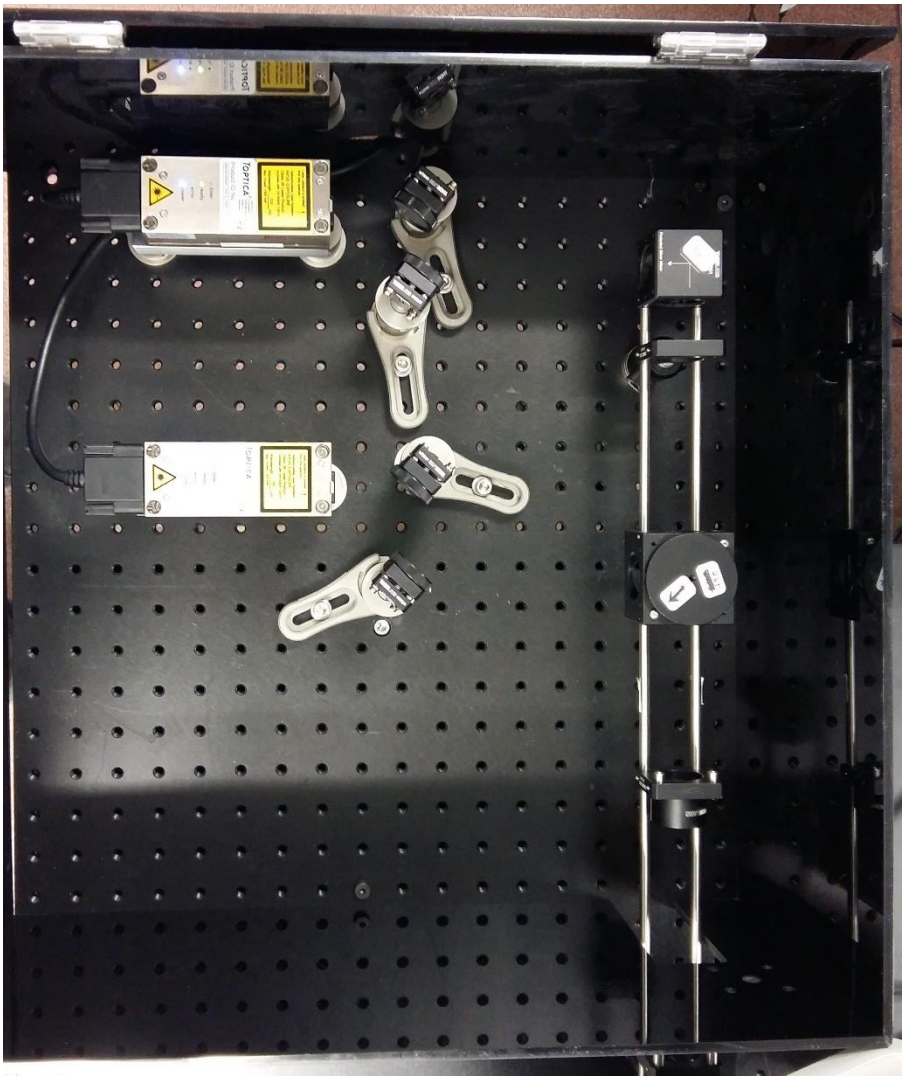

FIGURE 17. LASER ALIGNMENT SETUP

Once the beams are aligned with the cage system, this does not guarantee they are collimated. A first target should be located near the exit of the dichroic cage cube. A second target should be located very far away from the cage system (~20 meters). The orientation of the kinematic mirrors should now be adjusted so the blue spot and the red spot both hit the center of the two targets.

Hitting only the center of one of those targets means the beams are focused at that point in space, but it does not mean they are parallel to each other. Both beams are parallel only when the close target and the far target are hit at the same spot. Note that no beams remain parallel at infinity (e.g.: a distance of several kilometers). A distance of around 20 meters is sufficient because it is much greater than the length of the optical path in the system (around 500mm). If the beams are accurately coaligned for 20 meters, they will be for the effective length of the system.

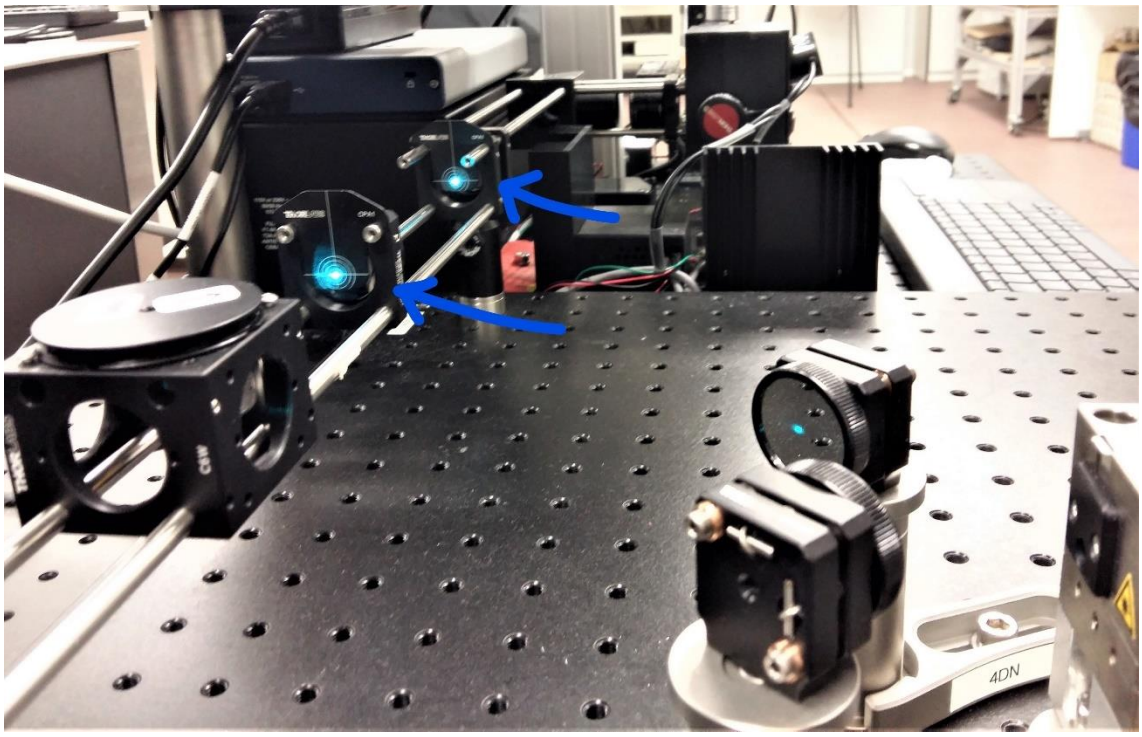

FIGURE 18. TARGETS FOR ALIGNMENT
Blue arrows point to the two targets in the cage system used for alignment. Additionally, a spot 20 meters away should also be hit. The same should be done for the red laser.

Fun fact! To make collimation easier and faster, I started a video call from the computer to my cell phone. The cell phone camera was placed far from the optical table, focused on the target 20 meters away. The image was sent to the screen of the computer next to the breadboard where I was adjusting the kinematic mirrors by using both the target and the image on the screen. The phone camera captured the blue and red spots corresponding to each laser, that would turn into a white spot when collimated.

3.2.1.3. Beam expansion

The collimated light beam in the optical axis of the cage system now experiences an expansion phase. Originally, the red and blue beams generated by the laser diodes have a 1mm diameter. Wider beams are preferred to generate planes of light with smaller focal spot diameter (better spatial resolution).

Endless widening the beam is limited by several factors. Firstly, obeying distance requirements between expansion lenses conflicts with space restrictions in the optical breadboard. Secondly, the beam must be narrow enough to fit within the galvo mirrors' and the lenses' area. Severe distortions are caused by a beam that is wider than the optical components it interacts with. Finally, there is the depth of focus to account for. This parameter determines the effective field of view and is inversely proportional to the beam width. Large beam widths risk having a field of view that is too short.

The math behind Keplerian beam expansion is quite simple and usually covered in physics or optics courses. The diagram below illustrates this principle.

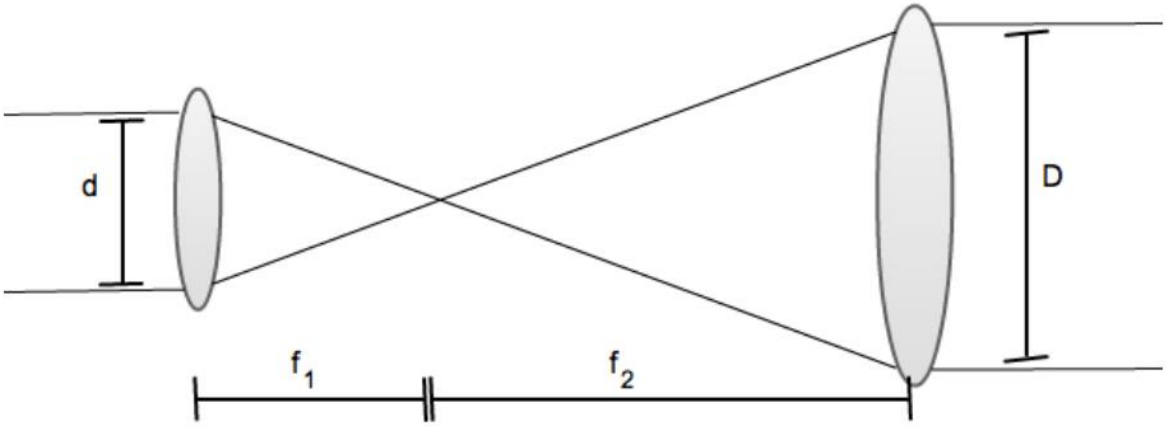

FIGURE 19. KEPLERIAN BEAM EXPANSION [74]

EQ. 2: BEAM EXPANSION MAGNIFICATION

$$\text{Magnification Power } = {}^{f_2}/_{f_1} = {}^{D}/_{d}$$

The plano-convex spherical lenses utilized have focal spots of f_1 = 30mm and f_2 = 150mm. The magnification power is 5, so an initial beam of 1mm in diameter will exit the second lens as a 5mm beam. The cage system requires a length of at least 180mm (plus an extra for the casing and mounting of the lenses) dedicated to beam expansion.

To check for correct beam expansion, the output beam diameter should be 5mm at the exit of the second lens and in the far field (at the 20-meter target, like the one used for collimation). If the diameter is not constant then there is a cone of light instead of a beam of light, and the focal distances should be properly readjusted.

3.2.1.4. Entering the Galvo

Before entering the galvo, two pieces of optical equipment are arranged in the cage system: a kinematic mirror and an electrically tunable lens (ETL).

A. Cage-mounted kinematic mirror

After expansion, this mirror directs the beam into the galvo; there are two purposes behind. The first concerns direction and space of the cage system. The galvo output is 90º with respect to the input. With this mirror at -90º (90º opposite direction), the directionality is maintained. This exploits the length of the table and not its width, allocating space for linear stages, camera rails, and to give the user room for sample preparation.

Apart from the spatial issue, which a fixed 45º mirror could solve, this kinematic mirror provides fine adjustments to ensure the collimated beam enters the galvo aligned with the optical axis. Arguably, this task is performed by the four kinematic mirrors that face the laser diodes. However, a kinematic mirror in this position removes the need of

adjusting alignment of each laser through the compact kinematic mirrors, a very laborious task that risks uncollimating the two beams.

B. First tunable lens (excitation light)

The role of this lens is to adjust the focal spot of the excitation laser so it lies just under the center of the objective lens. In theory, the job of this lens is not necessary if the three spherical lenses (two for beam expansion and one for focal spot focusing) and the objective are located exactly at ideal immutable distances.

Any person mounting the lenses in a cage system can rarely achieve the micrometer precision required by the microscope. Although minimal, there are also inherent deviations caused by machining imperfections of the optomechanical components. An ETL can correct for the differences in focal spot position by adjusting the current passing through the lens. This is done by the user from the software interface in the computer and requires a calibration step discussed later in the report.

Future development of the control software is planned to allow this lens to move the focal spot back and forth within the image plane. This aims to achieve higher and homogeneous spatial resolution in the whole x-y image plane.

C. Mirror Galvanometer (Galvo)

The galvo transforms the beam directionality from static to dynamic by allowing light to be focused independently in two orthogonal directions: up-and-down (Y) and left-to-right (X).

(i) Setting up the galvo

There are several considerations to account for when mounting the galvo. Advantageously, an adapter is used to mount it into the cage system, placing the galvo accurately with respect to the optical axis. Care must be taken when changing the frame to not damage the mirrors. Apart from this, there are inconveniences that have to be dealt with.

As mentioned earlier, the input and the output inlets (or ports) are oriented at 90º from each other. There is also height offset of 14.7mm between the inlets which changes the elevation of the optical plane with respect to the breadboard. These two are inherent characteristics of the galvo device due to the positioning requirements of the mirrors inside.

The galvo system relies on two driver cards that interface the electronics and the mechanics of the device. This poses another spatial limitation as each driver card heatsink covers a 12.5 x 12.5mm area of the optical breadboard. The galvo also comes with a bulky linear power supply with long cables that has to be put somewhere, but at least it is not fixed to the optical table.

The inlets of the galvo have directionality: one is for input (the lower one) and the other for output (the higher one). The software is designed to control the X and Y motors assuming this directionality.

(ii) Operation of the Galvo:

The motors of the galvo rotate to direct the beam in space. As said previously, the horizontal (X) and the vertical (Y) directions are perpendicular and independent. The applications of each are discussed below.

- Y motor: scanning the sample in the z direction

Regardless of the LSFM method that is being used (virtual lightsheet or planar lightsheet), movement of the lightsheet in the vertical direction is paramount for volume scanning. The Y position indicates the sample section (z coordinate in the image volume) being excited.

The whole volume of the sample is imaged, plane by plane, by moving the lightsheet up and down (rotating the Y mirror) in synchrony with the focal point of the second tunable lens (emission) in the camera turret. The image acquisition protocol and the role of the Y motor and the second tunable lens is detailed in *3.2.2.3 Second tunable lens (emission focusing)* where the control of the SPIM system is described.

- X motor:

(a) Virtual lightsheet, DSLM

A virtual lightsheet can be created by oscillating a beam of light at a very high frequency. No cylindrical lens is required to generate a virtual lightsheet. This approach is also considered LSFM, but it is different from SPIM.

Compared to SPIM, Digital Scanned Laser Light Sheet Microscopy (DSLM) also requires lateral (X) scanning, leading to longer acquisition times and greater phototoxicity. It poses a problem when stitching the images because the registration algorithms are not as simple. Since our sample does not rotate, removing shadow artifacts is impossible with DSLM.

An advantage of DSLM over SPIM is that it provides more homogeneous illumination than a static planar lightsheet, thus increasing the quantitative value of the images. A virtual lightsheet is also more efficient (>90%) compared to a true lightsheet (5%), so less powerful excitation lasers can be used. The scanning beam is not subjected to possible artifacts from the cylindrical lenses.

Fun fact! Removing the cylindrical lenses from this SPIM system is pretty straightforward, so it could easily be used for DSLM imaging. The software is designed to oscillate the beam in the X direction for pivoting (see below): this implemented oscillatory motion can be exploited to create virtual lightsheet scans.

(b) Lightsheet pivoting

SPIM can be implemented with a single-axis galvo (1D) or a dual-axis galvo (2D) but, in any case, necessitates of at least one cylindrical lens. The Y dimension is a must for volume scanning of the illumination plane, while the X direction is a highly-recommended enhancement. Especially in this system, movement in X plays a major role in improving the quality of the images when two cylindrical lenses are employed.

Oscillating in the X direction produces a non-static planar lightsheet with higher illumination homogeneity and increased shadow artifact correction. Pivoting is highly important in this system because the sample does not rotate (only linear stages are implemented). The figure below shows how pivoting can partly correct the stripes.

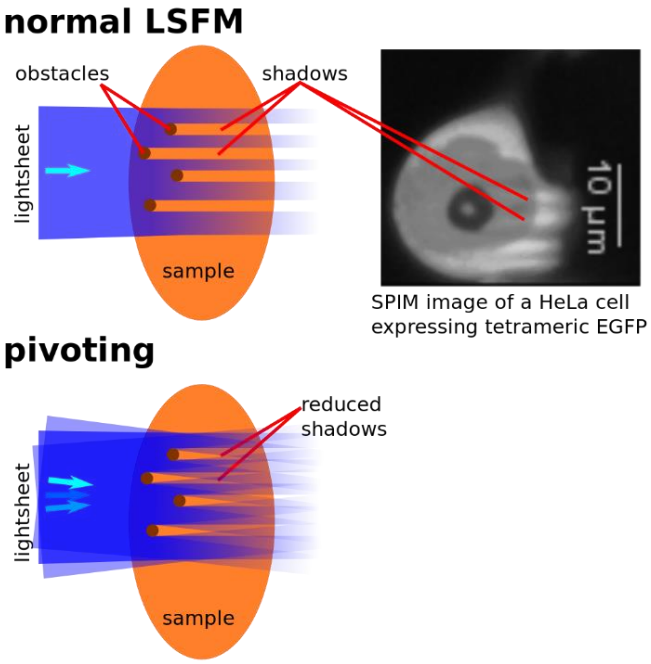

FIGURE 20. PIVOTING LIGHTSHEET DIAGRAM [75]

Many SPIM systems hold their sample in a rotary stage that can move 360º, producing images with minor shadow artifacts and minute illumination inhomogeneities. However, this leads to slower acquisition speed that would limit this microscope's applications in cell motion experiments, which are generally fast-changing phenomena.

On top of this, live cells are not welcoming to shear stress induced by fast rotation of the stage. If a microfluidic device with syringe pumps for medium renewal is used for cell culturing, rotation induces complex fluid inertia, apart from the motion restriction imposed by channels / tubes that connect to the microdevice.

The following table summarizes the possibilities of the system given the number of cylindrical lenses and the axes of galvo.

TABLE VII. LSFM TECHNIQUES: CYLINDRICAL LENSES AND GALVO AXIS

Num. of cylindrical lenses	0	0	1	1	2
Num. of galvo axes	1	2	1	2	2
DSLM	No	Yes	No	Yes	Yes
SPIM	No	No	Yes	Yes	Yes
Pivoting SPIM (no shadow artifacts)	No	No	No	No	Yes

Coordinate system

The coordinates being referred to can be somewhat confusing. This subsection aims to clarify what it's meant (spatially speaking) when referring to each of them.

The upper-case X and Y coordinates refer to the direction of the beam exiting the galvo. A change in X means a horizontal change in the laser beam direction, while a change in Y refers to variations of the beam vertically.

The X and Y coordinates for the galvo are not the same as the x, y and z coordinates of the image volume and linear stages. The table below shows the relationship between both coordinate systems.

TABLE VIII. GALVO, ETL AND LINEAR STAGE COORDINATES

Tunable lens focal depth (f_0)	Galvo horizontal steering (X)	Galvo vertical steering (Y)
↕	↕	↕
Linear stage in-out (x)	Linear stage left-right (y)	Linear stage up-down (z)

3.2.1.5. Lenses

The following lenses are set into the optical path defined by the cage system in the order they appear in the list. These lenses are encountered by the excitation beam after leaving the galvo and before arriving to the sample.

1. Generating the plane of light: 1st cylindrical lens

This round cylindrical lens generates a plane of light from a beam. Since it is a plano-convex lens, it has directionality. The beam enters the planar side and diverges into a plane when exiting at the convex surface. The focal length (50 mm) has to be selected so that the diverging beam does not widen too much, losing significant intensity (excitation power). This round lens is mounted in a rotation mount to control the orientation of the cylindrical surface and therefore the orientation of the plane.

Fun fact! When the cylindrical lens is not at an angle of π * *n*/2 (*n* natural number) the emerging plane is said to have an S shape.

2. Focusing on the sample: spherical lens

This spherical lens should have its focal spot (100mm) just below the objective. At the focal spot lies the minimal focal spot diameter of a Gaussian beam which is where the plane of light is thinnest. This lens cannot be placed with micrometer position, so the first tunable lens (mentioned earlier) is in charge of slight adjustments to the focal spot created by this lens.

3. Pivoting the lightsheet: 2nd cylindrical lens

Pivoting reduces stripes in the image arising from shadow artifacts. Without horizontal oscillation (for example, in a 1D galvo) there is no pivoting and this cylindrical lens would be unnecessary. Luckily, our system setup contains a dual-axis mirror galvanometer, so pivoting is implemented to produce images of higher quality.

The second plano-convex cylindrical lens has a focal length of 20mm and is fixed (unlike the first cylindrical lens). Similar to the cylindrical lens that precedes it, the planar side faces the beam, and the convex side faces the sample.

The X motor from the galvo oscillates the plane horizontally which causes it to pivot around an axis marked by the center of the cylindrical lens. The plane is redirected from different angles to the focal spot where the sample is located. This simulates a moving excitation light source that, although limited in angle range, strikes the sample from different viewpoints reducing shadows.

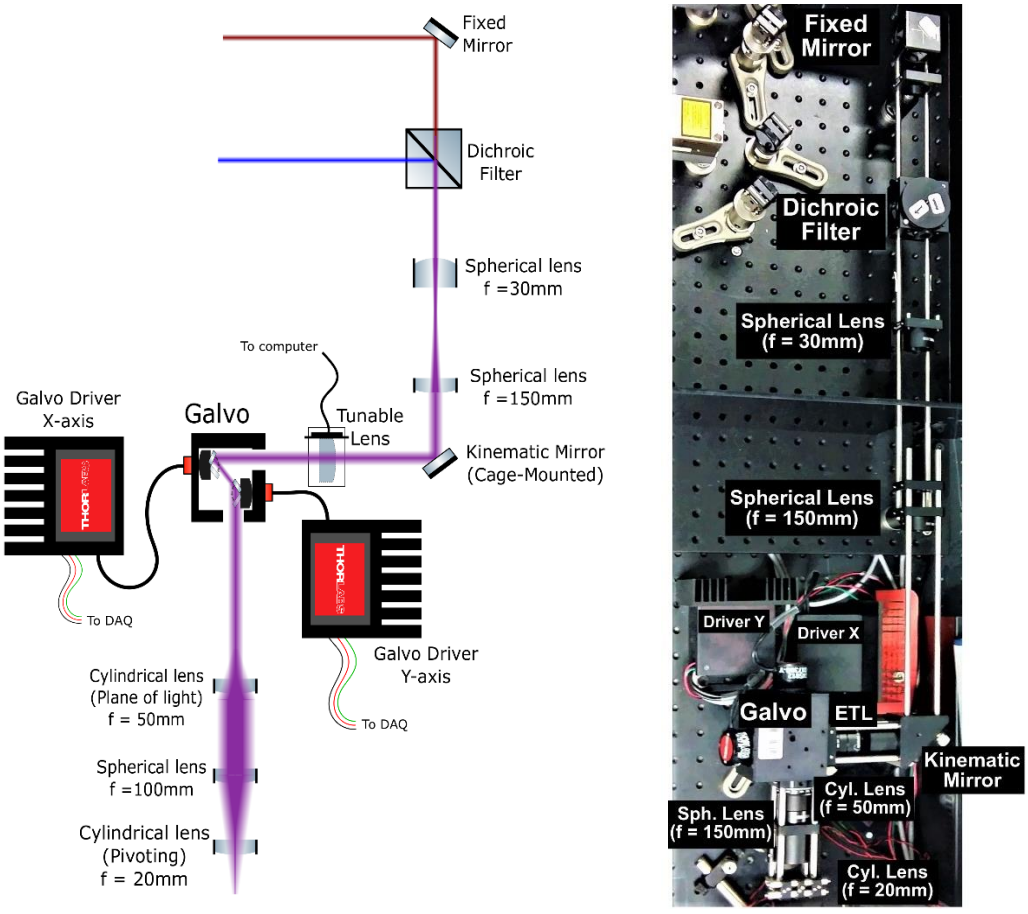

FIGURE 21. CAGE SYSTEM: BEAM EXPANSION, GALVO AND LENSES

3.2.1.6. Camera turret

In LSFM, the objective is oriented 90º with respect to the lightsheet to achieve a single in-focus excitation plane with maximum contrast and spatial resolution. The camera turret is supported upwards (vertically) by a long construction rail of 500mm. The rail, with the camera as the final element and the objective as the first, has several posts attached to rail clamps to support a lens tube system.

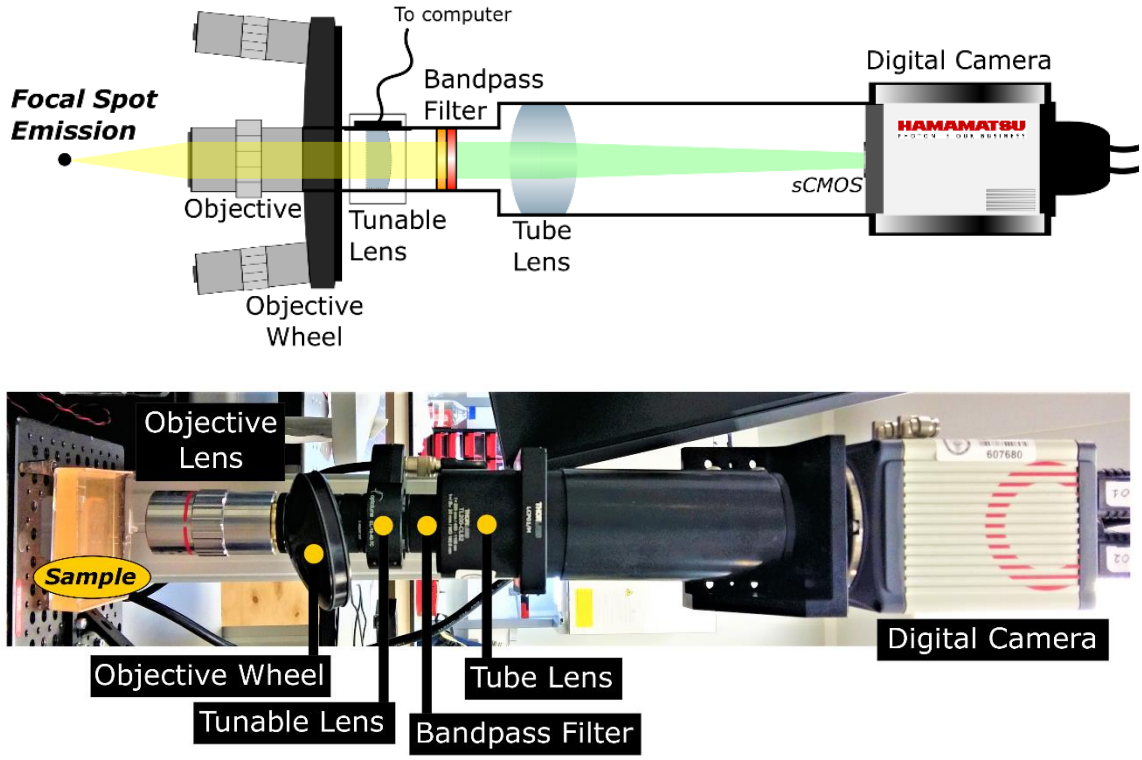

FIGURE 22. CAMERA TURRET

1. Tube system

The lens tube system carries the light from the objective to the sCMOS sensor in the camera. A series of extension tubes block the outside light from entering the optical path of the emitted light. These tubes are fitted with adapters to annex several optical elements. In sequence, as reached by the emitted light from the sample, these are: objective lens, objective wheel, second tunable lens (emission), bandpass emission filter, tube lens, and sCMOS pixel array sensor.

2. Objective lens and Infinity Space

The objective lens receives the emission light from the excited fluorophores in the sample. The image created by this light is enlarged by a magnification factor determined by the lens composing the objective. Parallel rays exit the objective forming what is called *infinity space*. Within the infinity space, optical components can be mounted to alter the properties of the emitted light while causing few aberrations.

Two objective lenses were bought for this system:

- 5x Air Plan Apochromat: 34mm working distance (WD), 0.14 numerical aperture (NA)
- 10x Water immersion Semiapochromat (fluorite): 3.5mm WD, 0.3 NA

This level of magnification has a large field of view and is adequate for cell tracking in migration experiments or for quickly navigating the sample in search of regions of interest. The purpose of this SPIM microscope is to image live cell which is why air and water objectives are preferable over oil.

Other objectives of higher magnification are available in the lab: 63x Water immersion and 40x and 50x Air. These should be used for traction force microscopy (TFM) imaging of single cells, pseudopods, and fluorescent beads embedded in the matrix.

3. Objective wheel

The objective wheel is a piece of optomechanical equipment that allows the user to easily switch between the objective lens being used. For example, a 5x objective could be used to navigate the sample in search of a region of interest. Once this region is centered in the image, a turn of the wheel allows switching to a 50x magnification objective and observe greater details. Navigating with a 50x objective is challenging because of the narrow field of view.

4. Second tunable lens (emission)

The second tunable lens enables dynamic adjustment of the focal distance of the objective. There are two important functions that arise from this property.

(1) Focus on the plane being selectively excited by the laser light. LSFM would not be possible without this tunable lens. The refocusing speed of the lens and the moving speed of the galvo will determine how fast the sample volume can be imaged. The control mechanism of how this lens works with the galvo is further described in section *3.2.2.5 Scanning the sample in the z direction*:.

(2) Adjust the parfocal and focal distances between different objectives. Although this should preferably be optomechanically adjusted, there is always some amount of focus error. This lens can adapt to the objective in use to focus it precisely.

5. Bandpass emission optical filter

A dual bandpass emission filter is used. The first bandpass is centered at 577nm with a bandwidth of 24nm, while the second is centered at 690nm with 50nm bandwidth. The passbands are selected to match the emission energies of the fluorophores in the sample, effectively erasing or diminishing noise from several sources, mainly excitation scatter and background illumination.

An emission filter significantly improves contrast-to-noise ratio (CNR) and signal-to-noise ratio (SNR), more so in a sensor that is not color sensitive. Using color pixel arrays would reduce spatial resolution (individual pixels are dedicated to each RGB color).

In future upgrades of the system, a manual or automatic filter wheel (similar to the objective wheel) could be implemented. This would allow to change between single bandpass filters of narrower bandwidth that are more specific to the fluorophore being excited.

6. Tube lens

Tube lens mark the end of the infinity space by focusing the parallel light rays into the sCMOS. The tube lens has a focal length of 200mm which establishes the fixed distance they should keep from the camera sensor.

7. Camera

The filtered and magnified emission photon flux from the sample is captured by the sCMOS pixel array sensors in the camera. The actual sensor is composed of two independent adjacent sensors for higher readout speed. Two Camera Link cables, one for each of those sensors, send the digital images to the computer where post-processing is applied to stitch them into a volume image.

3.2.1.7. Linear stages and Sample-holding platform

Three linear stages support the sample and allow it to be translated in three orthogonal independents directions. The mounting position of each motor and its movement direction are shown in the table below.

TABLE IX. MOVING DIRECTIONS OF MOUNTED STAGES

Linear stage position	Direction	Corresponds with
Lowermost	y (left-right)	Galvo X motor
Middle	x (in-out)	Tunable lens depth of focus
Uppermost	z (up-down)	Galvo Y motor
The directions are described with respect to the incident illumination plane.		

Linear stages are mounted on top of each other. When the lowermost stage moves, it drags with it the other two stages mounted on top of it. Likewise, the movement of the middle stage displaces the vertical stage (uppermost). The up and down movement of the last stage only affects the sample holder. Careful consideration has to be taken when calibrating the movement range of the motors as they do not only move the sample holder, but also each other.

The sample holder is a platform rigidly held by a right-angle adapter to the z motor. Its function is to support the cuvette and the microdevices. An opening exposes the sample to light coming from the LED.

3.2.1.8. LED circuit

The LED was constructed by soldering several electrical components into an electronic breadboard. The circuit schematic is shown in the figure below.

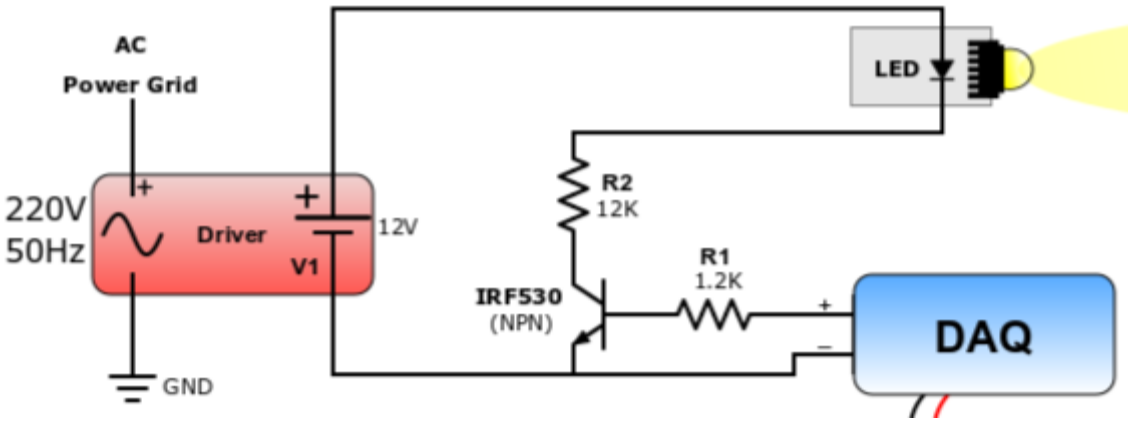

FIGURE 23. LED CIRCUIT DIAGRAM

Electronic elements:

- NPN Transistor: serves as an electronic switch that can be activated from the DAQ by a 5V digital output.
- LED: emits white light when a 12V current passes through it (electroluminescence).
- LED driver: converts the 220V 50Hz AC (alternating current) from the mains to a 12V DC (direct current) that powers the LED. It also regulates the power delivered to the LED by responding to the changing needs of the circuit. For example, it provides a constant quantity of power when temperature rises.
- Resistances: theoretically not required but may help protect the circuit in case of sudden high currents. The value of the resistance in series with the LED, R_2 = 12kΩ, also softens the intensity of the LED. If the light was too bright, another resistance could be soldered in series.
- Physical switch: the switch (not shown on the diagram) is connected with the AC supply to manually turn on or off the power to the LED.
- Cables: take electricity from one place to another, connecting the electrical components between themselves and with the power supply.

Non-electronic elements:

- Adapter: an optomechanical adapter connects the LED to lens tube system that shines the light under the objective.
- Heat sink: glued directly to the back of the LED by a thermally conductive adhesive. Enhances heat dissipation and prevents overheating of the diode.

- Spherical lens: cheap spherical lens diverges light and broadens the effective illumination area under the sample.
- Optical diffuser: scatters light to transmit soft light.
- Plastic case: protects the electronic components. Manual machining of the case is required to fit the breadboard inside. Pierced and polished openings are used to fix the switch (so it is connected to the circuit but can be pressed from the outside) and two screw terminals: one connecting to the mains and the other to the DAQ.

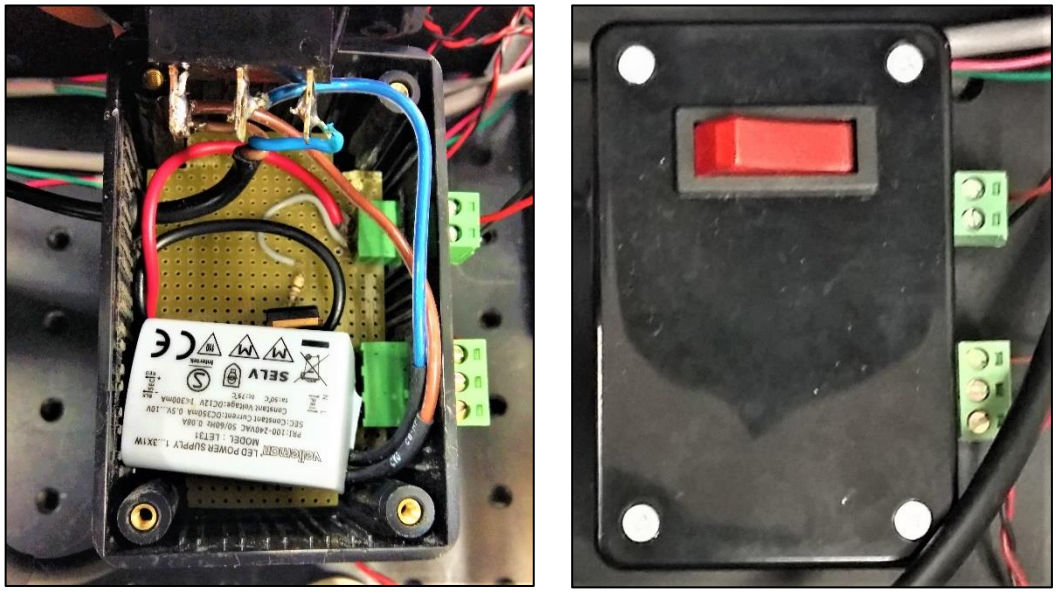

FIGURE 24. LED CIRCUIT CASE
Left: Case open; the soldered circuit can be seen inside. *Right*: Case closed; as seen from outside.

Fun fact! A blank piece of paper can be used as a diffuser; the paper fibers serve to scatter light.

3.2.1.9. DAQ connections

The DAQ has I/O (input/output) pins with different functions. Two pieces of equipment interface the computer through the DAQ: the mirror galvanometer and the LED. The rest of the equipment (camera, linear stages, tunable lenses) is directly connected to the computer.

A. Connecting the galvo:

In this microscope, the two driver cards from each axial galvo motor are connected to the DAQ by three cables:

- **Red cable** → carries the analog signal that controls the movement of the mirror from an AO pin to the magnetic motor. DAC transforms the digital signal that arrives from the computer to the analog signal that is sent to the galvo.
- **Black cable** → connects to a ground (GND) pin.
- **Green cable** → contains information from the capacitive position sensor and connects to an AI pin. At the AI pin, the signal undergoes ADC so it can be understood by the computer.

B. Connecting the LED:

The LED is also connected to the DAQ as shown in the diagram from Figure 23**.** The **red cable** carries a digital signal from a digital I/O pin to the transistor base (B). When the digital pin is set to High (1), the current flows from the collector (C) to the emitter (E) and the LED shines; the contrary occurs when the pin is Low (0). The **black cable** is connected to ground (GND).

3.2.1.10. Computer connections

Apart from the galvo and LED which connect to the DAQ, the rest of the electrical devices are directly connected to the computer. This includes:

- DAQ: connects to the computer via USB 3.0 port.
- Lasers: each connects via USB 2.0 port.
- Linear stages: connected to each other in sequence by a daisy chain which carries power and information. The first of these devices in the series connects to the computer by a single USB 2.0 port and to the mains electricity for power.
- Tunable lenses: connect to the computer via USB 3.0 port which powers and controls the lens.
- Camera: two Camera Link cables connect to the computer at two SDR ports.

3.2.1.11. Ergonomics

Ergonomics: The study of people's efficiency in their working environment.

The designer of a device has to account for the convenience of its operation in terms of hardware and software. During the design of the hardware there were several considerations taken to improve the user-friendliness of the microscope.

1. A completely opaque methacrylate box covers the lasers, kinematic mirrors and beam expansion. It serves the purposes of safety, aesthetics and protection of the aligned mirrors.

   There are openings in the box for:
   - The expanded beam to exit into the kinematic mirror cage mount.
   - Connecting the cables of the lasers to the power supply and the computer.
   - A ventilation grid to prevent overheating.

2. The height of the optical plane should be kept horizontal and levelled with the waist to prevent laser beams from reaching the eyes of the user and/or lab mates.

3. Distance from sample-holding platform and the objective can be adjusted thanks to the infinity space. It should be such that the objective lens does not risk crushing against the platform. Enough space for comfortable sample preparation, movement and focusing is desirable as well.

4. Linear stages have to be set so they occupy the minimum useful space within the breadboard. The zero-distance point (origin) of the stages should prevent the sample-holding platform from colliding against the second cylindrical lens, the LED tube system and the rail that supports the camera turret.

5. Non-optical component placement:

Non-optical components such as cables, DAQ, linear power suppliers, computer and screen have to be placed somewhere. The placement of these should be considered for convenience of space and usability.

i. A wooden platform under the optical workstation supports the computer. The dimensions (in millimeters) sent for fabrication are shown in the figure below.

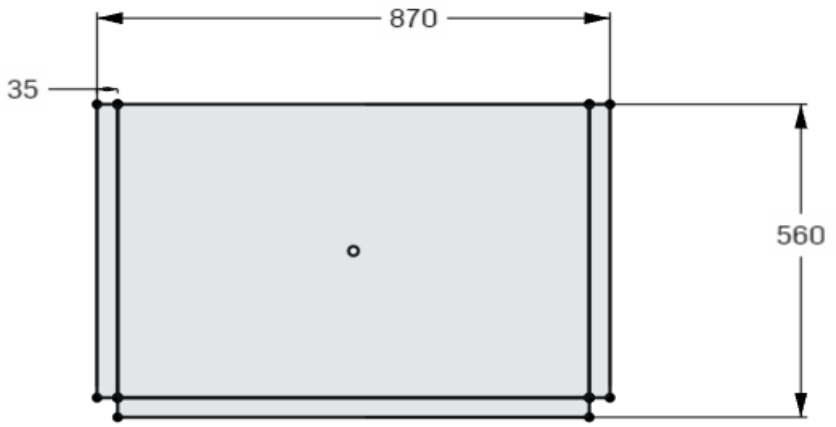

FIGURE 25. CAD DESIGN OF COMPUTER WOODEN BOARD

ii. A screen shelf attached to a 130mm mounting post holds the computer screen. The height and orientation are adjustable for both the screen and for the clamp fixing the shelf to the post. The combination of these can orient the screen in any direction and at heights for sitting down and standing up.

iii. The DAQ and linear power supplies are stacked from smallest to largest in the unused space behind the camera turret.

iv. Cables are hidden in the space between the main optical breadboard and the extension breadboard.

v. Two power strips, held by cable ties to the legs of the workstation, power the whole SPIM system. The main power strip (connected to the mains) has sockets with individual switches and labelled stickers: “Computer”, “Screen”, and “SPIM”. The secondary power strip feeds from the socket marked “SPIM” and connects all the electronic components that form the microscope. This allows the user to turn off the SPIM device without switching off the computer.

vi. In front of the sample holder there is just enough space for a small wireless keyboard (with mouse pad) that can be used to control the computer while being at distance to manipulate the sample.

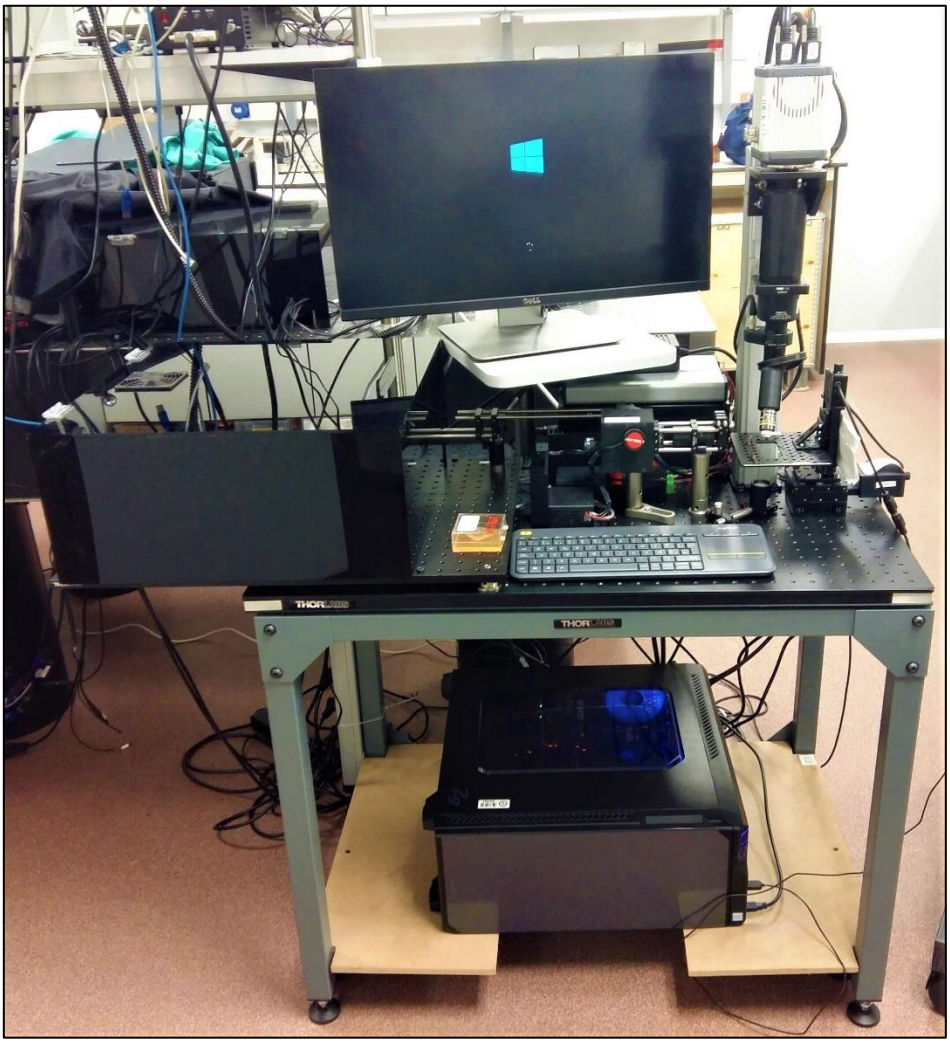

FIGURE 26. PHOTOGRAPH OF THE ASSEMBLED SPIM WORKSTATION

3.2.2. SPIM Control System

Now that the hardware composing the microscope has been described, it is time to elaborate on how it serves to acquire images in combination with the software. The events below enumerate the steps involved in this process and are illustrated in the control diagram in Figure 27**.**

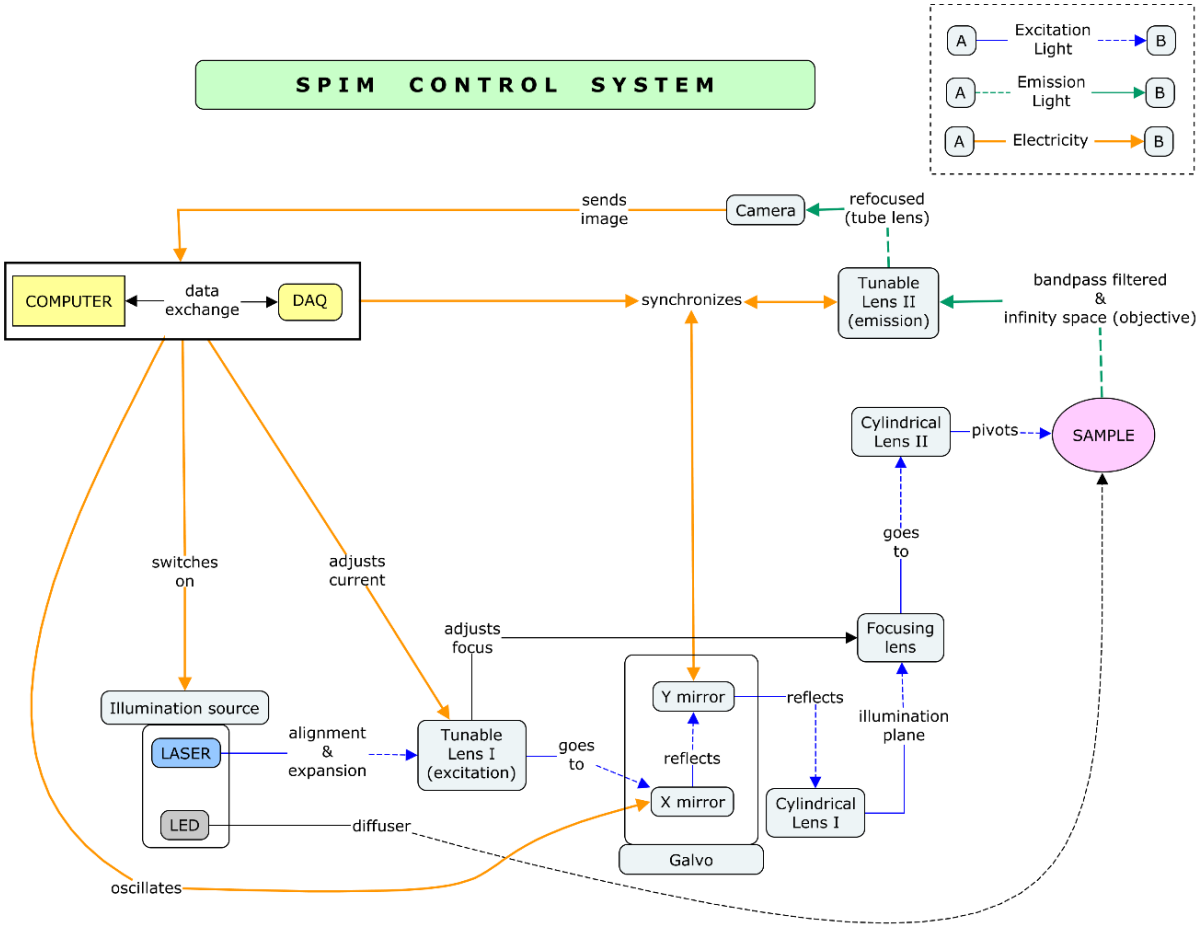

FIGURE 27. SPIM CONTROL SYSTEM DIAGRAM

It is not a sequential (in series) control process. Some of the steps are carried out simultaneously (in parallel) or back-and-forth. It is actually a feedback/feedforward system in which changing one of the steps may affect other processes in the control diagram.

3.2.2.1. Switch the illumination source on.

Illumination can either come from a laser (633nm or 488nm) or a white LED. If the white LED is switched on, then the sample is directly illuminated and only the processes in *3.2.2.3*, *3.2.2.4* and *3.2.2.7* apply. If instead a laser is switched on, the beam is expanded and converted into a plane of light which selectively illuminates a slice of the sample. In the case of lasers, more operation mechanisms apply.

3.2.2.2. First tunable lens (excitation focusing)

The slice of the sample being illuminated can be wider or narrower depending on the focal length of this tunable lens. When setting the focal spot directly under the objective, the focal spot diameter is minimum and the spatial resolution maximal. A narrower lightsheet is more selective and less blurry.

Note that this focal distance can change depending on the refractive index of the immersion medium (air, water, oil). Widefield illumination can also be obtained if the plane is focused as far away as possible (far field).

3.2.2.3. Second tunable lens (emission focusing)

The second tunable lens - placed in the infinity space between the objective and tunable lenses - affects the emitted light from the fluorophores or the scattered light from the LED. At this stage, current delivered to this lens can be adjusted to focus the image exactly on the slice being illuminated.

3.2.2.4. Moving the linear stages

Now that the sample is in focus, linear stages can translate the sample in the x, y, z space to find the region of interest (ROI). Note that changes in the z direction will change the slice being illuminated, while movements in the x and y directions occur within the same slice. During navigation with the linear stages, smaller binning and short exposure times in the camera are preferable to refresh the screen faster.

3.2.2.5. Scanning the sample in the z direction:

This is the basics of what SPIM is about. It relies on the synchronized action of the tunable lens and the galvo motor.

- Galvo Y-axis mirror motor: Directs the beam to shine a plane of light selectively at a given slice in z.
- Second tunable lens (emission focusing): Focuses the camera on the emission image given off by the fluorophores at the illuminated slice.

This synchronized movement is calculated by interpolation. The user manually defines initial, medial and final positions where the image is in focus. At these positions, the galvo Y-coordinate (angle in degrees) matches the z-coordinate focal point (current in milliamps) of the tunable lens. Quadratic interpolation on the Y and z coordinates defines the entire trajectory of the Y and z values for selective slice excitation and imaging.

Within the z scan trajectory, two parameters can be defined: the range $[z_{min},z_{max}]$, the number of differential steps *dz*, and the number of measurements per scan.

3.2.2.6. Galvo X motor oscillation

The X-axis of the galvo is set to oscillate sideways to homogenize illumination and reduce shadow artifacts. Several parameters control the oscillatory motion:

- Frequency: preferably high frequencies (100Hz) of oscillation.
- Range: the mirror is rotated between values of X belonging to the range [X_{min}, X_{max}].
- Waveform: the shape of the oscillation can be square, sinusoidal or triangular.

3.2.2.7. Capturing the image (Camera)

Some capabilities of the camera have already been described in *3.1.4 Digital sCMOS Camera*. Here, the parameters that can be controlled from the software interface are discussed:

a. Frames/Second (FPS)

Not controlled by the user but given as feedback to estimate the duration of a scan and keep track of the refreshing rate of the live image. Low FPS are preferred when manually navigating and focusing the sample so the live image display does not lag. FPS is equivalent to the sampling frequency. If the FPS rate matches or surpasses 2-times the speed of the oscillating galvo (Nyquist) sampling aberrations can be seen (aliasing).

b. Number of shots:

The final slice image will be an average of the number of shots taken of that slice. When increasing the number of shots, the FPS remain constant, but the acquisition time is longer.

c. Autoscale histogram:

Normalizing the intensity values comes in handy when navigating along the sample. Significant differences in brightness arise from varying concentrations of fluorophore, changes in background illumination, and when different light sources are used.

d. Binning:

A user-defined parameter $M = 2^{n-1}$ (n = 1, 2, 3…) determines an M×M binning. Binning does not affect the FPS. Binning can improve SNR when the signal is low at the expense of spatial resolution.

TABLE X. EFFECTS OF BINNING IN SPATIAL RESOLUTION AND MEMORY SIZE

Images of a USAF (U.S. Air Force) target were taken with a 5x Air objective and LED illumination. These targets are engraved with patters to calculate the planar resolving power of the system.

1x1 Binning	2x2 Binning	4x4 Binning
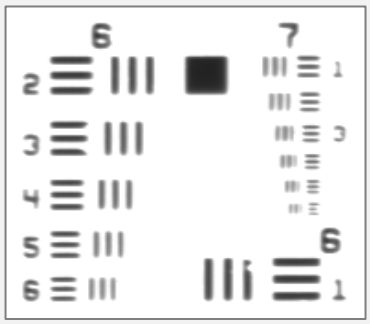	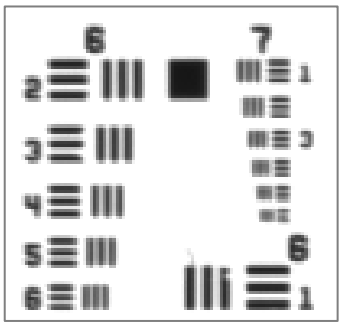	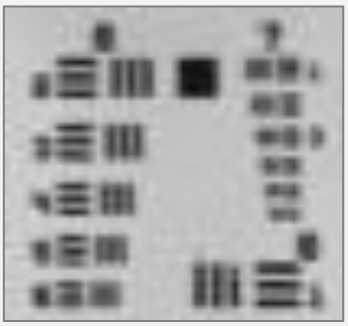
File size: 8MB	File size: 2MB	File size: 512KB

e. Exposure time:

The exposure time (in milliseconds) determines the amount of time in which the sensor receives photons. It is directly related to the FPS. Long exposure times can improve SNR when the signal is low at the expense of temporal resolution.

Binning and Exposure time: Binning is integration (summing) of the signal over space. Exposure is integration over time. If brightness is high, then large binning and long exposure times can saturate the image.

f. Image dimensions:

Sometimes measuring the entire field of view (FOV) is unnecessary. With certain objective lens (e.g.: non-planar), the exterior of the image appears distorted. The height and length (as a percentage) of the field of view can be restricted to avoid this.

g. Region of Interest (ROI):

Before the image is acquired, a ROI has to be defined within the field of view of the sensor. The ROI contains the part of the sample that is relevant to the user. A ROI smaller than the FOV enables faster image acquisition and requires less memory space in the computer.

3.2.2.8. Stitching

Stitching is a post-processing reconstruction algorithm performed by the software that builds the image volume from the acquired slices. It does this by knowing the position of each slice and performing a weighted average of the intensities of each pixel. There are other stitching options implemented such as the standard average or maximum intensity projection (MIP).

3.2.3. Software Calibration

To function, the code reads system-specific parameters from a folder containing text files. Software calibration is the final stage of the set-up and consists of modifying these text files so the parameter values match those of the equipment.

Fun fact! You can easily disrupt the software by modifying a file incorrectly. Having a backup copy of the folder containing the text files is highly recommended.

3.2.3.1. Software installation:

Installing the software is the first step in this process. The software that runs the control was provided by 4DNature (http://4dnature.eu/), the spin-off company of Dr. Jorge Ripoll. The code is based on LabVIEW and only installed in customized systems.

Since custom-made optical devices differ, there are specific parts of the code that must be readjusted during installation. The main code is quite generalized, so adjustments involve suppression of certain non-implemented functions. For example, a rotary motor or an automatic filter wheel are not included in this particular system, so the code in charge of operating them would be hidden or deleted.

It is advised to check the functioning of the software whenever parts of the original code are changed to prevent it from malfunctioning after the installation process is complete. Trying to detect a bug by tracing back the changes can be stressful and tiring.

3.2.3.2. Computer ports and DAQ pins

The DAQ and the computer interface with other electronics devices. For future troubleshooting, or if the SPIM workstation is relocated, it is important to document where and how each connection occurs.

Table XI and Table XII list the type of connection and the port / pin number. In the case of the computer, the text file storing the ports' information is mentioned. For the DAQ, the function of each pin is stated.

TABLE XI. COMPUTER CONNECTIONS

Computer Connections		
Element	Port	Text file
ETL Excitation Focus	COM5	*Opt3D_IllumFocus_Defaults*
633nm Laser	COM14	*Opt3D_LaserSelect_Defaults*
488nm Laser	COM13	*Opt3D_LaserSelect_Defaults*
LED	Dev2/port0/line1	*Opt3D_LaserSelect_Defaults*
Linear stage x	COM12::1	*Opt3D_Movement_Defaults*
Linear stage y	COM12::3	*Opt3D_Movement_Defaults*
Linear stage z	COM12::2	*Opt3D_Movement_Defaults*
ETL Emission Focus	COM3	*Opt3D_Defaults*

TABLE XII. DAQ PIN CONNECTIONS

DAQ Connections		
Connection	Pin	Function
LED black	82	D GND (Digital Ground)
LED red	66	P0.1 (Digital I/O)
Galvo X Black	16	AO GND (Analog Output Ground)
Galvo X Red	15	AO 0 (Analog Output)
Galvo X Green	16	AO GND
Galvo Y Black	32	AO GND
Galvo Y Red	31	AO 1
Galvo Y Green	32	AO GND

The function of each of the DAQ pins is listed on the cover behind the device. A picture of this reference list is available in Figure 85.

3.2.3.3. Stage motor positions

When the software is initiated the linear stages are sent to the zero-position which is the physical origin of the motors. This is required because, unlike the galvo motor, the linear stages have no capacitive sensor: they estimate the current position based on how much they have previously moved. Since the motors have no memory, the zero-reference point must be set when they are initiated.

Calibration of the motors involves finding the values of several important positions and saving them in the corresponding text files that are read by the software.

The file *Opt3D_Movement_Defaults* contains the data from the manufacturer like the step increment units of the motor. In this file, the maximum and the minimum thresholds for the range of movement of each stage can be modified.

In practice, the minimum threshold has no use in this setup because the software is started at zero (physical minimum). This requires careful design and placement of the stages and platform to prevent them from crashing against other hardware. The calibration of the maximum displacement value is important for this same reason.

Apart from the range of movement and the manufacturer's parameters, there are additional calibration values. Labelled buttons in the GUI can send the linear stages to the locations indicated by the following files:

- *Opt3D_origin*:

The software sends the motors to these x, y, z positions after the zero-reference point.

```
>> Stage Origin <<
==================
# X position (in mm)
22.2
# Y position (in mm)
20.3
# Z position (in mm)
4.3
```

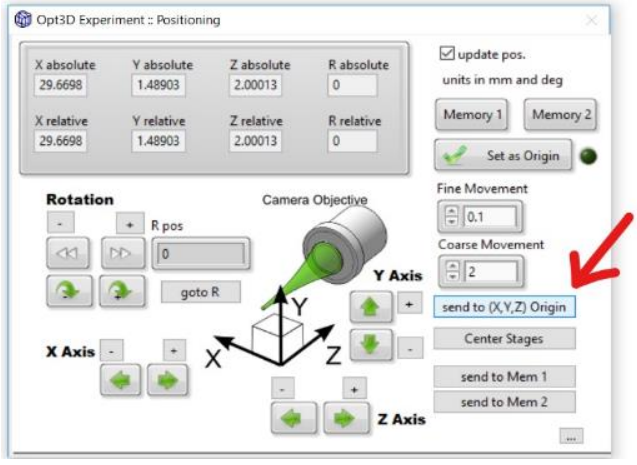

FIGURE 28. MOVE TO X, Y, Z ORIGIN GUI

- *Opt3D_center:*

Establishes the central position of the platform where the sample will be imaged. The center position puts the sample in focus under the objective.

```
>> Stage Center <<
==================
# X position (in mm)
15.3
# Y position (in mm)
20.3
# Z position (in mm)
4.3
```

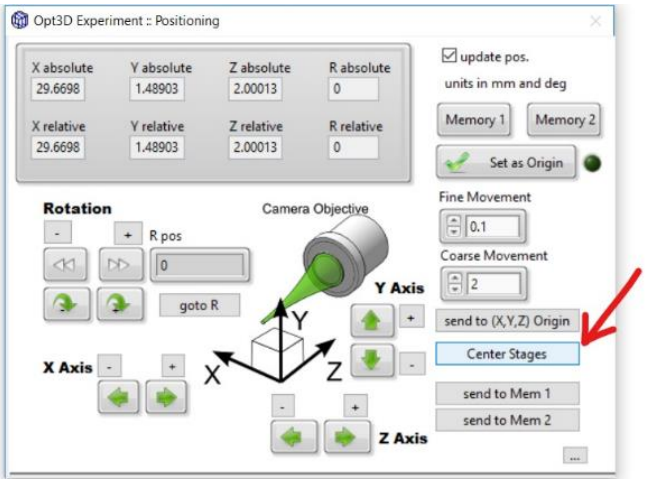

FIGURE 29. MOVE TO CENTER STAGES GUI

- *Opt3D_change_sample*:

The change sample button sends the platform to a comfortable position from where the sample can be changed or manipulated.

```
Change Sample action
--------------------
X position
35.5
Y position
0
Z position
115
```

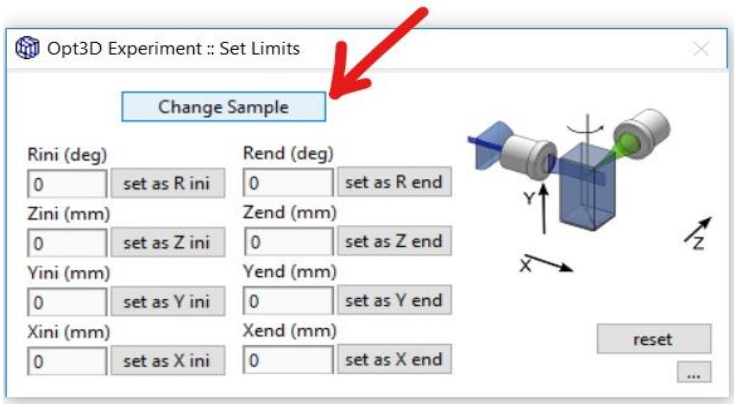

FIGURE 30. CHANGE SAMPLE GUI

3.2.3.4. Tunable lens

As mentioned, this microscope implements two ETLs for variations in the focal length of the illumination and of the objective.

1. Focusing the beam:

The default focus of the first tunable lens is dictated by the file *Opt3D_IllumFocus_Defaults*.

```
== Laser Select Defaults ==
============================
...
# Media for correction
Oil,Water,WideBeam          ←          (1)
...
# Laser Name
488 [Toptica]               ←          (2)
# Laser Wavelength (nm)
488
#Focus Address (optotune position):
0.0,105,299.0               ←          (3)
...
# Laser Name
633 [Toptica]               ←          (4)
# Laser Wavelength (nm)
633
#Focus Address (optotune position):
0.0,105,299.0               ←          (5)
```

(1) This line of code creates a list of different focusing options which will become available as a dropdown menu in the GUI. These can correspond to imaging specifications (e.g.: widefield) or immersion media corrections (e.g.: oil, water).

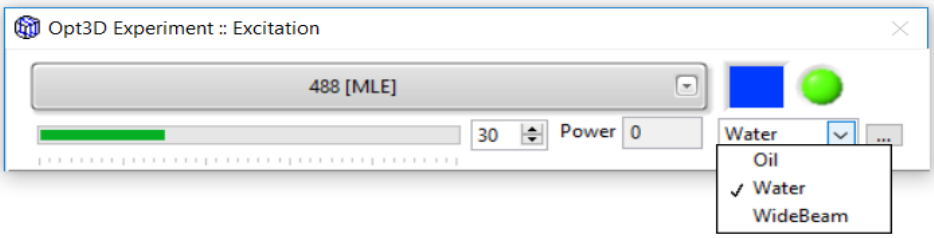

FIGURE 31. MEDIA FOR CORRECTION MENU

(2) and **(4)** The Laser Name identifies each laser. When that specific laser is switched on, the calibrated focus position will be automatically applied.

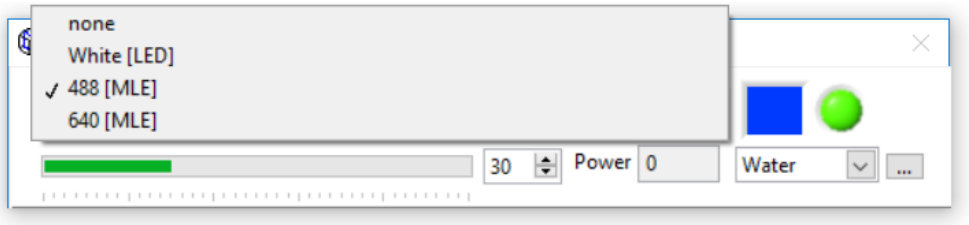

FIGURE 32. ILLUMINATION SOURCE MENU

(3) and **(5)** The Focus Address specifies the amount of focusing of the lens. The order of the numbers in the list corresponds to the focusing options from **(1)**. Different media will require different adjustments. The numbers must be empirically determined by imaging the laser beam in a soluble fluorophore medium.

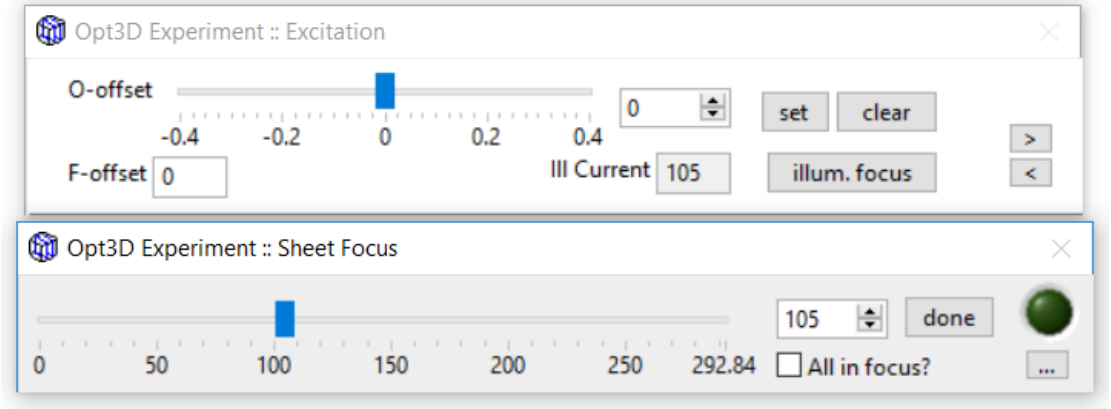

FIGURE 33. ILLUMINATION FOCUS MENU

2. Focusing the image:

Opt3D_Defaults is the core text file which contains information about more comprehensive aspects of the system such as the number and types of cameras and some parameters regarding the galvo.

```
>> OPT3D DEFAULTS <<
==================
...
# Optotune com port? (or none)
COM3                          ←              (1)
...
# Optotune center, min, max (mA):
177.5,100.0,300.0             ←              (2)
...
```

The lines above specifically relate to the second tunable lens which is designed to focus the image.

(1) Established the port where the lens connects to.

(2) Establishes the current range (in milliamps) around which the user can play to focus the sample and perform the interpolation algorithm to run a SPIM scan. The center value will be the default focus position. The minimum and the maximum establish the range [min, max] available in the scroll bar displayed in the GUI. There is also an input option which accepts values outside this range from -300 to 300, although using negative numbers is not recommended.

FIGURE 34. FOCUS POSITION AND SHEET DISPLACMEMENT MENU

3.2.3.5. Characterizing the system

Characterizing the system involves finding several dimensionless numbers, such as the magnification, and other numbers with dimensionality like the spatial resolution. The quality and capabilities of an optical system are defined by these parameters.

Fun fact! Microscopes, like cars (e.g.: horsepower) or printers (e.g.: dots-per-inch), have properties that are quite important to its buyers and must be given together with the product.

1. Magnification and Pixel size

Although manufacturers sell objectives labelled by magnification, the theoretical values provided are never exact. An important part in characterizing the system is finding the magnification. This allows to calculate the pixel size in the image plane, quite important to know the real size of the objects being viewed.

Calculating the magnification is a relatively simple mathematical problem:

- The laser beam is first focused and a snapshot is taken.
- Then, the galvo is turned a known angle (α) and a second snapshot of the beam is acquired. The displacement (d) of the beam in units of length is calculated by trigonometry (see Figure 35 below).
- Now, the number of pixels from the center of one beam to the other are measured. The ratio between the displacement of the beam and the size of the CMOS pixels reveals the magnification (M).

EQ. 3: OBJECTIVE LENS MAGNIFICATION

MAGNIFICATION

CMOS pixel size: 6.5µm

Focal Distance : 10mm

$$M = \frac{6.5\mu m \cdot \#\ pixels}{d}$$

$$d = f \cdot \tan(\alpha)$$

FIGURE 35. FINDING THE MAGNIFICATION

Once the magnification for an objective is found, the value is saved to the text file *Opt3D_Objective_Defaults*. The table below shows the values obtained for the current objectives.

TABLE XIII. OBJECTIVE LENSES MAGNIFICATION

Objective	Angle α (degrees)	# pixels	M	Pixel size (µm)
5x Air	0.40000±0.0009	563	5.241±0.001	1.2402±0.0002
10x Water	0.40000±0.0009	997	9.286±0.001	0.7000±0.0002

2. PSF and Spatial Resolution

Calculation of the point-spread function (PSF) and axial spatial resolution were performed with the 5x air objective. The procedure is standard and can be reapplied to other systems and objectives.

The point-spread function describes the response of an imaging system to an impulse function (delta). The PSF acts on the signal by convolution, and its effects are similar to those of gaussian blurring in image processing.

Finding the PSF is important in determining the resolution of the system. Also, it allows application of deconvolution algorithms that improve the sharpness of fluorescent images.

To simulate an impulse in these systems, fluorescent beads of 0.5μm are imaged. The beads were embedded in a rigid PDMS gel during synthesis; PDMS rigidity can be modified according to the concentrations of crosslinker. The number of beads has to be kept low to avoid aggregation and overlap between the signals coming from them.

Once an image of the gel is acquired, beads will show as intensity balls. Note that the size of the bead is smaller than the size of the pixel in the image plane, so theoretically a bead should correspond to a single pixel in the image (an impulse). The x, y and z intensity profiles of the bead are extracted and plotted. Fitting Gaussian curves to the profiles obtained reveals the three-dimensional PSF.

In reality, the bead profiles are Airy functions, but the center of an Airy function can be fit by a Gaussian. Following the Rayleigh criterion, the spatial resolution corresponds to the FWHM (full width at half maximum) of an Airy function. The FWHM is extracted from the PSF in each axial direction. The number of pixels in the FWHM is multiplied by the pixel size to obtain the spatial resolution in micrometers.

The table below shows the PSF for a single bead. However, beads are not perfectly round: small differences are expected from bead to bead. To be rigorous, statistical analysis should be performed to the profiles obtained from several beads. Doing this shows the resolution in x and y to be isotropic, while being anisotropic in z. This relation in the PSF is a common characteristic of SPIM microscopes.

TABLE XIV. POINT-SPREAD FUNCTION AND RESOLUTION

x	y	z
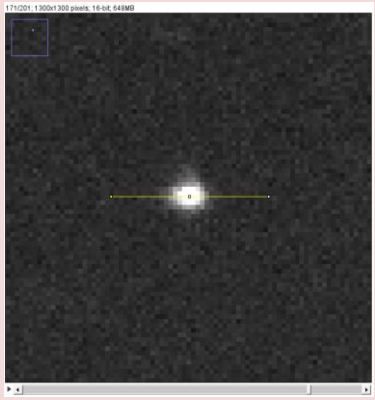 FIGURE 36. BEAD IMAGE: X PROFILE	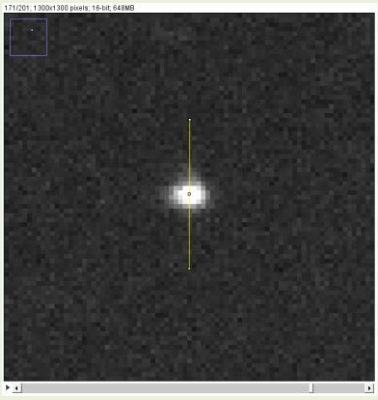 FIGURE 37. BEAD IMAGE: Y PROFILE	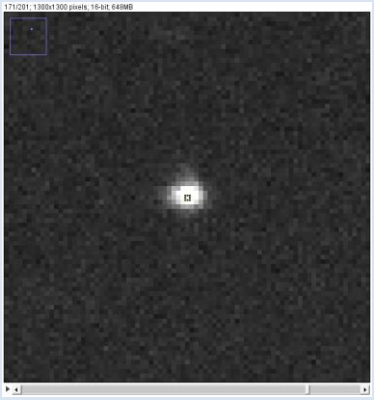 FIGURE 38. BEAD IMAGE: Z PROFILE
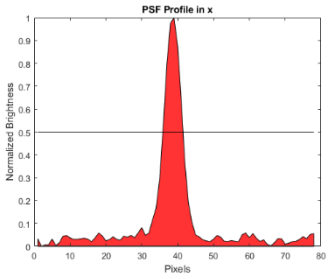 FIGURE 39. BEAD PROFILE IN X	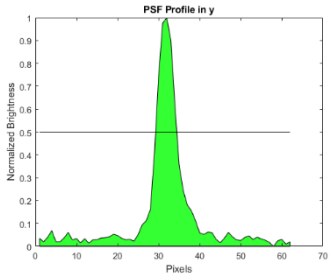 FIGURE 40. BEAD PROFILE IN Y	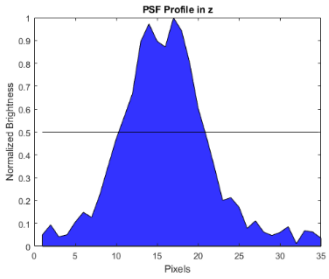 FIGURE 41. BEAD PROFILE IN Z
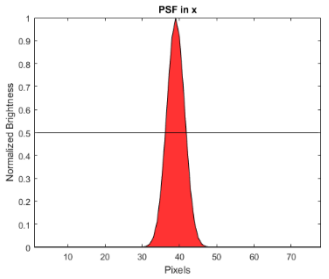 FIGURE 42. PSF IN X	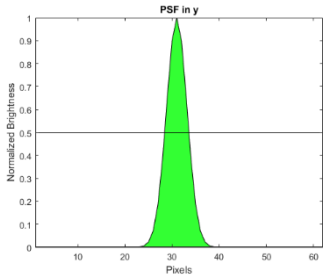 FIGURE 43. PSF IN Y	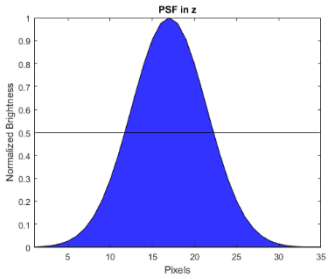 FIGURE 44. PSF IN Z
Sigma PSF: 2.39	Sigma PSF: 2.18	Sigma PSF: 4.47
FWHM: 5.4907	FWHM: 5.0350	FWHM: 10.5388
x resolution: 6.81µm	y resolution: 6.24µm	z resolution: 13.07µm

A simple MATLAB code in the Annex outlines the mathematical operations involved in calculating the values in this table from the intensity profile of a single bead.

3. Spatial Resolution with USAF target

Spoiler: US Air Force targets have nothing to do with the military. It is an optical tool used to measure spatial resolution (resolving power) in two directions by having a pattern of labelled lines which gets smaller and smaller. The smallest one that can be distinguished corresponds to the spatial resolution.

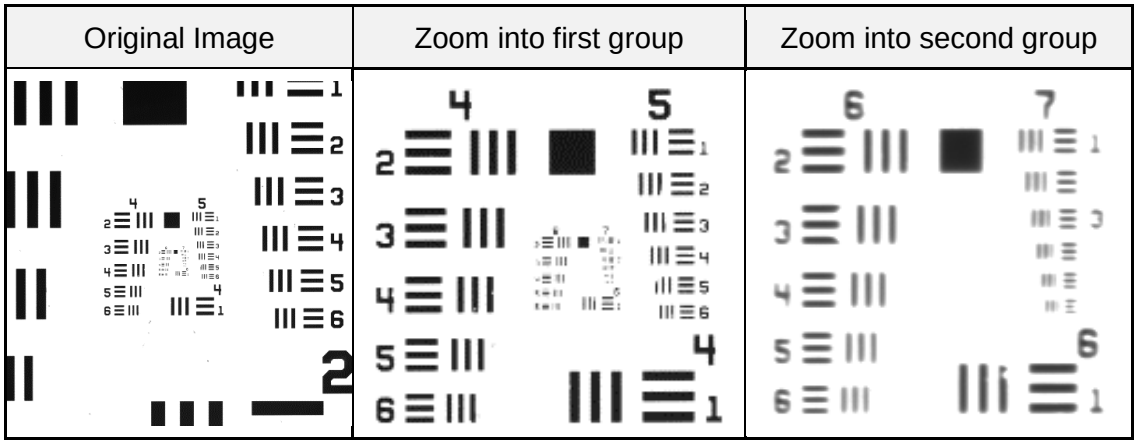

FIGURE 45. USAF TARGET AND RESOLVING POWER

The lines in Group 7 up to Element 5 can still be distinguished with clarity, but the pattern in Element 6 of that same group is diffused. The resolution of our system corresponds to that defined by Group 7 Element 5 which is 203.0 lines / mm, and each line 2.46μm in width. Hence, the resolving power is 2.46μm.

The spatial resolution given by this approach is completely planar, compared to that of the PSF which is three dimensional. The differences in the values obtained are due to the "integration" of signal coming from the depth of field of the objective lens when comparing planar and volume structures.

4. Field of view (FOV)

Knowing the pixel size in the image plane and the number of pixels in the sensor, the x-y field of view can be calculated:

EQ. 4: FIELD OF VIEW

$$\text{FOV} = \text{pixel size} \times \#\ \text{pixels in sensor}$$

$$\text{FOV} = 1.240\mu\text{m/pixel} \cdot 2048\ \text{pixels} = 2539.52\mu\text{m}$$

The field of view of the image plane is slightly over 2.5-by-2.5mm and symmetrical since the sensor has a squared shape.

5. Beam waist and Focal depth

The beam waist is closely related to the spatial resolution in z and is commonly calculated when characterizing the microscope. The beam waist is equivalent to the diameter of the focal spot. Although it can theoretically be estimated, the way to accurately determine it is empirical. In this report, both approaches are shown and compared.

The focal depth is the length along which the beam waist is minimum. This determines the effective field of view, where resolution in z is constant.

a. Theoretical Beam Waist and Focal Depth

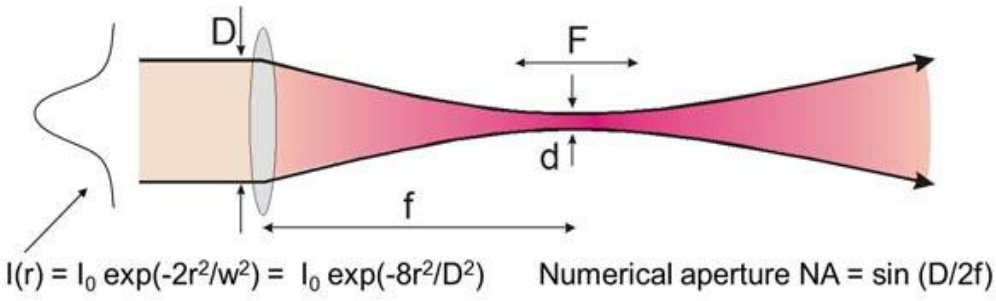

For a Gaussian laser beam:

Diameter of the focal spot

$$d = \frac{4 \cdot f}{\pi \cdot D} \lambda \cong \frac{2 \cdot \lambda}{\pi \cdot NA}$$

Focal depth

$$F = \frac{8 \cdot f^2}{\pi \cdot D^2} \lambda \cong \frac{2 \cdot \lambda}{\pi \cdot NA^2}$$

FIGURE 46. FOCUSING OF A GAUSSIAN BEAM [76]

EQ. 5: DIAMETER OF THE FOCAL SPOT

$$\mathrm{d} = 4 \cdot f \cdot \lambda / (\pi \cdot \mathrm{D})$$

EQ. 6: FOCAL DEPTH

$$\mathrm{F} = 8 \cdot f^2 \cdot \lambda / (\pi \cdot \mathrm{D}^2)$$

By following the diagram and the equations listed above, with the system's beam diameter (D = 5mm) and focal distance (f = 100mm), then:

For λ = 488nm: d_{488nm} = 12.4 µm F_{488nm} = 497.1 µm

For λ = 633nm: d_{633nm} = 16.1 µm F_{633nm} = 644.8 µm

The calculations do not account for effects such as the change in propagation medium. The simple application of the formulae above only suffices as approximations of the real values in the system. In a conservative way, the depth of focus can be said to be 500µm.

The depth of focus is 5 times smaller than the FOV. This indicates that, when acquiring images with the 5x objective lens, it is recommended to use a ROI of 500-by-500µm (400-by-400 pixels). Images can be obtained outside this range but the resolution in z will be worse and non-constant. For objectives of high magnification (50x) the depth of focus will be larger than the field of view, so this issue is negligible.

b. Empirical Beam Waist

The correct way to determine the beam waist is by finding the FWHM from acquired images. Beams of low power (10mW) avoid saturating the sensor or the fluorophore. When too powerful beams are used the FWHM widens giving incorrect results.

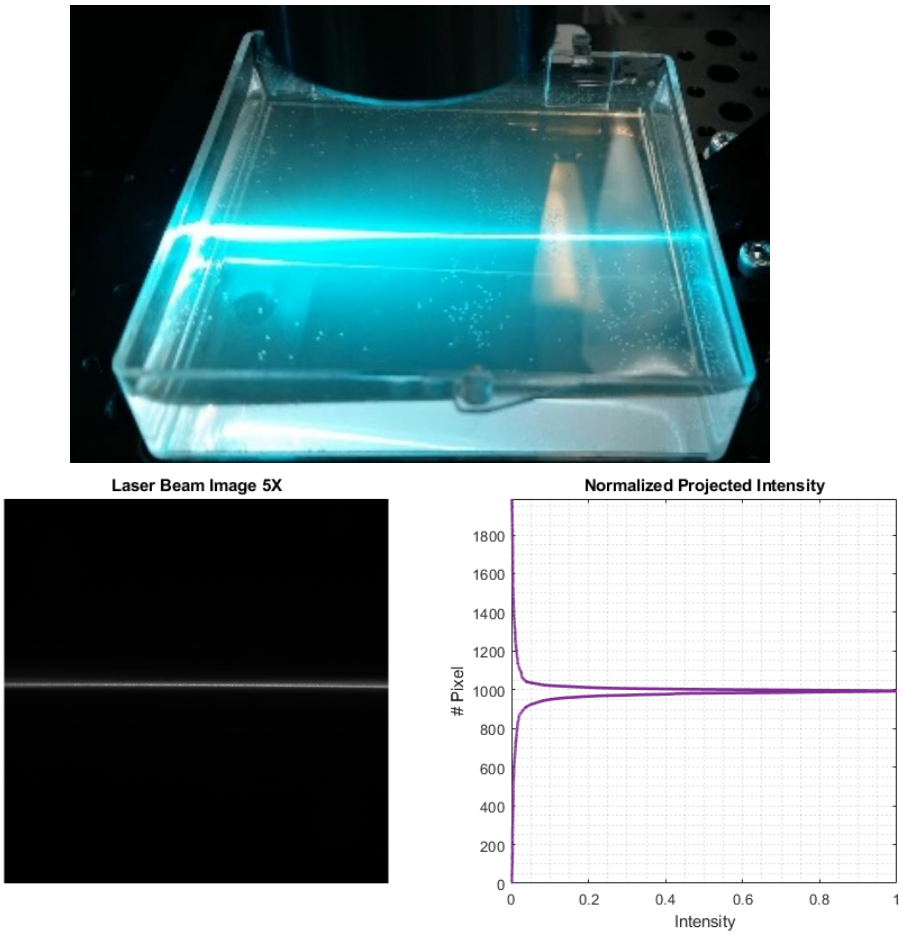

FIGURE 47. LASER BEAM:
Top: Physical image of laser beam traversing the fluorophore solution. *Bottom left*: Laser beam image acquired by the system. *Bottom right*: The projection profile of the image.

Along the entire image:

FWHM = 19.9913
Beam waist = 24.789µm

Within the depth of field (~500 pixels):

FWHM = 15.2626
Beam waist = 18.926µm

Additional note: When the power of the laser is increased, there is a non-linear relationship between the beam waist (FWHM) and the intensity (mWatts). This relationship is due to the saturation of fluorophores as shown in Figure 48 below.

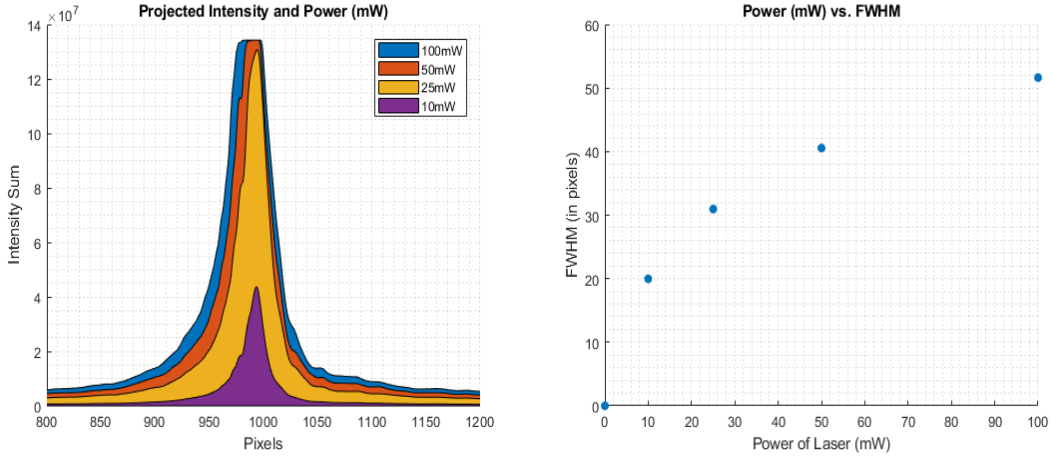

FIGURE 48. LASER BEAM POWER:

Left: Projected intensity profile for a given beam power (mW). *Right*: Beam power against FWHM of the projected intensity profile.

Additional figures showing the intensity projections of 10, 25, 50 and 100mW are attached in Figure 86 in the Annex.

3.2.4. Timeline

The timeline on the next page (Figure 49) shows estimated time requirements for each setup stage. It also serves as a schematic of the assembly process.

As mentioned in [77], a SPIM microscope takes a person skilled in optical equipment about one month to build. For a beginner, this process has taken an approximate 200 days (part-time). However, this is an unfair measure since not all of the equipment was available from the start. Orders of parts could take up to a couple of weeks to be processed and delivered. Hence, if the time dedicated to writing the thesis is removed and a step-by-step guidebook is available, an undergraduate student should be able to assemble a SPIM microscope in no longer than 100 full-time work days.

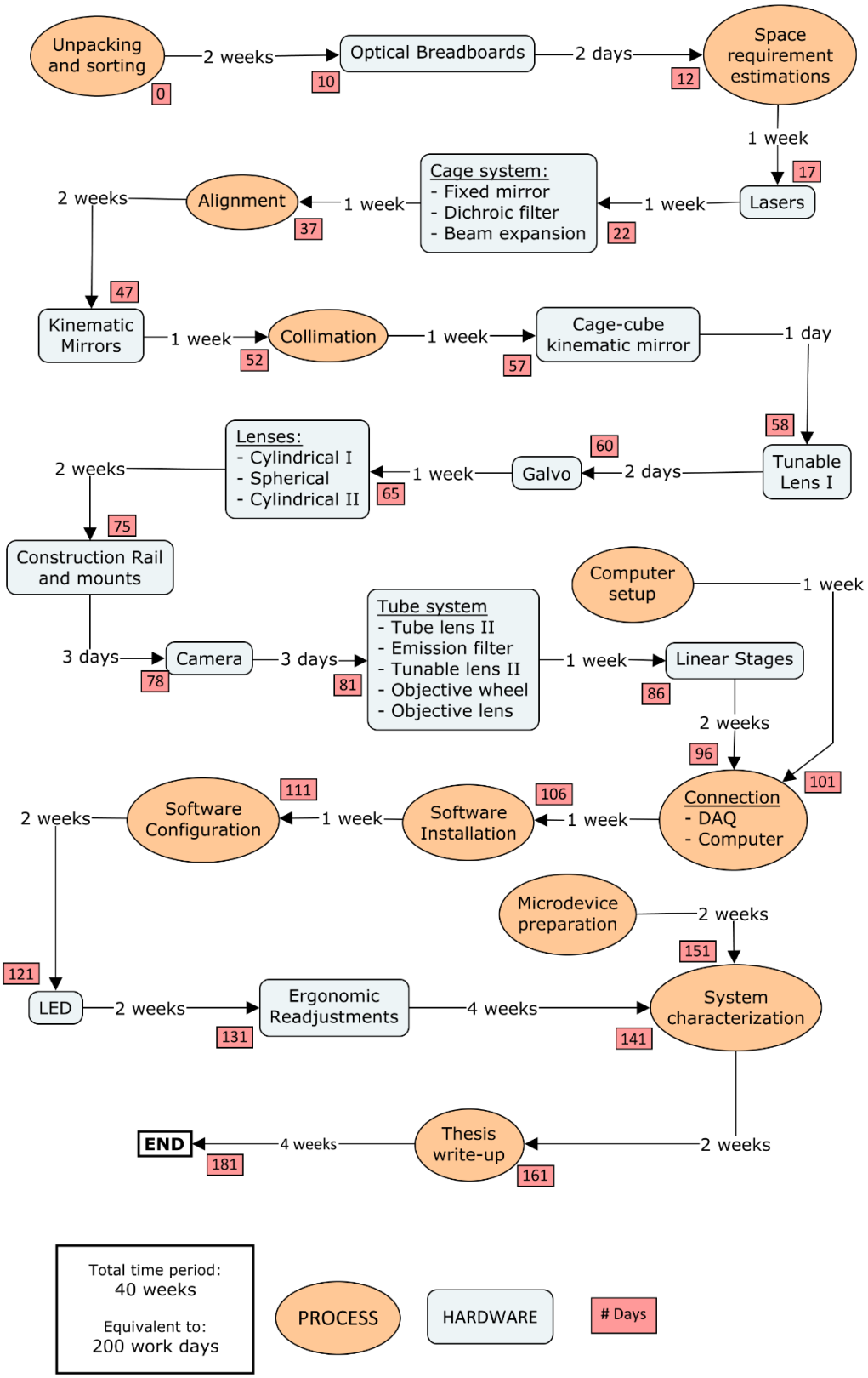

FIGURE 49. TIMELINE OF THE PROJECT:

All the steps shown in this diagram have been carried out by Ignacio Albert Smet (undergraduate) with the exception of *Microdevice Preparation* by Mario González Arjona and *Software Installation* by Dr. Jorge Ripoll. All the work prior to *Unpacking and Sorting* was done by Dr. Arrate Muñoz-Barrutia and Dr. Jorge Ripoll. The general workflow followed broadly the protocol described in [77].

3.3. SAMPLE PREPARATION

3.3.1. PDMS microfluidic devices

Microdevices, also known as bioMEMS, have become increasingly popular as a means for cell culturing. Most are made from PDMS because it is a cheap, optically transparent well-studied biocompatible polymer. Those bioMEMS that contain microchannels are named “microfluidic devices”.

Microchannels are characterized by having laminar flow which is controllable and predictable. The microdevice our research group employs for TFM experiments is shown in Figure 50**.** Two lateral channels surround the loading channel and keep the cells alive by circulating medium and removing waste products. Solutes are exchanged by diffusion gradient, and not by the drag of the fluid. This prevents fluid forces from disturbing cell traction forces and/or their measurement.

Microfluidic devices enable finer control over the delivered medium. Also, lower reagent needs results in more economical experiments than those carried out on a Petri dish or culture well.

3.3.2. Manufacturing procedure of microdevices

Microdevices are created by casting polydimethylsiloxane (PDMS) on a master silicon wafer with the desired pattern. Silicon master molds are microfabricated in clean room facilities by photolithography, the same manufacturing process as integrated circuits.

Liquid sylgard and a curing agent are poured into the mold and cured by organometallic crosslinking to give an optically transparent elastomeric polymer: PDMS. During the following procedure [78], chemical gloves are required for safety:

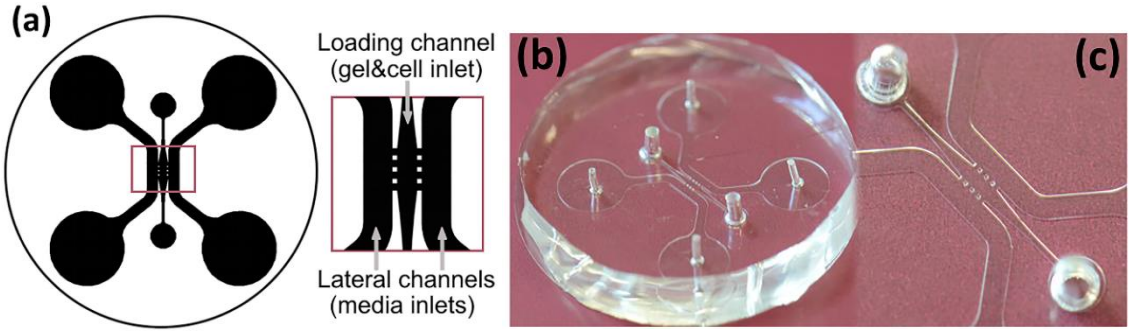

FIGURE 50. MICROFLUIDIC DEVICE FROM [79].
(a) Device architecture. (b) Cast PDMS microdevice. (c) View of the mold.

1. Take the master silicon wafer with the microdevice design. The architecture consists of two microchannels that flow parallel to the sides of the cell culturing channel (see Figure 50).

2. Prepare the PDMS chemicals: sylgard polymer base and curing agent in a 10:1 ratio. Typically, 60.0g of Sylgard polymer and 6.0g of curing agent is enough to make a few devices.
3. Air bubbles trapped during the mixing of the viscous chemicals degrade the optical qualities of cured PDMS and must be removed. These bubbles eventually rise to the top of the liquid, where blowing across the surface will break them.

   Vacuum is a simple and faster way of removing the bubbles from the PDMS. Applying a vacuum while mixing the PDMS can be done by connecting the mixing cup to a vacuum mixer for 10 min.
4. PDMS is cast into the wafer by confining it within a methacrylate or 3D printed open container (see Figure 51 below).

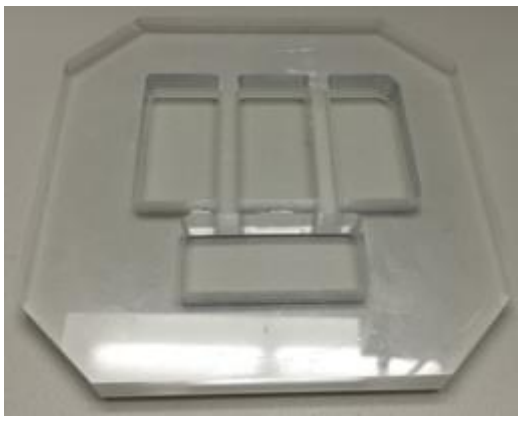

FIGURE 51. CASTING CONTAINER

Fun fact! Another option is to create a "wall" around the wafer with wrinkled aluminum foil. This is good enough for confocal or widefield microscopy, but *terrible* for SPIM because light enters laterally into the microdevice through a rugged surface. The plane of light would be deformed and scattered.

5. After the PDMS is casted on the wafer, it is cured in an oven at 70ºC for 60 min. Then allowed to cool for 4-5 minutes and removed from the wafer.
6. Undesired areas can be removed with a cutter or scissors.
7. In order to create the channels of the patterns, a glass coverslip needs to be chemically bonded to the PDMS by oxygen plasma treatment. Before the treatment, the surfaces of PDMS and the coverslips are cleared from impurities with tape.
8. Both PDMS and coverslips are placed into an O_2 plasma chamber for 3 minutes at a pressure of 300 milliTorr, after which treated surfaces are put in contact.
9. Finally, the devices are placed in an oven for 2 hours at 80ºC. Then, they are taken out and light weight is applied against them for 12 hours to ensure perfect binding.

3.3.3. Seeding the cells

According to [79], cells should be seeded in the following way:

- Seed cells in a medium made of Dulbecco's Modified Eagle Medium (DMEM) + 10% fetal bovine serum (FBS) + 1% Antibiotic-Antimycotic solution
- Incubate at 37ºC and 5% CO_2 for 2 days.
- The third day, detach the cells and mix them with collagen. First, mix all the components that are not collagen. This avoids fluctuations of pH that may damage the collagen. These components are:
  - 128µL of collage (3.43g/mL)
  - 20µL phosphate buffered saline (PBS) 10X
  - 45µL H_2O MilliQ
  - 7µL NaOH 0.5N (mol/L) to attain a 7pH neutral environment.
- From the 200µL of the collagen mixture, 100µL will be used to place the cells (around 100.000 of them).
- Take 5µL of the collagen-cell mixture can be seeded into the microdevice at the loading channel. DMEM is then added through the auxiliary channels.
- Incubate at 37ºC and 5% CO_2 for 2 hours to allow the cells to attach to the collagen matrix.
- Place the sample under the microscope for image acquisition.

3.3.4. Sample preparation for SPIM imaging

Once the cells are seeded with collagen into the microdevice, placing it on the platform that holds the sample and acquiring an image is not as obvious as it might seem.

For calibration and evaluation purposes, it suffices to place the microdevice on the platform immediately after introducing the cells. Simple actions such as focusing the beam and/or plane, checking oscillatory motion, moving the linear stages, switching between objective lens, and other tests serve to validate the equipment and software. Some can be carried out on microdevices without cells, or directly on a cuvette with dissolved fluorophores.

When preparing the sample for imaging, there are a few optical phenomena to account for: scattering, refraction and reflection. All the interfaces facing the objective lens and the illumination direction should be clear, smooth and free of impurities to prevent scattering of the excitation and emission rays. Few material interfaces and of similar refractive indices are desirable to limit the effects of refraction and reflection. These should be as flat (non-circular) as possible and completely perpendicular to the light path.

3.3.5. Current limitations of LSFM

Most biology microscopes are not designed to be illuminated from the sides, so cell culture dishes are generally round, sometimes rugged and disposable. The same happens with microdevices, where most are designed for confocal microscopy. This makes LSFM challenging with the current means but opens new possibilities of research in developing novel designs of bioMEMS for light-sheet applications.

A cuvette with excellent optical properties may allow the use of some state of the art microdevices of confocal microscopes for SPIM. The microdevice can be placed inside the cuvette and immersed on medium, which reduces considerably refractive index differences and guarantees planar incidence of the excitation rays.

As it is a SPIM set-up for live imaging, the preparation can become much more complex. The current system does not implement temperature control (see *4.2. Limitations*) which is paramount for long-term imaging of spheroid culture or cell migration experiments.

Also, immersing the microdevice in PBS or non-biocompatible oil, as suggested above, does not seem to be a viable solution. The microfluidic device requires tubes connecting pumps and reservoirs to the inlets of the microchannels for medium renewal. Having this submerged in a liquid-replete cuvette would be complicated to assemble.

The most fitting solution, as contemplated in *4.3. Future Directions*, is to redesign bioMEMS so they can be illuminated horizontally and have the image captured vertically.

3.4. IMAGE ACQUISITION

The previous section (*3.3. SAMPLE PREPARATION*) described microdevice synthesis and cell seeding procedures. Here, the tasks performed on the computer by the user after the sample is placed on the sample holder are listed.

3.4.1. Starting the program

Clicking on the shortcut on the desktop executes Opt3D.

FIGURE 52. OPT3D SHORTCUT.

A window will appear with the button *Initialize* to start the software. Before clicking it, all the electronics should be connected to the computer. If the camera is not connected or switched on, the initialization process will abort.

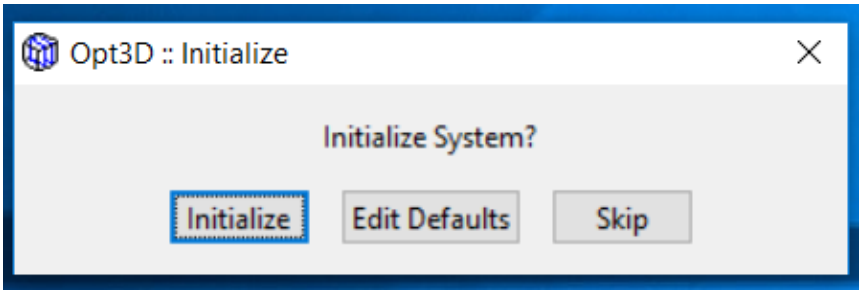

FIGURE 53. INITIALIZE SYSTEM WINDOW.

The *Log* display lists sequentially the operations and errors which also get saved to a text file in the installation folder. This information can be accessed by the developers for technical support.

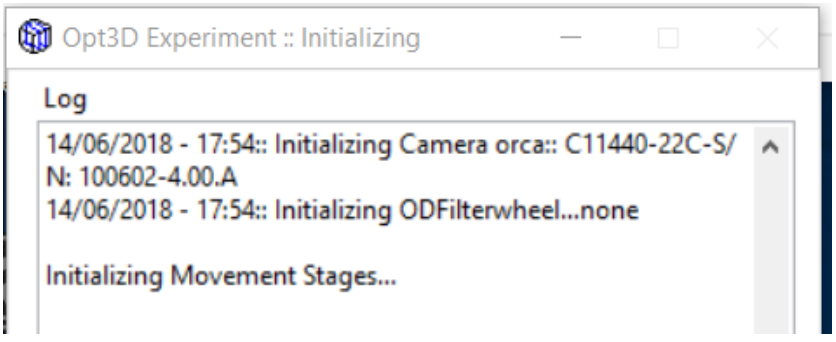

FIGURE 54. LOG DISPLAY.

The next window asks whether or not the stage motors are sent to the *Home* position. If a sample has been placed, care must be taken to ensure there is no collision during movement. Sending the motors to zero (Home) sets the reference point so that translation distances can be calculated.

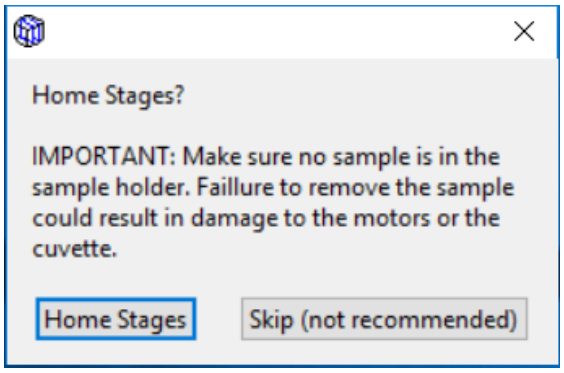

FIGURE 55. HOME STAGES WINDOW.

The motors will move to zero, after which another window shows asking the user whether they want to move the stages to the *Center* position. This is not an essential command and can be done at any time from the interface.

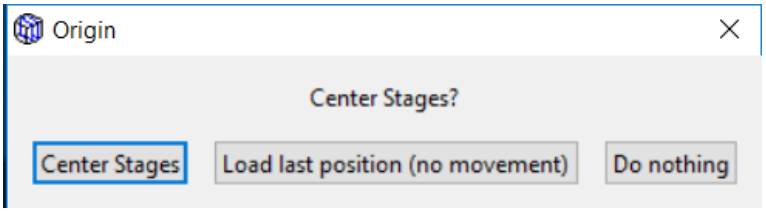

FIGURE 56. CENTER STAGES WINDOW.

After the motors have moved, the folder for saving files is selected. For long studies the folder should be located in the SSD. After selecting the folder, the main interface opens.

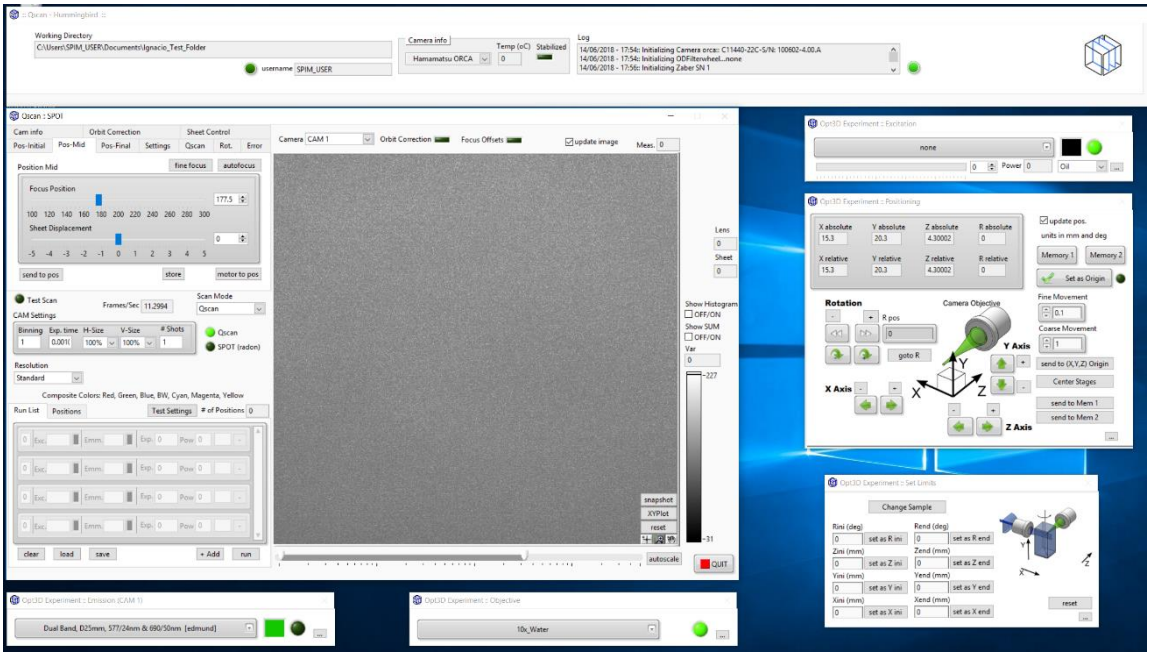

FIGURE 57. SOFTWARE MAIN INTERFACE.

3.4.2. Navigation

A window of the graphical user interface (GUI) is dedicated to navigate the sample with the motors. Pressing the arrows labelled with each coordinate (x, y, z) will move the linear stage in that direction by an amount in millimeters defined by the *Coarse Movement* parameter. Fine movement is controlled through the smaller buttons with "+" and "-" signs.

The sample should be navigated until the area of interest is under the objective. Focusing the imaging plane while navigating is suggested. The image displayed in the center of the GUI will be updated in real time and orients the user with respect to the sample.

Focusing can be done by moving the sample in the z direction, or by adjusting the tunable lens with the scroll bar in section *3.4.4 Focusing the illumination plane*.

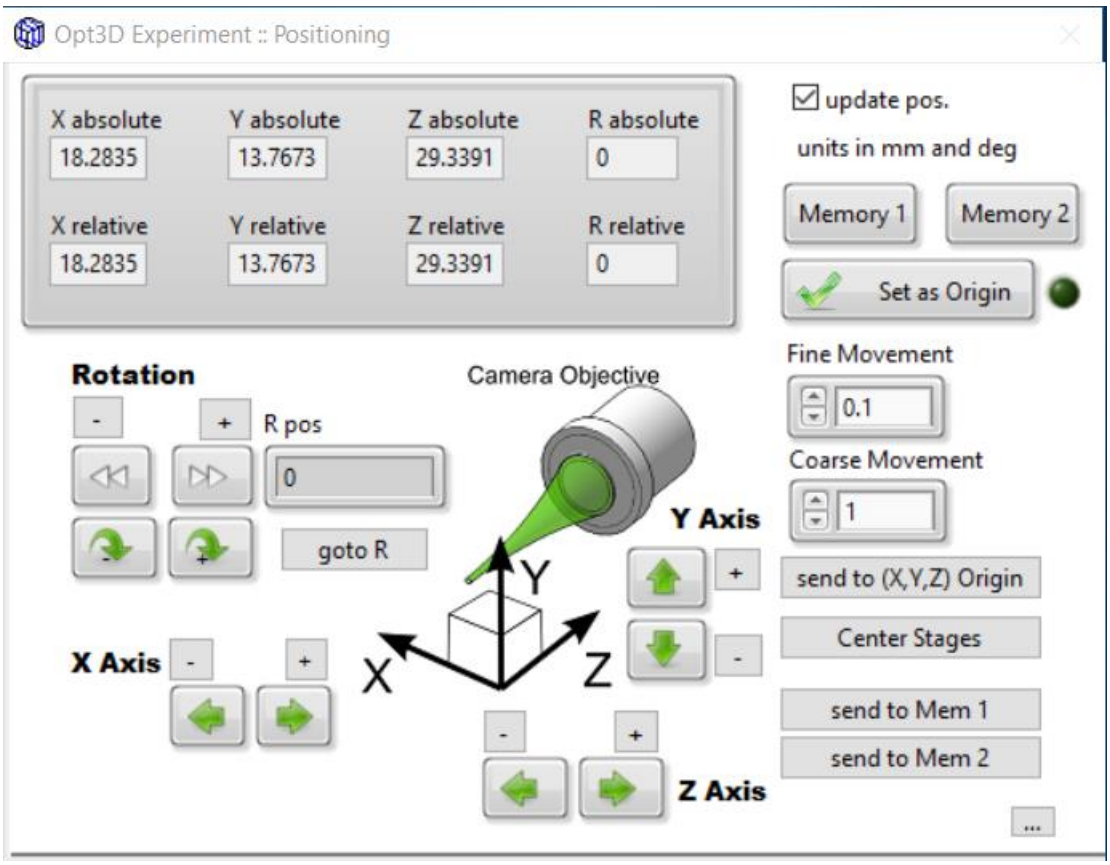

FIGURE 58. GUI FOR MOVING LINEAR STAGES.

3.4.3. Switching the laser

Now that the sample is centered under the objective, the excitation source is switched on. The power can be regulated from the same interface. The illumination focus has been previously calibrated (see *3.2.3.4 Tunable lens*) for each specific medium. For the experiments in this microscope, the medium will almost always be water.

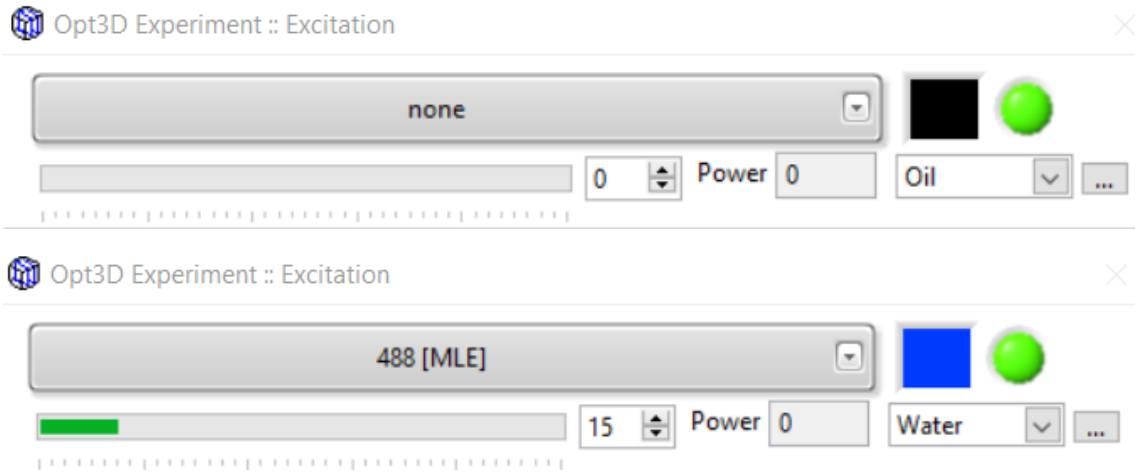

FIGURE 59. ILLUMINATION CONTROL GUI:
Top: Excitation is switched off (Default). *Bottom*: 488nm laser switched on with a power of 15mW and illumination focus on water.

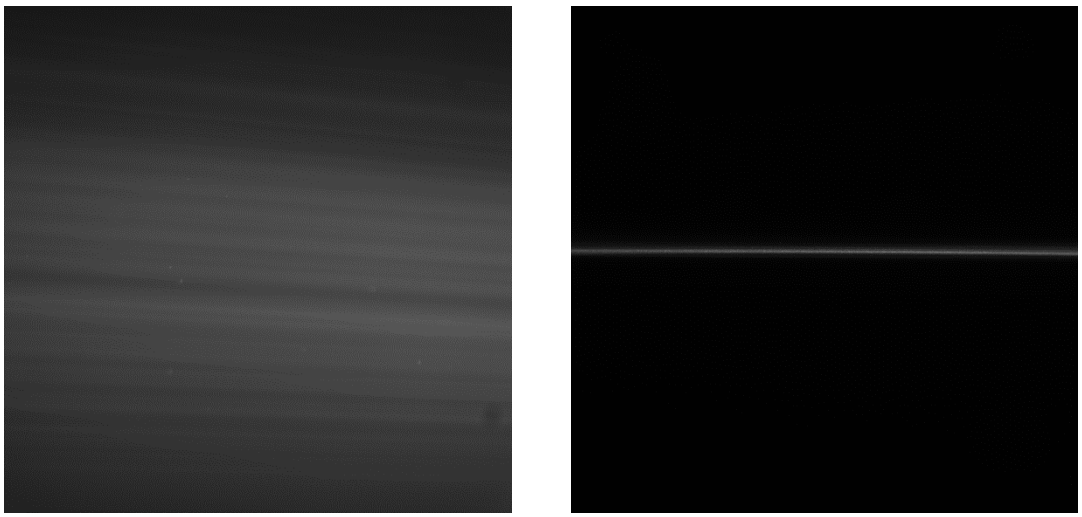

FIGURE 60. EXCITATION PLANE VS. BEAM.
Left: shows an illumination plane created by the cylindrical lens as seen under the microscope. *Right*: shows a focused laser beam.

3.4.4. Focusing the illumination plane

SPIM relies on single excitation planes that are focused along the z direction producing slices of a volumetric image stack. Three distinct planes must be illuminated and focused so that the interpolation algorithm can calculate the synchronized trajectories of the galvo and the tunable lens. Each of these planes is selected via three separate tabs: *Pos-Initial*, *Pos-Mid* and *Pos-Final*.

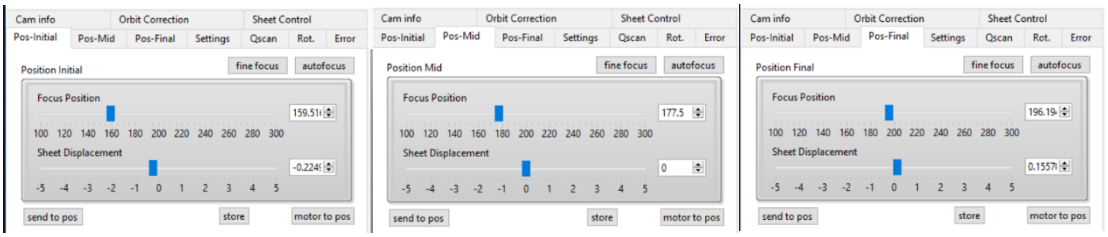

FIGURE 61. FOCUS POSITIONS AND SHEET DISPLACEMENTS FOR INTERPOLATION.

3.4.5. Oscillating the illumination source

DSLM requires an oscillating beam to form a virtual lightsheet. In SPIM, oscillations increase the quality of images by reducing shadow artifacts. The *Sheet Control* tab is used to define the waveform, frequency and width of the oscillation. When the green button under *Oscillate?* is pressed, oscillation begins.

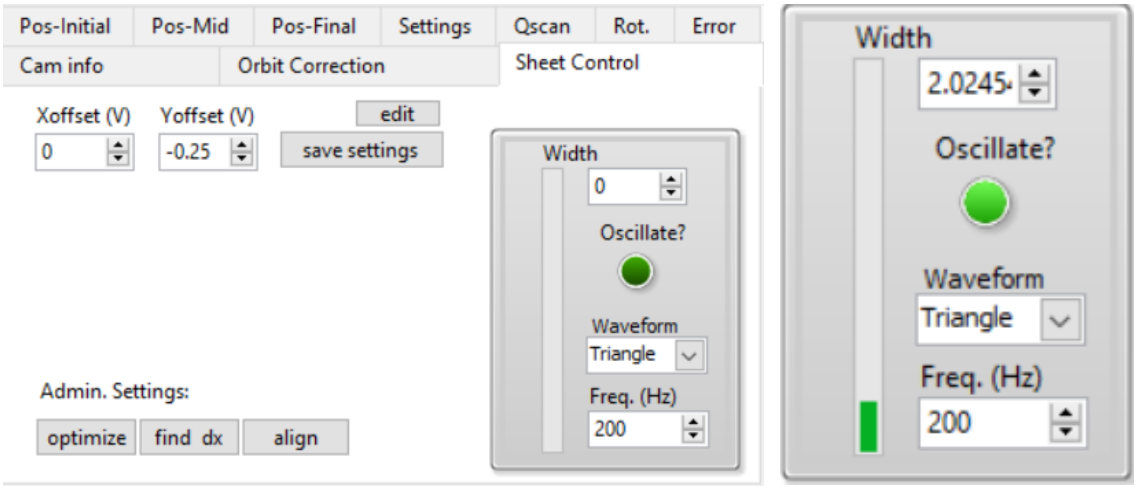

FIGURE 62. OSCILLATION CONTROL MENU.
Left: Control menu with oscillation turned off (Default). *Right*: Oscillation display turned on.

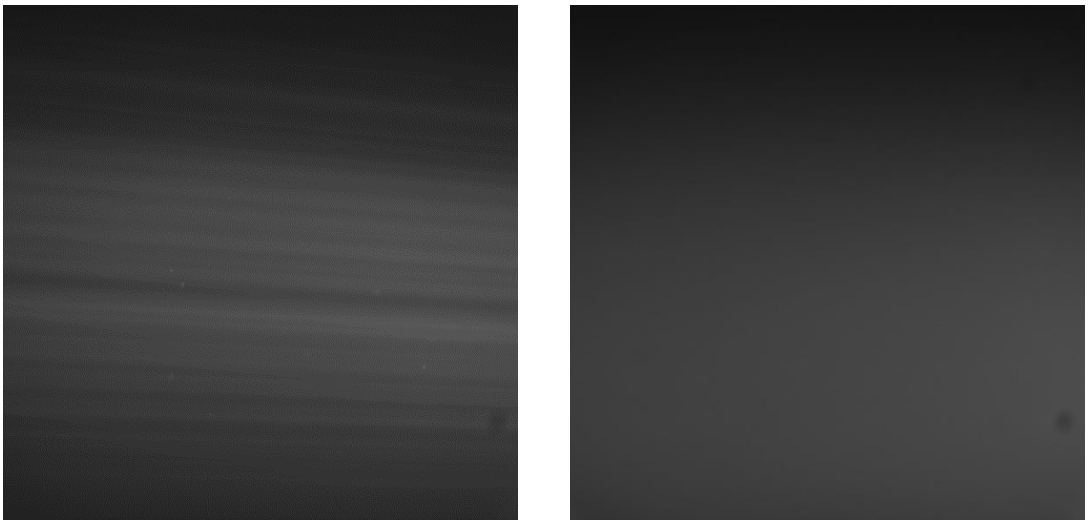

FIGURE 63. EFFECTS OF OSCILLATIONS.
Left: Image of a **static plane** of light shone into a fluorophore bath as seen under the microscope. The directionality of the light can be appreciated. *Right*: An **oscillating plane** of light. Note how illumination is highly homogeneous and the rays non-unidirectional.

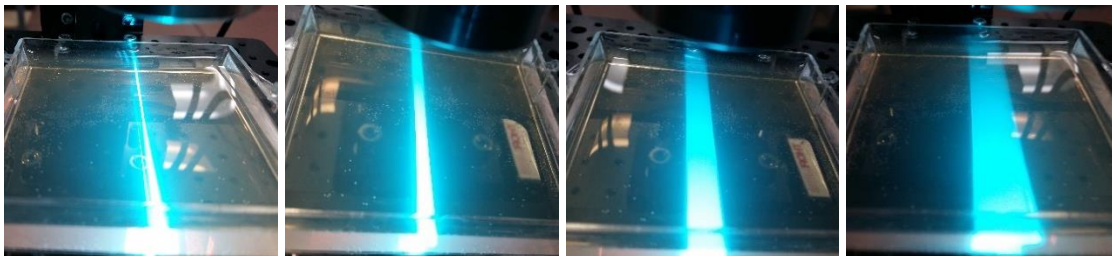

FIGURE 64. DSLM AT DIFFERENT OSCILLATION WIDTHS.
From left to right: (a) A static beam of light traversing a fluorophore bath. (b), (c), (d) The beam of light from (a) oscillating at high frequency with increasing amplitudes: 0.5 (b), 1.0 (c) and 2.0 (d) millimeters, respectively. These are images of virtual lightsheets used for DSLM.

3.4.6. Other acquisition parameters

The pixel size has been calculated for each objective during calibration and affects the units shown in the interface. Although normal images can still be acquired, the objective being used for imaging should be selected from the drop-down menu.

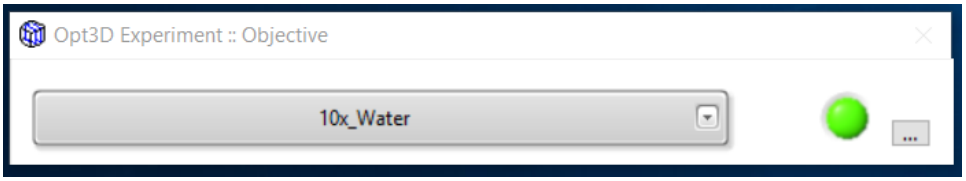

FIGURE 65. SELECT OBJECTIVE DROP-DOWN MENU.

Parameters related to the camera sensor can be changed on the main window. These are: binning, exposure time, horizontal size, vertical size, and number of shots. The properties of how each of these affects spatial and time resolution is described in *3.2.2.7 Capturing the image (Camera)*.

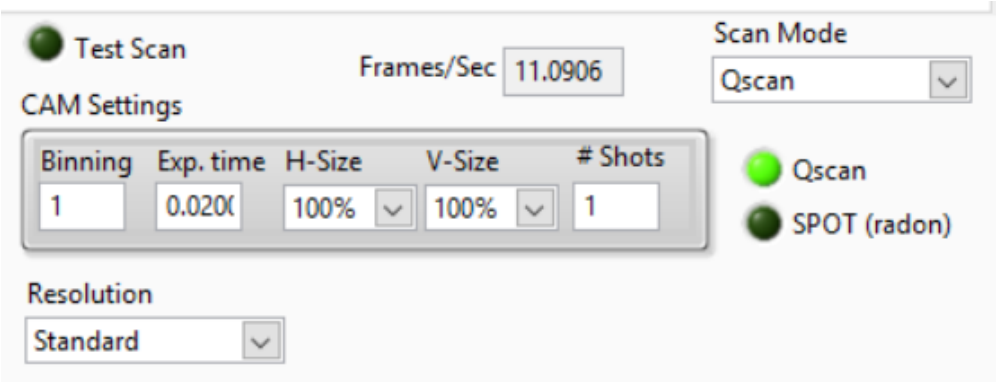

FIGURE 66. MENU FOR ADJUSTING THE CAMERA PARAMETERS.

3.4.7. Running a 3D scan

Snapshots can be taken by pressing the button labelled *Snapshot* next to the image display in the GUI. Performing a 3D scan involves several steps.

It first starts under the tab *Settings*, where the user can see and define parameters regarding a SPIM scan. By default, the *Sheet Initial* and *Sheet Final* positions are set to zero (single slice). These two values refer to the initial and final positions of the Y-coordinate in the galvo. The test scan will occur from *Sheet Initial* to *Sheet Final* in the number of steps specified by the variable *# of Meas. / scan*.

In order to maintain the highest interpolation accuracy, the values of *Sheet Initial* and *Sheet Final* must lie within the range defined by the sheet displacement values of *Pos-Initial* and *Pos-Final* described in *3.4.4. Focusing the illumination plane*. When outside this range, interpolation cannot guarantee that the illuminated plane is exactly in focus.

When the values are set to the desired range, the system will automatically start scanning in the z direction. The focus position and sheet displacement values will appear to the right of the image display in the GUI as they change (see Figure 67).

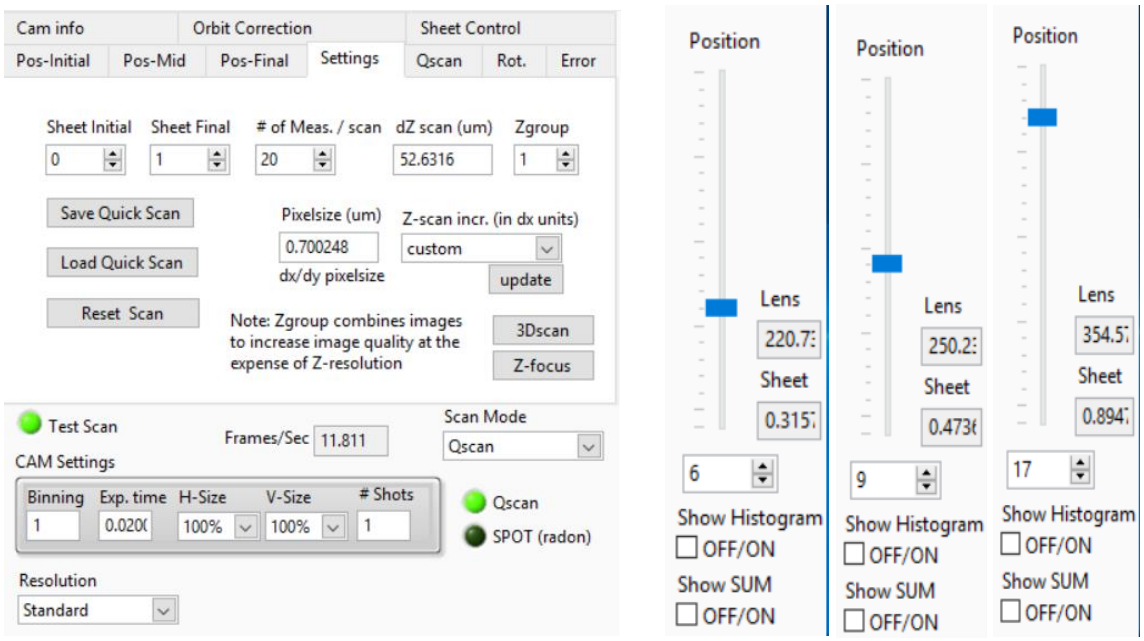

FIGURE 67. SCANNING THE SAMPLE.
Left: Menu showing the parameters that control the z-scan. *Right*: While the test scan runs, the focus position of the lens and the Y-axis displacement of the galvo change in a number of steps determined by *# of Meas. / scan*.

To perform the acquisition and save the image stack, the button *3Dscan* is pressed. This opens a pop-up window which allows the user to select the scan width and the step size, and the region of interest (ROI).

The total width divided by the increment gives the total number of images per stack. Attention should be paid to not abuse from slices that are too thin, as this may result in two problems. Firstly, the size of the image can be too large and saturate the RAM. For example, a 1mm scan with 1µm increments of all the pixels in the sensor would give an image stack of 8.4GB. Secondly, the z resolution cannot improve beyond the spatial resolution limits given for the system (listed in *4.1.* Current Capabilities), which is a waste of time and memory.

The ROI is delimited by the yellow lines (the middle square). These mark the boundaries of the pixels of the sensor that will be read during the scan. The area of interest in the sample does not necessarily occupy the whole image plane. The ROI limit imaging to where it is useful.

Additionally, the illumination focal depth can be smaller than the FOV. This occurs especially in lower magnification objectives; whose images show decreasing z resolution at pixels further away from the illumination focal spot. The ROI can constrain imaging to the areas of maximal and homogeneous resolution.

Following the example above, if the 1mm scan with 1µm increments was taken of an area of 500-by-500 pixels, the image stack would be of 500MB with an improvement in temporal resolution.

The button *Run 3D scan*, as the name indicates, initiates the scan under the given parameters. Stitching is automatically performed and the image is saved.

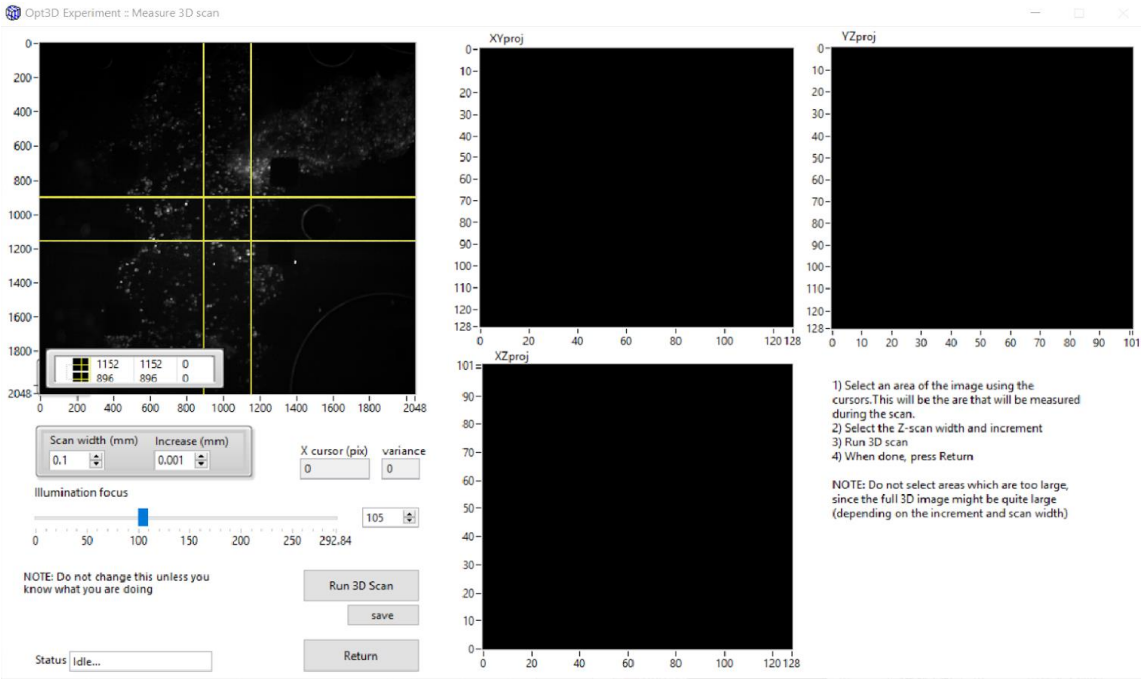

FIGURE 68. RUN 3D SCAN GUI.

The parameters of a scan can be saved into a list that fulfills two purposes. First, it can execute several scans in sequence and even move the motor positions around. This allows, for example, to automate scans across several culture wells. Also, and most importantly, saving them conserves the settings for future use, which avoids having to redo the parameter-defining steps covered in this section over and over again.

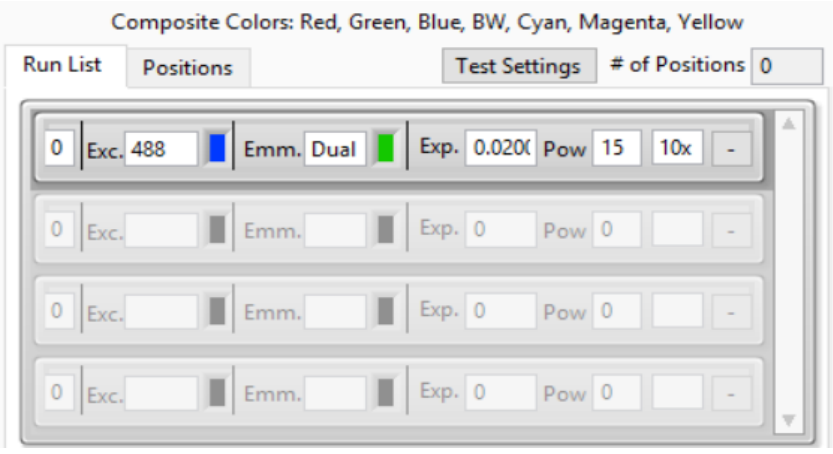

FIGURE 69. RUN LIST MENU AND DISPLAY.

3.4.8. Closing the program

After image acquisition is finished, the program is closed by clicking on the large red button labelled *QUIT*. To safeguard from accidental clicks, another window is opened which asks the used for confirmation to shut down the software.

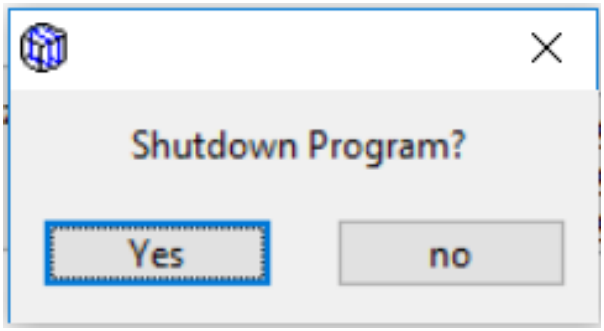

FIGURE 70. SHUTDOWN PROGRAM WINDOW.

4. Results and Discussion

4.1. Current Capabilities

This section recapitulates the characteristics that define the microscopy capabilities of this device. A number of tables and figures display this information and also show examples of real images taken by SPIM scans.

4.1.1. Characteristics of this system

The table below presents the essential information regarding and affecting spatial resolution. The researcher can use the values of these parameters to get an idea of the imaging power, the limits and the possible applications of the system.

The values were acquired for the 5x air objective. To recalculate for other objective lenses, or if changes were made to the hardware, the procedure to follow is outlined in *3.2.3.5. Characterizing the system*.

TABLE XV. CHARACTERISTICS OF THE SYSTEM

Parameter	Description	Value
Beam waist (focal spot diameter)	Closely related to resolution. The thinner the beam waist the higher the resolution in z.	18.93±0.01μm
Illumination Depth of field (estimate)	Related to the FOV outside which the quality of the image decreases.	500μm
Field of View	The extent of the area seen by the sensor.	2.5 x 2.5mm
Magnification	The apparent enlargement of a specimen by the objective.	5.241±0.001
Pixel size at focal spot	Closely related to resolution. Every pixel in the image represents pixels of this size in the sample.	1.2402μm (±0.0002)
x resolution	Smallest detail resolvable in a given direction in space.	6.5±0.2μm
y resolution		6.5±0.2μm
z resolution		13.0±0.4μm
Resolving Power	Smallest detail resolvable in a given direction in planar imaging.	2.46±0.01μm

4.1.2. Examples of images

Showing examples of images is proof that the system works as expected. The quality of the images obtained is high and suitable for image processing. The images shown in the report might appear small and with low contrast, however the original ones are 2048x2048 pixels with 16-bit intensity range of values, equivalent to 8MB per slice.

TABLE XVI. GFP-EXPRESSING CELLS IN MICRODEVICE (5X AIR).

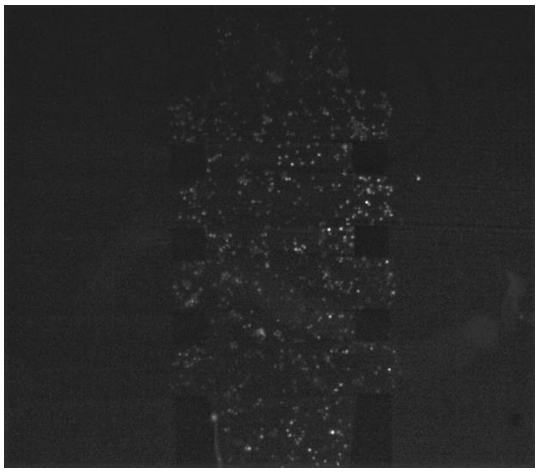

FIGURE 71. FLUORESCENCE RAW (5X).
Grayscale intensity values obtained directly from a snapshot have been contrast-enhanced for visualization purposes. The size of the image is 2095-by-1830 μm.

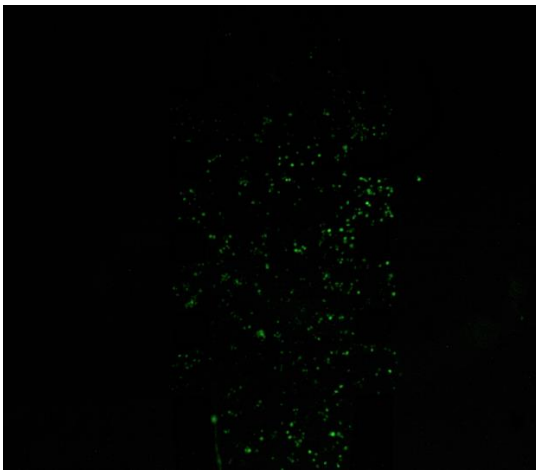

FIGURE 72. FLUORESCENCE CORRECT (5X).
The median value of the image has been subtracted to remove background effects. The intensity values have been colored for pure green (510nm) which is the emission maxima of GFP.

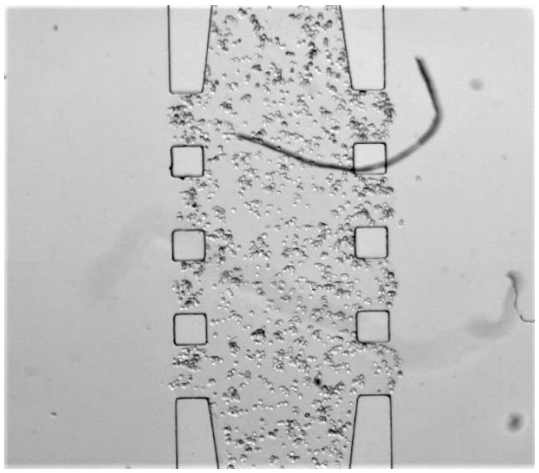

FIGURE 73. LED RAW (5X).
Same image obtained with LED illumination instead of laser plane. Contrast enhancement for visualization.

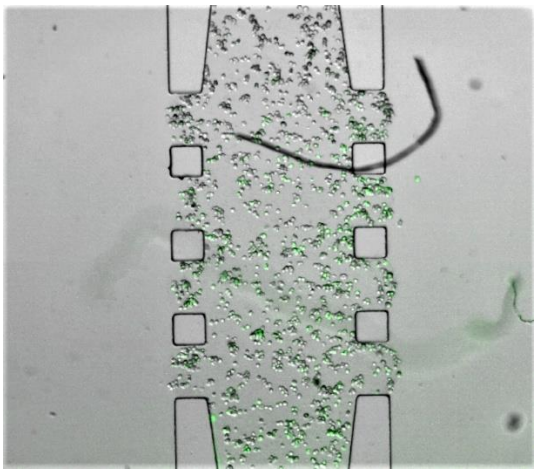

FIGURE 74. LED AND FLUORESCENT CORRECTION SUPERIMPOSED (5X).
Shows the cells that have been successfully transfected and lie within the illuminated slice. The upper part of the microdevice is not receiving light from the incident plane so the cells in that area appear dark.

TABLE XVII. GFP-EXPRESSING CELLS IN MICRODEVICE (10X WATER)

FIGURE 75. FLUORESCENCE RAW (10X).
The size of the image is 1183 x 1033 µm.

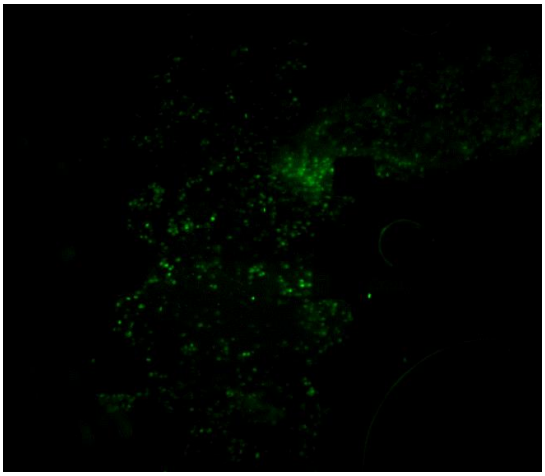

FIGURE 76. FLUORESCENCE CORRECT (10X).

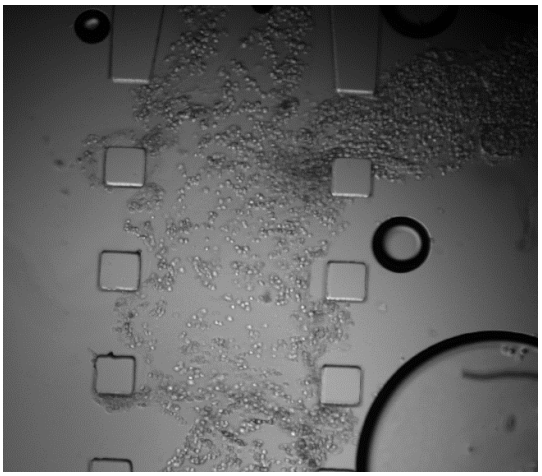

FIGURE 77. LED RAW (10X).
A small and a large bubble can be seen in the image. Microfluidic-device designers avoid certain shapes (such as sharp edges) to prevent bubbles from accumulating. Achieving a completely biocompatible bubble-free environment is quite complicated, as soluble gases (CO_2) and temperature differences are prone to accumulate gas.

Also, notice how the cells and gel in the loading channel have entered the side channels. This can happen if pipetting too forcefully or at an angle towards the microchannels.

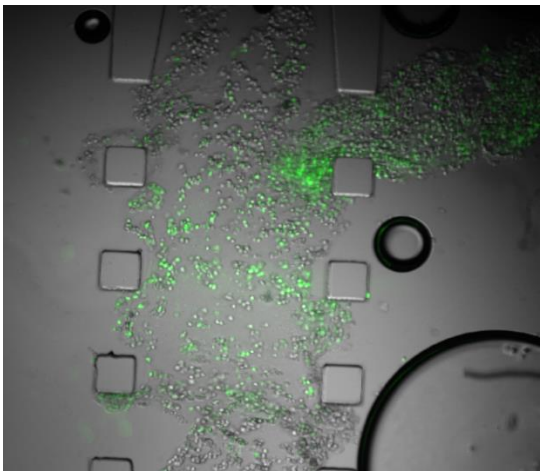

FIGURE 78. LED AND FLUORESCENT CORRECTION SUPERIMPOSED (10X).
This image is interesting because it shows how bubbles interact with the signal. The edges of the bubble appear fluorescent (zoom-in to see) but, of course, they do not contain GFP. The signal received is emission light being reflected at the surface of the bubble. This is well seen in the small bubble, where only the areas facing fluorophores show green.

Also, bubbles seem to block the illumination coming from the side. The cells behind bubbles do not show fluorescence.

TABLE XVIII. 3D SCAN OF GFP-EXPRESSING CELL IN MICRODEVICE (50X AIR).

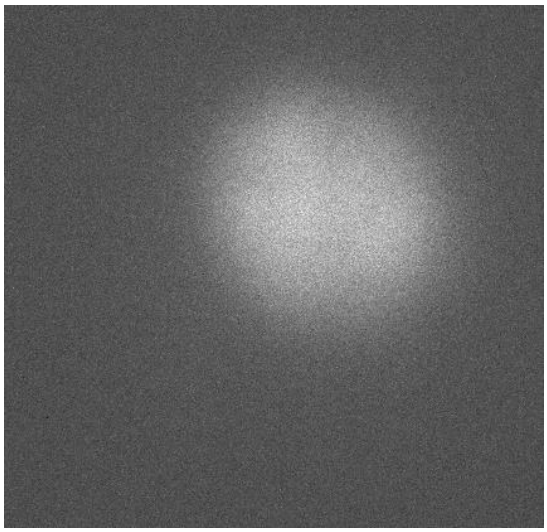

FIGURE 79. FLUORESCENCE RAW IMAGE OF THE MIDDLE SLICE (50X).

GFP was not associated to any particular structure but metabolized and released into the cytoplasm. This can be appreciated in the images.

The round shape is characteristic of cells not attached to the collagen matrix usually because of being outside of culture conditions for some time.

The estimated* image size is 56 x 54 μm.

* The real magnification of the 50x objective has not been obtained yet so the pixel size is calculated from the theoretical magnification: 50.

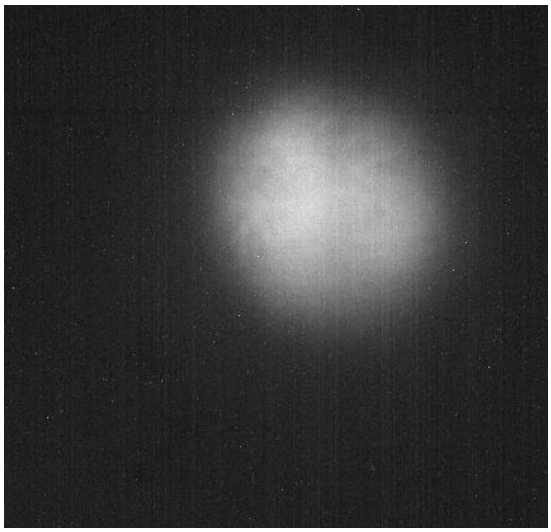

FIGURE 80. FLUORESCENCE STANDARD DEVIATION PROJECTION (50X).

The STD projection of an image stack effectively removes background and highlights relevant changes in variance.

Fun fact! The vertical stripes seen in the image represent the read lines of the CMOS sensor.

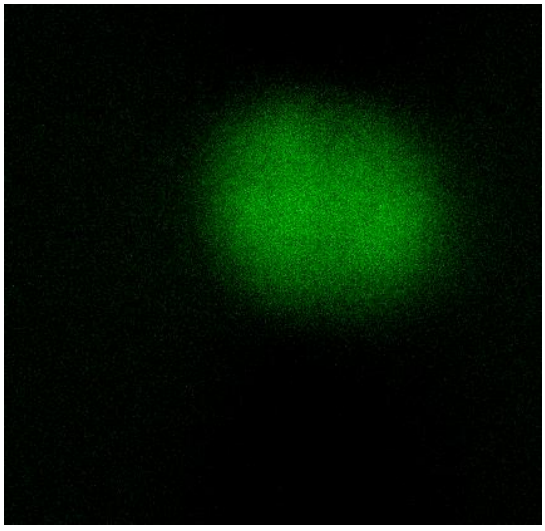

FIGURE 81. FLUORESCENCE CORRECTION OF MIDDLE SLICE (50X).

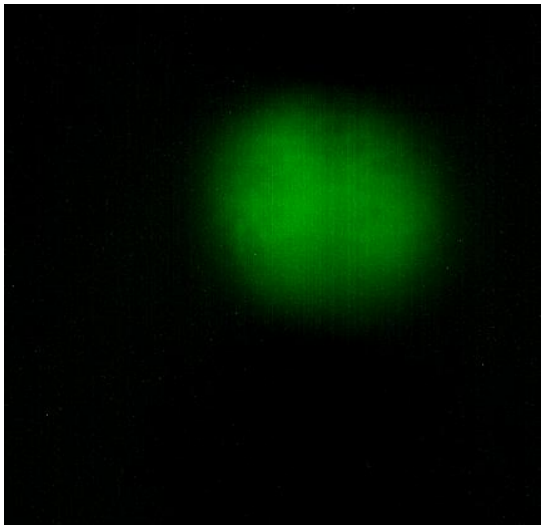

FIGURE 82. FLUORESCENT STD PROJECTION CORRECTION (50X).

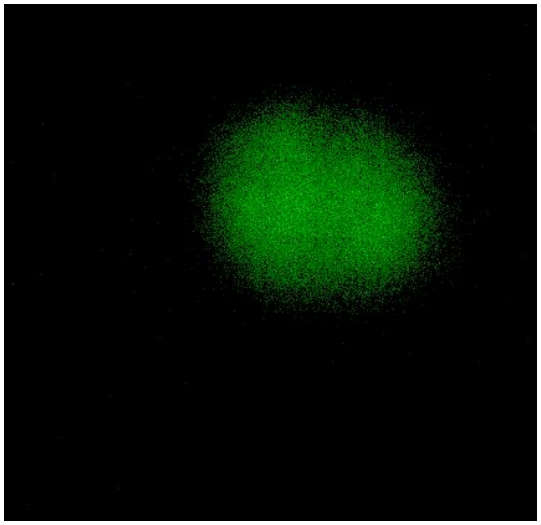

FIGURE 83. INTENSITY THRESHOLDING CORRECTION OF MIDDLE SLICE (50X).
This image is not as clear as it would be expected. To reduce blurring, deconvolution has to be performed. Increasing the exposure time should also sharpen the edges at the expense of time resolution and phototoxicity.

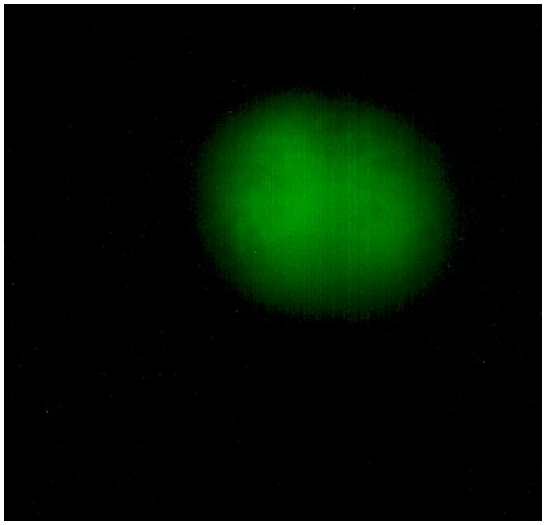

FIGURE 84. INTENSITY THRESHOLDING STD PROJECTION CORRECTION.
Intensity thresholding is neater for projection images than it is for slices. This makes sense because projection images integrate information from all the slices.

4.2. Limitations

The project was completed as expected. A few improvements remain that should be addressed for long-term imaging and traction-force experiments before the microscope is completely functional for research. These are:

I. Calibration of more objectives

So far, the system has been characterized for a 5x magnification air objective lens. It is important to do this for more objectives, including those of water immersion and of higher magnification. Water immersion objectives have higher NA and can capture more light. Higher magnification enables traction force microscopy (TFM) by being able to detail cell movement and shape, and deformations of the extracellular matrix (ECM). Attached in the Annex is Table XXI which lists the objectives available in the laboratory.

II. Parfocal distance adapters

The use of objectives from various manufacturers often requires adjusting for the differences in parfocal distances (equivalent to the length of the objective plus its working distance), a task that can sometimes be performed by the tunable lens located in the infinity space. However, this is not practical because the user must refocus the sample every time the objective is changed. Parfocal distance adapters solve this issue and maintain the image plane constant regardless of the objective in use.

III. Prolonged *in vitro* imaging

At present, the system can only image cells for a brief period of time (5 minutes) before they die. Temperature, CO_2 and medium control must be implemented for live imaging. The sample holder should be able to generate a controlled heat environment with a constant temperature of 37ºC. Pumps and microfluidics connections can exploit the advantages of bioMEMS culturing by regularly replenishing the medium to keep the cells alive. This was beyond the scope of the project due to time limitations.

4.3. Future Directions

This section presents a few pointers on how this system can be utilized or improved by someone doing research in SPIM imaging of microdevices.

4.3.1. Microdevices for LSFM

Designing and microfabricating bioMEMS is not an easy task. The process of microfabrication is expensive, so molds should be ordered once a design has been validated exhaustively with flow simulators and prototypes.

Apart from designing them, microfluidic devices integrate sensors and actuators (pumps, valves) to automate the culture process. Assembling the entire bioMEMS and programming the controllers for specific experiments is a fundamental step towards live imaging.

4.3.2. System enhancement possibilities

If desired, a few perks can be added to the existent hardware and software to extend the applications and quality of SPIM.

1. Adding lasers

With a higher number of lasers of different wavelengths more fluorophores can be excited. This allows to mark simultaneously several structures like the nuclei, the plasma membrane or the extracellular matrix. Also, tagging different cell types in co-cultures or proteins that can identify gene expression would make this system suitable for drug tests and organoid experiments. For now, the system has the mandatory minimum of excitation wavelengths required for traction force microscopy (TFM).

2. Emission filter wheel

A manual or automated filter wheel improve detection of fluorescence and reduce background illumination. It can potentially detect several fluorophores with similar absorption peaks but different emission bands (e.g.: quantum dots) without the need of adding extra lasers.

3. Simultaneous dual-laser excitation

Dual-laser excitation requires two cameras and an emission dichroic filter to redirect light into each of the cameras. It increases temporal resolution and scan speed by concurrently imaging two fluorophores. The dichroic filter can slightly reduce the amount of signal reaching each camera (this becomes relevant in systems with many cameras). The actual setup would require thorough redesign of the camera turret structure to implement a second camera.

4. Scanning the illumination focal spot

The company supplying the software is planning to include illumination focal spot scanning in future versions of the control system. With this code, the tunable lens that focuses the excitation light would be focused back and forth within the image plane. This achieves homogeneous and maximal spatial resolution in z throughout the whole x-y field of view. The drawback to this approach is an increase in phototoxicity.

5. Conclusion

The report has discussed the setting-up of a SPIM instrument capable of imaging cells seeded in PDMS microfluidic devices. The fluorescence microscope is proven to work for its intended purpose in *4.1.2. Examples of images*.

A few adjustments (*4.2. Limitations*) remain before the overall system is completely ready for researchers to record traction forces and cell migration. Most importantly, integrating temperature control and bioMEMS into the sample-mounting workflow to generate the conditions to keep cells alive for longer periods of time.

Since life does not end after the Bachelor Thesis, fundamental procedures to the functioning of the microscope have been described in *3.2.3. Software Calibration*, *3.3. SAMPLE PREPARATION*, and *3.4. IMAGE ACQUISITION.* These will be especially useful for people continuing with and expanding the work here proposed.

For researchers interested in setting up similar devices, the report is a perfect guideline to follow, more so for someone inexperienced in optics. The principal costs and challenges have been outlined and a full list of the material is available in Table XXII. Project Costs..

The new SPIM device at the Biomedical Imaging and Instrumentation Group is expected to mark a significant difference to the research the group has been performing up-to-date in the development of algorithms for cell migration and traction-force quantification.

6. Socio-Economic Impact

6.1. Research Impact

The integration of bioMEMS and LSFM is a novel field requiring collaborative research that can produce more quantitative experiments of increased biological significance. So far, two-dimensional microscopy experiments been extensively studied and research has progressed towards the 3D analysis of the cell environment. A research group that wants to produce the latest discoveries has to necessarily move in this direction. The system designed for this project will reinforce the role of Universidad Carlos III de Madrid as a leading research institution in the country by allowing nonconventional experiments of increased complexity beyond the scope of other laboratories.

Technology wise, integrating LSFM and bioMEMS can potentially reduce laboratory costs through automation of culturing and analysis. It should be possible to synchronize imaging and microdevice technology if these tasks are performed from the same control center (computer). If this is accomplished, the department could commercialize the device or rent it for drug tests.

Additionally, the study of cell migration and traction forces in a volume can lead to new image processing algorithms which will become of widespread demand when more groups approach 3D fluorescent imaging. The installation of this microscope next to the laboratories of the tissue engineering group could spark collaborations for organoid research in the future.

6.2. Project Costs

Table XIX below summarizes the costs for this project. This data has been created using an Excel dynamic spreadsheet from Table XXII in the Annex which offers a breakdown of all the items used for this project together with the quantity, price and link to the manufacturer's website. Table XX shows the breakdown of hours devoted by each employee towards the completion of the project.

TABLE XIX. PROJECT COSTS SUMMARY

Costs Summary	
Concept	**€**
Optical and Optomechanical Hardware	42,709
Software	17,000
Electronic and Computer Hardware	5,129
Other	2,458
Subtotal Purchasing Costs	67,296
Taxes (21% of Purchasing Costs)	14,132
Human Resources	26,500
Subtotal Costs	107,928
Overheads (15% / Total) *	19,046
Total	**126,975**

* Percentage taken from UC3M Agreement on the distribution of the retention of research projects (Government Council 25/10/12), referring to projects of the Spanish National Plan (items defined by the Ministry of Economy are among others: furniture, general equipment, computer equipment, general and computer maintenance, electricity, water, gas) and European Union projects (including some additional ones such as: part of the personnel cost of the Administrative and Legal Office, amortizations, etc.) [80].

TABLE XX. COSTS ASSOCIATED TO HUMAN RESOURCES

Human Resources			
Employee	**Hours**	**Cost / hour**	**€**
Project Manager	80	70	5,600
Optics Expert	80	70	5,600
Research Assistant (chemist)	60	25	1,500
Laboratory technician (electronics)	60	20	1,200
Laboratory technician (IT)	20	20	400
Laboratory technician (biology)	10	20	200
Undergraduate Researcher	800	15	12,000
Total general	1.110	23.87	**26,500**

The 800 hours dedicated to this project encompass 500 hours from a Research Collaboration Scholarship from the Spanish Ministry of Education plus 360 hours (12 ECTS) from the Bachelor Thesis course at Universidad Carlos III de Madrid.

After being built, the whole setup is estimated to have a useful lifespan of 10 years. During this period, a maximum of three software updates are expected, each with a cost of 2000€. Up to 15,000€ of the optical and optomechanical hardware is reusable. The outdated electronics can potentially be recycled for academic purposes or less accuracy-demanding applications. Accounting for this, the cost of the system is calculated to be **11,700€ / year** for a period of **10 years**.

Bibliography

[1] L. O. Björn, "The nature of light and its interaction with matter," in *Photobiology: The Science of Light and Life (3rd Ed.)*, 3rd ed. New York: Springer-Verlag New York, 2015.

[2] Thomas Thomson, Richard Phillips and Edward William Brayley, *The Annals of Philosophy*. London: C. Baldwin Printer New Bridge street, 1819*14*.

[3] G. G. Stokes, "On the Change of Refrangibility of Light," *Philosophical Transactions of the Royal Society of London*, vol. 142, *(2)*, pp. 463-562, 1852. Available: https://www.jstor.org/stable/108550. DOI: 10.1098/rstl.1852.0022.

[4] J. Lee, *Structure and Spectra in Bioluminescence*. 2014. DOI: 10.13140/RG.2.1.5084.2080.

[5] Thermo Fisher Scientific, *Spectra Viewer*. Available: https://www.thermofisher.com/order/spectra-viewer.Spectra viewer

[6] J. Ripoll, B. Koberstein-Schwarz and V. Ntziachristos, "Unleashing Optics and Optoacoustics for Developmental Biology," *Trends Biotechnol.*, vol. 33, *(11)*, pp. 679-691, 2015. DOI: S0167-7799(15)00174-2.

[7] C. A. Combs, "Fluorescence microscopy: a concise guide to current imaging methods," *Current Protocols in Neuroscience / Editorial Board, Jacqueline N. Crawley ... [Et Al.]*, vol. Chapter 2, pp. Unit2.1, 2010. Available: http://www.ncbi.nlm.nih.gov/pubmed/20066655.

[8] R. S. Fischer *et al*, "Microscopy in 3D: a biologist's toolbox," *Trends in Cell Biology*, vol. 21, *(12)*, pp. 682-691, 2011. Available: https://www.clinicalkey.es/playcontent/1-s2.0-S096289241100198X. DOI: 10.1016/j.tcb.2011.09.008.

[9] Steven Ruzin, "Techniques in Light Microscopy," Dec 1, 2017.

[10] J. Jonkman and C. M. Brown, "Any Way You Slice It-A Comparison of Confocal Microscopy Techniques," *J. Biomol. Tech.*, vol. 26, *(2)*, pp. 54-65, 2015. DOI: 10.7171/jbt.15-2602-003 [doi].

[11] Y. Wu *et al*, "Advanced optical imaging techniques for neurodevelopment," *Current Opinion in Neurobiology*, vol. 23, *(6)*, pp. 1090-1097, 2013. Available: https://www.clinicalkey.es/playcontent/1-s2.0-S095943881300127X. DOI: 10.1016/j.conb.2013.06.008.

[12] R. M. Power and J. Huisken, "A guide to light-sheet fluorescence microscopy for multiscale imaging," *Nature Methods*, vol. 14, pp. 360, 2017. Available: http://dx.doi.org/10.1038/nmeth.4224.

[13] P. A. Santi, "Light Sheet Fluorescence Microscopy: A Review," *Journal of Histochemistry and Cytochemistry*, vol. 59, *(2)*, pp. 129-138, 2010. Available: http://www.ncbi.nlm.nih.gov/pmc/articles/PMC3201139/. DOI: 10.1369/0022155410394857.

[14] Jordi Andilla *et al*, "Imaging tissue-mimic with light sheet microscopy: A comparative guideline," *Scientific Reports (Nature Publisher Group)*, vol. 7, *(44939)*, pp. 44939, 2017. Available: https://search.proquest.com/docview/1903384966. DOI: 10.1038/srep44939.

[15] Jan Huisken and Didier Y. R. Stainier, "Selective plane illumination microscopy techniques in developmental biology," *Development*, vol. 136, *(12)*, pp. 1963-1975, 2009. Available: http://dev.biologists.org/content/136/12/1963.abstract. DOI: 10.1242/dev.022426.

[16] F. Pampaloni, B. Chang and E. Stelzer, "Light sheet-based fluorescence microscopy (LSFM) for the quantitative imaging of cells and tissues," *Cell Tissue Res*, vol. 360, *(1)*, pp. 129-141, 2015. Available: http://www.ncbi.nlm.nih.gov/pubmed/25743693. DOI: 10.1007/s00441-015-2144-5.

[17] J. R. Allen, "Light Sheet Fluorescence Microscopy," *MicroscopyU - NIKON INSTRUMENTS INC.*, Available: https://www.microscopyu.com/techniques/light-sheet/light-sheet-fluorescence-microscopy.

[18] F. O. Fahrbach *et al*, "Light-sheet microscopy in thick media using scanned Bessel beams and two-photon fluorescence excitation," *Optics Express*, vol. 21, *(11)*, pp. 13824-13839, 2013. Available: http://www.ncbi.nlm.nih.gov/pubmed/23736637. DOI: 10.1364/OE.21.013824.

[19] Z. Yang *et al*, "A compact Airy beam light sheet microscope with a tilted cylindrical lens," *Biomedical Optics Express*, vol. 5, *(10)*, pp. 3434, 2014. Available: http://www.ncbi.nlm.nih.gov/pubmed/25360362. DOI: 10.1364/BOE.5.003434.

[20] Yicong Wu *et al*, "Inverted selective plane illumination microscopy (iSPIM) enables coupled cell identity lineaging and neurodevelopmental imaging in Caenorhabditis elegans," *Proceedings of the National Academy of Sciences of the United States of America*, vol. 108, *(43)*, pp. 17708-17713, 2011. Available: https://www.jstor.org/stable/41352582. DOI: 10.1073/pnas.1108494108.

[21] J. Huisken *et al*, "Optical Sectioning Deep Inside Live Embryos by Selective Plane Illumination Microscopy," *Science*, vol. 305, *(5686)*, pp. 1007-1009, 2004. Available: http://www.sciencemag.org/cgi/content/abstract/305/5686/1007. DOI: 10.1126/science.1100035.

[22] P. J. Keller *et al*, "Reconstruction of Zebrafish Early Embryonic Development by Scanned Light Sheet Microscopy," *Science*, vol. 322, *(5904)*, pp. 1065-1069, 2008. Available: http://www.sciencemag.org/cgi/content/abstract/322/5904/1065. DOI: 10.1126/science.1162493.

[23] Paul J. Scherz *et al*, "High-speed imaging of developing heart valves reveals interplay of morphogenesis and function," *Development*, vol. 135, *(6)*, pp. 1179-1187, 2008. Available: http://dev.biologists.org/content/135/6/1179.abstract. DOI: 10.1242/dev.010694.

[24] E. G. Reynaud *et al*, "Light sheet-based fluorescence microscopy: More dimensions, more photons, and less photodamage," *HFSP Journal*, vol. 2, *(5)*, pp. 266-275, 2010. Available: http://www.tandfonline.com/doi/abs/10.2976/1.2974980. DOI: 10.2976/1.2974980.

[25] C. J. Engelbrecht *et al*, "Three-dimensional laser microsurgery in light-sheet based microscopy (SPIM)," *Optics Express*, vol. 15, *(10)*, pp. 6420, 2007. Available: http://www.ncbi.nlm.nih.gov/pubmed/19546948. DOI: 10.1364/OE.15.006420.

[26] E. J. Gualda *et al*, "Three-dimensional imaging flow cytometry through light-sheet fluorescence microscopy," *Cytometry Part A*, vol. 91, *(2)*, pp. 144-151, 2017. DOI: 10.1002/cyto.a.23046.

[27] R. Regmi, K. Mohan and P. P. Mondal, "High resolution light-sheet based high-throughput imaging cytometry system enables visualization of intra-cellular organelles," *AIP Advances*, vol. 4, *(9)*, pp. 7, 2014. Available: https://doaj.org/article/e102563f48ef47ad9fc792dfc5b888d2. DOI: 10.1063/1.4896260.

[28] R. Regmi, K. Mohan and P. P. Mondal, "Light sheet based imaging flow cytometry on a microfluidic platform," *Microscopy Research and Technique*, vol. 76, *(11)*, pp. 1101-1107, 2013. DOI: 10.1002/jemt.22296.

[29] F. Pampaloni, N. Ansari and E. Stelzer, "High-resolution deep imaging of live cellular spheroids with light-sheet-based fluorescence microscopy," *Cell Tissue Res*, vol. 352, *(1)*, pp. 161-177, 2013. Available: http://www.ncbi.nlm.nih.gov/pubmed/23443300. DOI: 10.1007/s00441-013-1589-7.

[30] M. Rimann Ursula, "Synthetic 3D multicellular systems for drug development," *Current Opinion in Biotechnology*, vol. 23, *(5)*, pp. 803-809, 2012. Available: https://www.clinicalkey.es/playcontent/1-s2.0-S0958166912000237. DOI: 10.1016/j.copbio.2012.01.011.

[31] C. Zoe and T. Kenichi, "Spheroid Culture of Mesenchymal Stem Cells," *Stem Cells International*, vol. 2016, pp. 1-11, 2016. Available: http://dx.doi.org/10.1155/2016/9176357. DOI: 10.1155/2016/9176357.

[32] B. Ducommun, "Engineering and Imaging multicellular tumour spheroids to study 3D cell proliferation," *L'Agence Nationale De La Recherche (ANR)*, 2012. Available: http://www.agence-nationale-recherche.fr/Project-ANR-12-BSV5-0008.

[33] M. Rimann and U. Graf-Hausner, "Synthetic 3D multicellular systems for drug development," *Current Opinion in Biotechnology*, vol. 23, *(5)*, pp. 803-809, 2012. Available: https://www.clinicalkey.es/playcontent/1-s2.0-S0958166912000237. DOI: 10.1016/j.copbio.2012.01.011.

[34] H. Jiang *et al*, "Droplet-based light-sheet fluorescence microscopy for high-throughput sample preparation, 3-D imaging and quantitative analysis on a chip," vol. 17, *(13)*, pp. 2193-2197, 2017. DOI: 10.1039/c7lc00164a.

[35] Peter G Pitrone *et al*, "OpenSPIM: an open-access light-sheet microscopy platform," *Nature Methods*, vol. 10, *(7)*, pp. 598, 2013. Available: http://www.ncbi.nlm.nih.gov/pubmed/23749304. DOI: 10.1038/nmeth.2507.

[36] Emilio J Gualda *et al*, "OpenSpinMicroscopy: an open-source integrated microscopy platform," *Nature Methods*, vol. 10, *(7)*, pp. 599, 2013. Available: http://www.ncbi.nlm.nih.gov/pubmed/23749300. DOI: 10.1038/nmeth.2508.

[37] European Comission, "COMMISSION DELEGATED DIRECTIVE (EU) 2015/863 amending Annex II to Directive 2011/65/EU of the European Parliament and of the Council as regards the list of restricted substances," Jun 4, 2015.

[38] University of California, Santa Barbara Staff, "Laser Safety Manual," *UCSB Environmental Health & Safety*, 2018.

[39] Iowa State University Staff, "Laser Safety Manual," *Iowa State University Environmental Health and Safety*, 2016.

[40] M. Kapałczyńska *et al*, "2D and 3D cell cultures – a comparison of different types of cancer cell cultures," *Archives of Medical Science*, 2016. DOI: 10.5114/aoms.2016.63743.

[41] K. Duval *et al*, "Studies in the Area of Tissue Engineering Reported from Dartmouth College (Modeling Physiological Events in 2D vs. 3D Cell Culture)," *Biotech Week*, pp. 326, 2017.

[42] M. Anguiano *et al*, "Characterization of three-dimensional cancer cell migration in mixed collagen-Matrigel scaffolds using microfluidics and image analysis," 2017. Available: http://hdl.handle.net/10016/24160.

[43] M. Maska *et al*, "Segmentation and Shape Tracking of Whole Fluorescent Cells Based on the Chan-Vese Model," *Tmi*, vol. 32, *(6)*, pp. 995-1006, 2013. Available: https://ieeexplore.ieee.org/document/6423287. DOI: 10.1109/TMI.2013.2243463.

[44] V. Ulman *et al*, "An objective comparison of cell-tracking algorithms," *Nature Methods*, vol. 14, *(12)*, pp. 1141, 2017. Available: http://urn.kb.se/resolve?urn=urn:nbn:se:kth:diva-221073.

[45] M. Maška *et al*, "A benchmark for comparison of cell tracking algorithms," *Bioinformatics*, vol. 30, *(11)*, pp. 1609-1617, 2014. Available: http://www.narcis.nl/publication/RecordID/oai:repub.eur.nl:58175. DOI: 10.1093/bioinformatics/btu080.

[46] W. J. Polacheck and C. S. Chen, "Measuring cell-generated forces: a guide to the available tools," *Nature Methods*, vol. 13, *(5)*, pp. 415-423, 2016. Available: http://www.ncbi.nlm.nih.gov/pubmed/27123817. DOI: 10.1038/nmeth.3834.

[47] A. Suñe-Auñon *et al*, "L1-regularized reconstruction for traction force microscopy," in Apr 2016, pp. 140-144.

[48] M. Gonzalez-Arjona *et al*, "Young's modulus measurement in polyacrylamide gels for Traction Force Microscopy in 2D," unpublished.

[49] A. Sune-Aunon *et al*, "Full L1-regularized Traction Force Microscopy over whole cells," *BMC Bioinformatics*, vol. 18, 2017. Available: https://search.proquest.com/docview/1934552294. DOI: 10.1186/s12859-017-1771-0.

[50] J. Cury and A. Muñoz-Barrutia, "Microspheres for Measuring the Elasticity of Gel Substrate for 2D Traction Force Microscopy Experiments.", Universidad Carlos III de Madrid, Leganes, 2017.

[51] D. M. Cohen *et al*, "Measurement of mechanical tractions exerted by cells in three-dimensional matrices," *Nature Methods*, vol. 7, *(12)*, pp. 969-971, 2010. Available: http://dx.doi.org/10.1038/nmeth.1531. DOI: 10.1038/nmeth.1531.

[52] J. A. Mulligan *et al*, "Measurement of dynamic cell-induced 3D displacement fields in vitro for traction force optical coherence microscopy," *Biomedical Optics Express*, vol. 8, *(2)*, pp. 1152, 2017. DOI: 10.1364/BOE.8.001152.

[53] T. M. Koch *et al*, "3D Traction Forces in Cancer Cell Invasion," 2012. Available: http://nrs.harvard.edu/urn-3:HUL.InstRepos:9807311.

[54] M. Cóndor *et al*, "Traction Force Microscopy in 3-Dimensional Extracellular Matrix Networks," *Current Protocols in Cell Biology*, [https://currentprotocols.onlinelibrary.wiley.com/doi/abs/10.1002/cpcb.24]. 2017. DOI: 10.1002/cpcb.24.

[55] Y. Abbas *et al*, "A microfluidics assay to study invasion of human placental trophoblast cells," *Journal of the Royal Society of London Interface*, vol. 14, *(130)*, pp. 20170131, 2017. DOI: 10.1098/rsif.2017.0131.

[56] I. K. Zervantonakis *et al*, "Three-dimensional microfluidic model for tumor cell intravasation and endothelial barrier function," *Proceedings of the National Academy of Sciences of the United States of America*, vol. 109, *(34)*, pp. 13515-13520, 2012. Available: https://www.jstor.org/stable/41700963. DOI: 10.1073/pnas.1210182109.

[57] Y. H. V. Ma *et al*, "A review of microfluidic approaches for investigating cancer extravasation during metastasis," *Microsystems & Nanoengineering*, vol. 4, pp. 17104, 2018. Available: https://search.proquest.com/docview/2022969690. DOI: 10.1038/micronano.2017.104.

[58] Toptica Photonics Staff, "iBeam smart Product Manual," 2018.

[59] Bio-Rad Antibodies. “Chapter 1 - Principles of the Flow Cytometer”, *Optics and Detection*. Available: https://www.bio-rad-antibodies.com/flow-cytometry-optics-detection.html.

[60] T. K. Gaylord. ECE 4500. Lecture Notes, Topic: “Aberrations in Optical Systems.” School of Electrical and Computer Engineering, Georgia Institute of Technology, Atlanta, GA, 2018.

[61] Wikimedia Commons, "Spherical aberration 2.svg," *Wikipedia*, 2006. Available: https://en.wikipedia.org/wiki/Spherical_aberration.

[62] Wikimedia Commons, "Lens6a.png," *Wikipedia*, 2006. Available: https://en.wikipedia.org/wiki/Chromatic_aberration.

[63] Thorlabs Inc, "Mounted Achromatic Doublets, AR Coated: 400 - 700 nm," 2018.

[64] J. S. Wolenski and D. Julich, "Fluorescence microscopy gets faster and clearer: roles of photochemistry and selective illumination," *The Yale Journal of Biology and Medicine*, vol. 87, *(1)*, pp. 21, 2014. Available: http://www.ncbi.nlm.nih.gov/pubmed/24600334.

[65] M. W. Davidson, "Numerical Aperture," MicroscopyU - NIKON INSTRUMENTS INC., Available: https://www.microscopyu.com/microscopy-basics/numerical-aperture.

[66] M. W. Davidson, "Introduction to Microscope Objectives," *MicroscopyU - NIKON INSTRUMENTS INC.*, Available: https://www.microscopyu.com/microscopy-basics/introduction-to-microscope-objectives.

[67] T. Goulette, C. D. Howard and M. W. Davidson, "Infinity Optical Systems," *MicroscopyU - NIKON INSTRUMENTS INC.*, Available: https://www.microscopyu.com/microscopy-basics/infinity-optical-systems.

[68] Thorlabs Inc, "Infinity-Corrected Tube Lenses," 2018.

[69] Zaber Technologies Inc, "T-LSM050A: Motorized stage, 50 mm travel, RS-232 plus manual control," 2018.

[70] Zaber Technologies Inc, "T-LS28M: Motorized linear stage, 28 mm travel, M6 thread, RS-232 plus manual control," 2018.

[71] S. Meroli, "CMOS Active Pixel Sensor Vs CCD. Performance comparison", Available: http://meroli.web.cern.ch/lecture_cmos_vs_ccd_pixel_sensor.html.

[72] Hamamatsu Photonics, "ORCA-Flash4.0 V3 Digital CMOS camera C13440-20CU," 2018.

[73] National Instruments, "What Is Data Acquisition?" 2018. Available: https://www.ni.com/data-acquisition/what-is/.

[74] Laser Teaching Center Staff, "Diffraction through a square aperture", Stony Brook University Department of Physics & Astronomy
Available: http://laser.physics.sunysb.edu/~melia/miniproject2.html#1.

[75] Wikimedia Commons, "Lsfm stripes.svg," 2013.
Available: https://commons.wikimedia.org/wiki/File:Lsfm_stripes.svg.

[76] D. Palanker, "Basic Laser Properties," 2013. Available: https://www.aao.org/munnerlyn-laser-surgery-center/basic-laser-properties.

[77] L. Gao *et al*, "3D live fluorescence imaging of cellular dynamics using Bessel beam plane illumination microscopy," *Nature Protocols,* vol. 9, *(5),* pp. 1083-1101, 2014.
Available: http://www.ncbi.nlm.nih.gov/pubmed/24722406. DOI: 10.1038/nprot.2014.087.

[78] A. Muñoz-Barrutia and N. Felix-Gonzalez, "PDMS microdevices," Universidad Carlos III de Madrid, Biomedical Microdevices 257-15564, Jan 24, 2018.

[79] M. Anguiano *et al*, "Characterization of three-dimensional cancer cell migration in mixed collagen-Matrigel scaffolds using microfluidics and image analysis," 2017.
Available: http://hdl.handle.net/10016/24160.

[80] Consejo de Gobierno, "ACUERDO SOBRE LA DISTRIBUCIÓN DE LAS RETENCIONES DE LOS PROYECTOS DE INVESTIGACION," *(Oct 25, 2012),* Jan 1, 2013.

Blank Page

Annex

TABLE XXI. LIST OF AVAILABLE OBJECTIVES IN THE OPTICS LAB 1.0.G12, UC3M

Objective Properties	Magnification / NA	Brand
M Plan Apo	5x / 0.14	Mitutoyo
U M PlanFL N	10x / 0.30	Olympus
EC-H Plan **Ph2**	40x / 0.65	Motic
M Plan Apo	1x / 0.025	Mitutoyo
Plan Apo ELWD	50x / 0.55	Edmund Optics
HCX Apo L	63x / 0.90	Leica
HCX Apo L	20x / 1.00	Leica
Plan Apo ELWD	20x / 0.42	Edmund Optics
EC-H Plan	40x / 0.65	Motic
EC-H Plan **Ph1**	10x / 0.25	Motic
EC-H Plan	4x / 0.1	Motic
EC-H Plan **Ph2**	20x / 0.45	Motic
EC-H Plan **Ph3** oil	100x / 1.25	Motic
EC-H Plan oil	100x / 1.25	Motic

WD: Working Distance
NA: Numerical Aperture
YELLOW: Air BLUE: Water GREY: Oil **Bold:** Phase-contrast

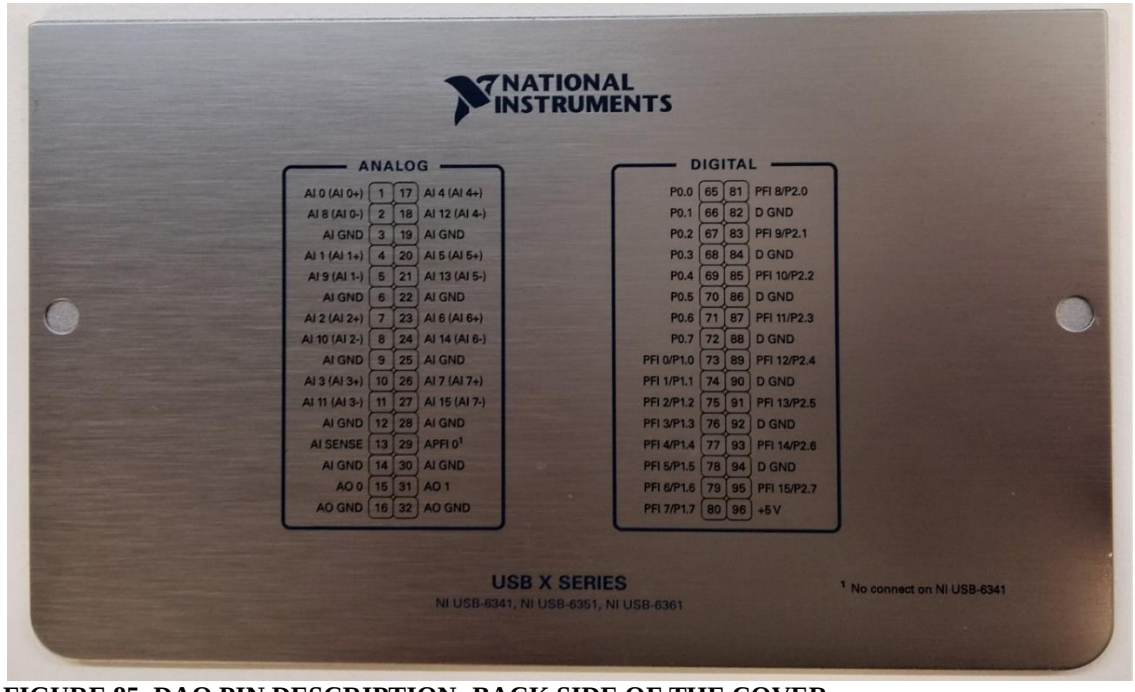

FIGURE 85. DAQ PIN DESCRIPTION: BACK SIDE OF THE COVER.

MATLAB CODE FOR PSF CALCULATION.

Finding the PSF and its standard deviation (Sigma) with the FWHM (Rayleigh criterion).

```
% Load the x,y,z profiles of a bead into a vector.
x; % Profile of the bead in x
y; % Profile of the bead in y
z; % Profile of the bead in z

x_Norm = (x - min(x(:)) ) ./ ( max(x(:)) - min(x(:)) );
y_Norm = (y - min(y(:)) ) ./ ( max(y(:)) - min(y(:)) );
z_Norm = (z - min(z(:)) ) ./ ( max(z(:)) - min(z(:)) );


Z = zeros(2048,2048);
D = Z;
D(1024,1024) = 1;
Sinc = fft(D);

Sigma_PSF = 1;
Sigma_increment = 0.01;

FWHM_profile = [fwhm(1:length(x_Norm),x_Norm),
fwhm(1:length(y_Norm),y_Norm), fwhm(1:length(z_Norm),z_Norm)];
val = [0,0,0];
FWHM = [0,0,0];
SIGMA = [0,0,0];

while not(all(val))

PSF = imgaussfilt(D,Sigma_PSF,'FilterDomain','frequency');
PSF = (PSF - min(PSF(:)) ) ./ ( max(PSF(:)) - min(PSF(:)) );
FWHM_PSF = fwhm(1:2048 , PSF(1:end,1024));

for i = 1:3
    if val(i) == 0
        if FWHM_profile(i) <= FWHM_PSF
            val(i) = 1;
            FWHM(i) = FWHM_PSF;
            SIGMA(i) = Sigma_PSF;
        end
    end
end

Sigma_PSF = Sigma_PSF + Sigma_increment;

end
```

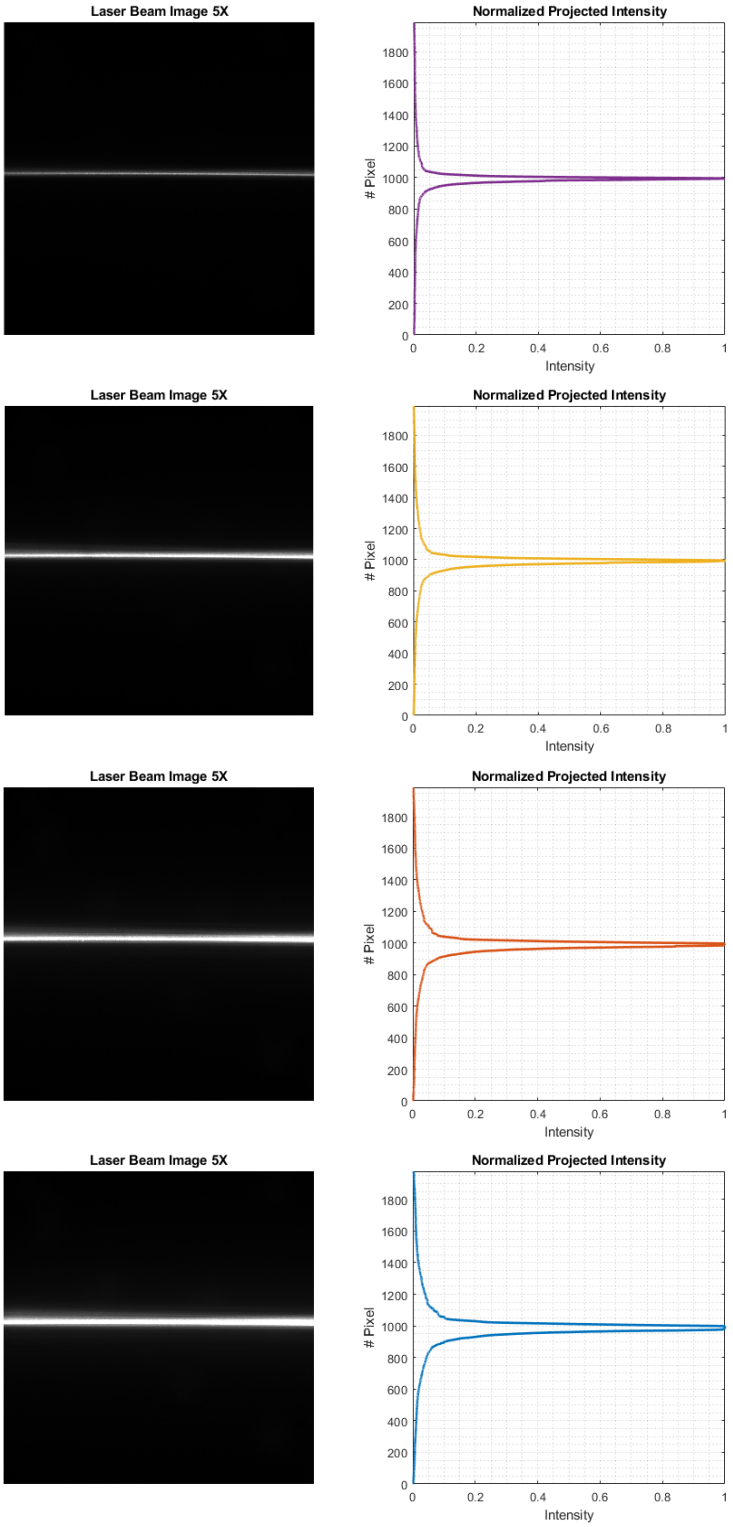

FIGURE 86. INTENSITY PROJECTIONS OF LASER BEAMS OF DIFFERENT POWER.

From top to bottom: beam power of 10mW, 25mW, 50mW, and 100mW.

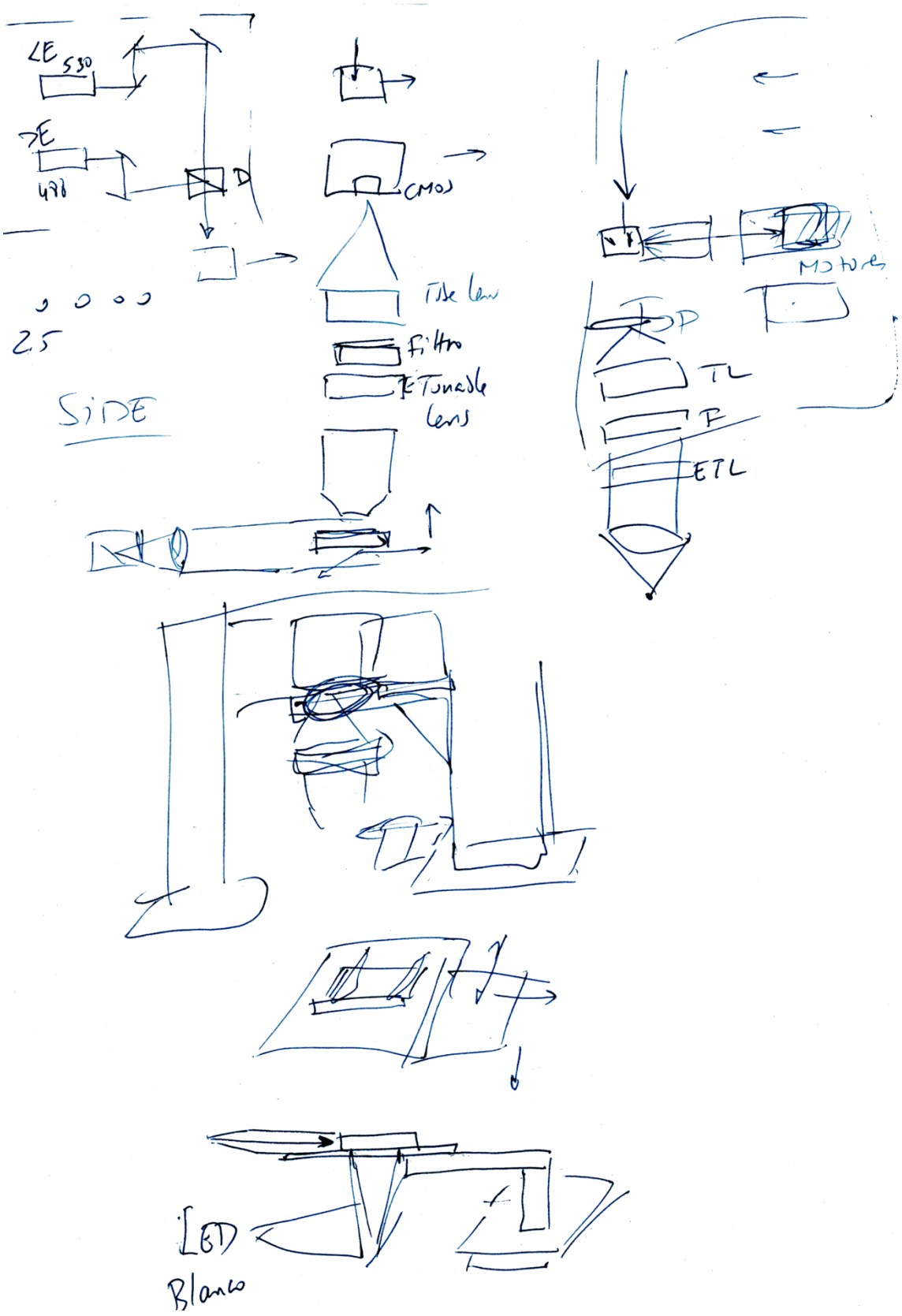

FIGURE 87. SCHEMATIC DRAWING OF THE SYSTEM.

By Jorge Ripoll, September 2017.

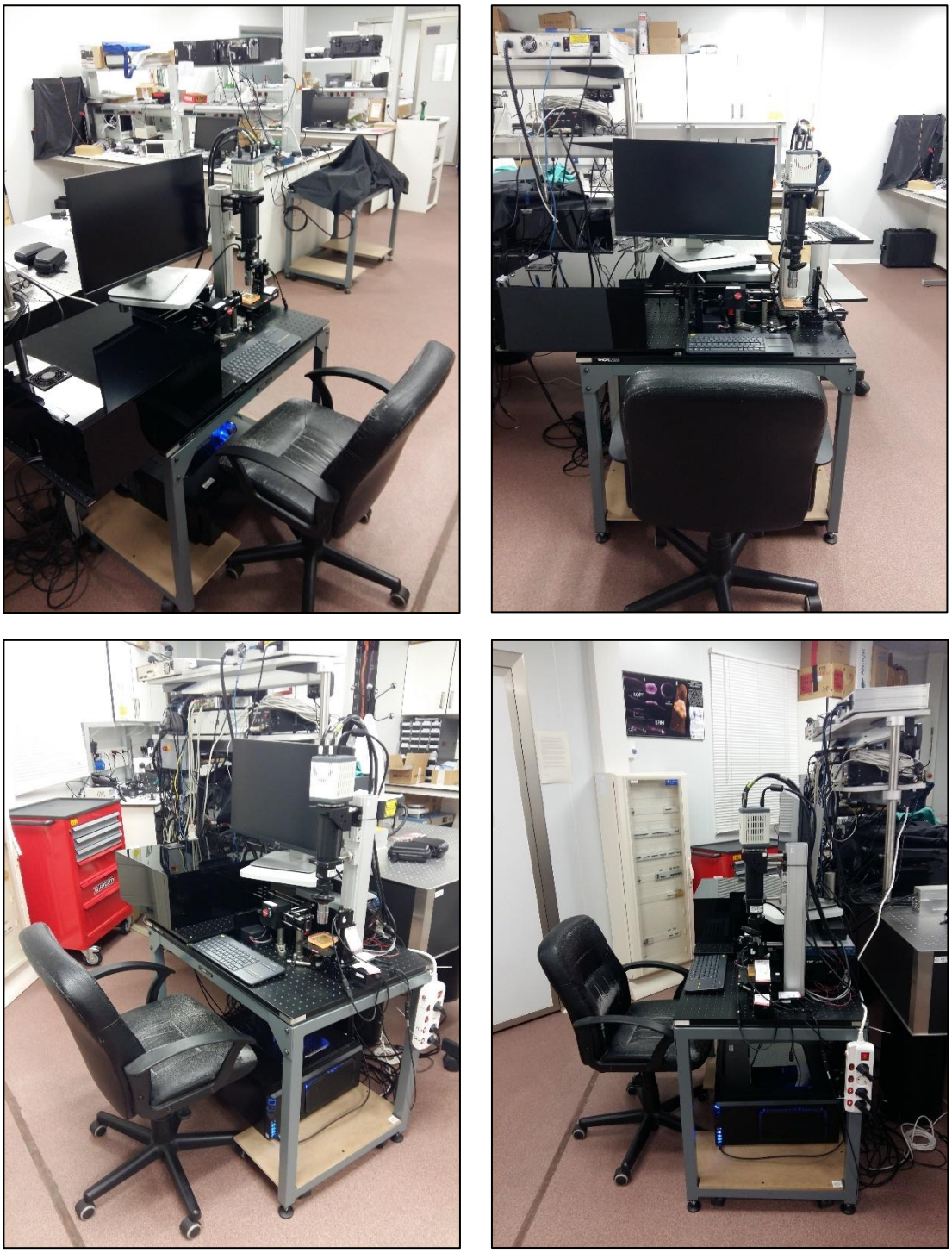

FIGURE 88. IMAGES OF THE SPIM WORKSTATION AT DIFFERENT ANGLES.

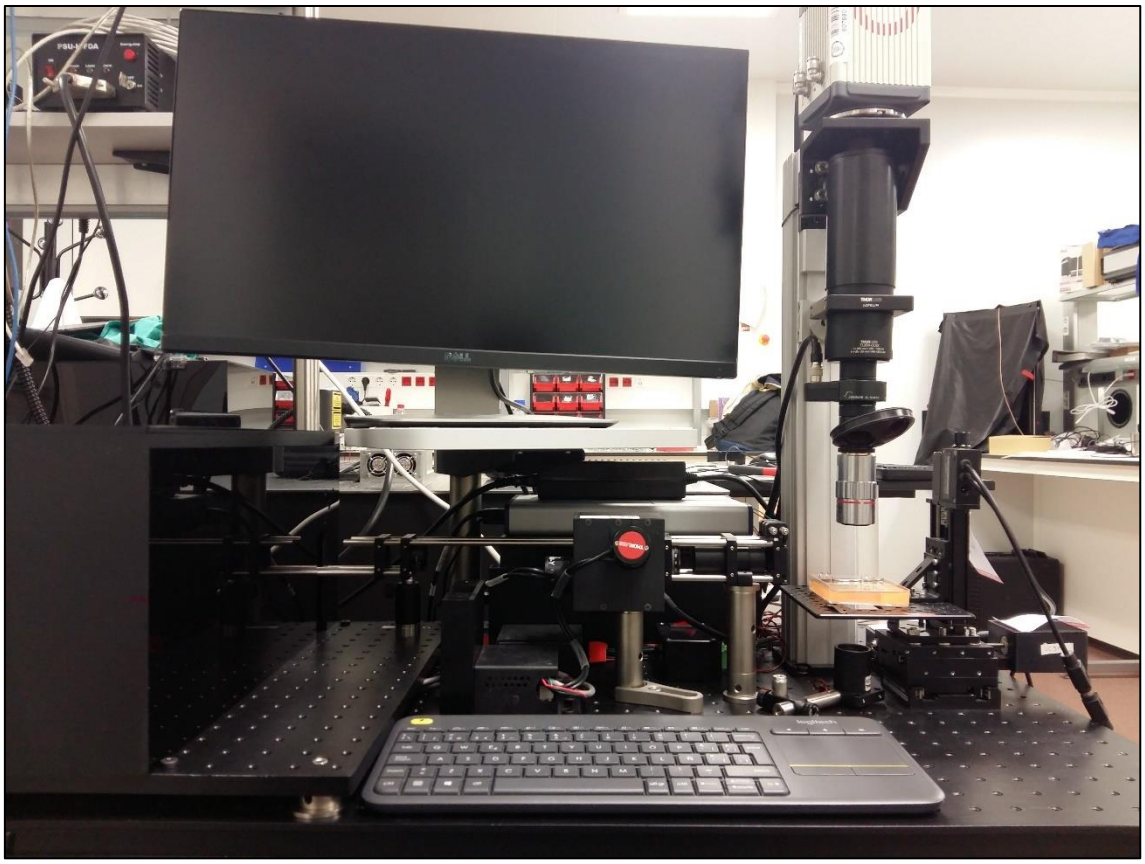

FIGURE 89. IMAGE OF THE SPIM WORKSTATION AS SEEN BY THE USER.

TABLE XXII. PROJECT COSTS.

Group	Subgroup1	Subgroup2	Item (CTRL + click for Link)	Quantity	Price (w/o VAT)	Total
Optical and Optomechanical Hardware	Motors	Galvo	2D Large Beam (10mm) Diameter Galvo System Silver-Coated Mirrors, Metric	1	2721,27	2721,27
Optical and Optomechanical Hardware	Motors	Galvo	GPS011 - 1D or 2D Galvo System Linear Power Supply	1	448,44	448,44
Optical and Optomechanical Hardware	Motors	Galvo	GCE001 - Galvo Driver Card Cover	2	53,08	106,16
Optical and Optomechanical Hardware	Motors	Galvo	GCM012/M - 30 mm Cage Adapter for 10 mm Galvo System, Metric	1	170,6	170,6
Optical and Optomechanical Hardware	Mechanical Support	Breadboard	MB4560/M - Aluminum Breadboard, 450 mm x 600 mm x 12.7 mm, M6 Taps	1	348,62	348,62
Optical and Optomechanical Hardware	Mechanical Support	Breadboard	PFM52501 - Lightweight Workstation for 600 mm x 900 mm Optical Breadboard	1	365,31	365,31
Optical and Optomechanical Hardware	Mechanical Support	Breadboard	PBG51506 - UltraLight Breadboard, 600 x 900 x 25 mm, M6 Taps	1	893,8	893,8
Optical and Optomechanical Hardware	Mechanical Support	Lens Tube SM1	SM1L03 - 0.30'' Thread Depth	2	11,05	22,1
Optical and Optomechanical Hardware	Mechanical Support	Lens Tube SM1	SM1L05 - 0.50" Thread Depth	3	11,44	34,32
Optical and Optomechanical Hardware	Mechanical Support	Lens Tube SM1	SM1L10 - 1.00" Thread Depth	3	12,95	38,85
Optical and Optomechanical Hardware	Mechanical Support	Lens Tube SM1	SM1L20 - 2.00" Thread Depth	1	15	15
Optical and Optomechanical Hardware	Mechanical Support	Lens Tube SM2	SM2L10 - 1.0" Thread Depth	2	27,35	54,7
Optical and Optomechanical Hardware	Mechanical Support	Lens Tube SM2	SC2L24 - SM2 Slip-On Lens Tube Cover, 24" Long	1	11,4	11,4
Optical and Optomechanical Hardware	Mirrors	Mirror	MH25 - Mirror Holder for Ø1" Optics 2.5 - 6.1 mm Thick	4	13,63	54,52
Optical and Optomechanical Hardware	Mirrors	Mirror	ME1-G01 - Ø1" Round Protected Aluminum Mirror, 3.2 mm Thick	5	12,7	63,5
Optical and Optomechanical Hardware	Mirrors	Mirror	KMSS/M - Compact Kinematic Mirror Mount, Hex Adjuster, M4 Taps for Post Mounting	4	32,45	129,8

Group	Subgroup1	Subgroup2	Item (CTRL + click for Link)	Quantity	Price (w/o VAT)	Total
Optical and Optomechanical Hardware	Mirrors	Mirror	KCB1/M - Right-Angle Kinematic Mirror Mount with Tapped Cage Rod Holes, 30 mm Cage System and SM1 Compatible, M4 and M6 Mounting Holes	1	129,99	129,99
Optical and Optomechanical Hardware	Mirrors	Mirror	CCM1-P01/M - 30 mm Cage Cube-Mounted Protected Silver Turning Mirror, M4 Tap	1	152,98	152,98
Optical and Optomechanical Hardware	Lenses	Tube Lens	CPA1 - 30 mm Cage System Alignment Plate with Ø1 mm Hole	1	11,59	11,59
Optical and Optomechanical Hardware	Lenses	Tube Lens	TL200-CLS2 - Laser Scanning Tube Lens, f = 200 mm, ARC: 450 - 1100 nm	1	4597,89	4597,89
Optical and Optomechanical Hardware	Lenses	Spherical Lens	AC254-030-A-ML - f=30 mm	1	97,35	97,35
Optical and Optomechanical Hardware	Lenses	Spherical Lens	AC254-100-A-ML - f=100 mm	1	90,86	90,86
Optical and Optomechanical Hardware	Lenses	Spherical Lens	AC254-150-A-ML - f=150 mm	1	90,86	90,86
Optical and Optomechanical Hardware	Lenses	Cylindrical Lens	CYCP/M - 30 mm Cage Mount for Cylindrical Lenses, M4 Tap	1	75,8	75,8
Optical and Optomechanical Hardware	Lenses	Cylindrical Lens	LJ1695RM-A - f = 50 mm, Ø1", N-BK7 Mounted Plano-Convex Round Cyl Lens, ARC 350-700	1	93,65	93,65
Optical and Optomechanical Hardware	Lenses	Cylindrical Lens	CRM1L/M - Cage Rotation Mount for Ø1" Optics, Double Bored with Setscrew, M4 Tap	1	85,07	85,07
Optical and Optomechanical Hardware	Lenses	Cylindrical Lens	LJ1328L2-A - f = 20.00 mm, H = 15.00 mm, L = 30.0 mm, N-BK7 Plano-Convex Cylindrical Lens, Antireflection Coating: 350-700 nm	1	83,45	83,45
Optical and Optomechanical Hardware	Lenses	Tunable Lens	EL-16-40-TC-VIS-5D-C: -2 to +3 Diopter, C-Mount to C-Mount Focus-Tunable Lens	1	780	780
Optical and Optomechanical Hardware	Lenses	Tunable Lens	EL-10-30-Ci-VIS-LD: +5 to +10 diopters, VIS, Optotune Industrial Focus-Tunable Lens	1	475	475
Optical and Optomechanical Hardware	Lenses	Tunable Lens	6-way Hirose Male/Female Cable, 1m Length	2	85	170
Optical and Optomechanical Hardware	Lenses	Tunable Lens	Optotune Industrial Electrical Lens Driver	2	280	560

Group	Subgroup1	Subgroup2	Item (CTRL + click for Link)	Quantity	Price (w/o VAT)	Total
Optical and Optomechanical Hardware	Lenses	Objective Lens	Navitar Machine Vision 1-60226 Mitutoyo 5X ICO 0.14 NA, 32 mm WD	1	600	600
Optical and Optomechanical Hardware	Lenses	Objective Lens	UMPLFLN10XW OLYMPUS long working distance, water immersion objective	1	899	899
Optical and Optomechanical Hardware	Mechanical support	Cage Mount	B5C1 - Ø1" Optic Mount for 30 mm Cage Cube with Setscrew Optic Retention	1	28,51	28,51
Optical and Optomechanical Hardware	Mechanical support	Cage Mount	C6W - 30 mm Cage Cube, Ø6 mm Through Holes	1	57,95	57,95
Optical and Optomechanical Hardware	Mechanical support	Cage Mount	B3C/M - Fixed Cage Cube Platform for C4W/C6W, Metric	1	22,62	22,62
Optical and Optomechanical Hardware	Mechanical support	Cage Mount	CP02/M - SM1-Threaded 30 mm Cage Plate, 0.35" Thick, 2 Retaining Rings, M4 Tap	7	14,91	104,37
Optical and Optomechanical Hardware	Mechanical support	Cage Mount	LCP01/M - 60 mm Cage Plate, SM2 Threads, 0.5" Thick, M4 Tap (2 SM2RR Retain. Rings Incl)	1	35,23	35,23
Optical and Optomechanical Hardware	Mechanical support	Post and Shelf	P100/M - Ø1.5" Mounting Post, M6 Taps, L = 100 mm	1	36,16	36,16
Optical and Optomechanical Hardware	Mechanical support	Post and Shelf	P30/M - Ø1.5" Mounting Post, M6 Taps, L = 30 mm	1	20,86	20,86
Optical and Optomechanical Hardware	Mechanical support	Post and Shelf	PSY191/S - Additional Instrument Shelf: 300 mm x 278 mm	1	109,41	109,41
Optical and Optomechanical Hardware	Mechanical support	Rails	XT66-500 - 66 mm Construction Rail, L = 500 mm	1	77,65	77,65
Optical and Optomechanical Hardware	Mechanical support	Rails	XT66P2/M - Rail Carriage for 66 mm Rails with M4 & M6 Taps	1	63,51	63,51
Optical and Optomechanical Hardware	Mechanical support	Rails	XT66C4 - Clamping Platform for 66 mm Rails, 1/4" Counterbored Slot, 40 mm Long	1	25,96	25,96
Optical and Optomechanical Hardware	Mechanical support	Rails	XT66RC - Counterbored Pivot Platform for 66 mm Rails	1	64,21	64,21
Optical and Optomechanical Hardware	Mechanical support	Rails	XT66P1 - Vertical Mounting Plate for 34 mm & 66 mm Optical Rails	1	32,91	32,91
Optical and Optomechanical Hardware	Mechanical support	Cage Rods	ER18 - Cage Assembly Rod, 18" Long, Ø6 mm	2	23,18	46,36

Group	Subgroup1	Subgroup2	Item (CTRL + click for Link)	Quantity	Price (w/o VAT)	Total
Optical and Optomechanical Hardware	Mechanical support	Cage Rods	ER6 - Cage Assembly Rod, 6" Long, Ø6 mm	2	7,86	15,72
Optical and Optomechanical Hardware	Mechanical support	Cage Rods	ER4 - Cage Assembly Rod, 4" Long, Ø6 mm	6	6,45	38,7
Optical and Optomechanical Hardware	Mechanical support	Cage Rods	ER3 - Cage Assembly Rod, 3" Long, Ø6 mm	3	6	18
Optical and Optomechanical Hardware	Mechanical support	Cage Rods	ERSCA - Rod Adapter for Ø6 mm ER Rods	3	10,29	30,87
Optical and Optomechanical Hardware	Mechanical support	Posts	CF125C/M - Clamping Fork, 31.5 mm Counterbored Slot, M6 x 1.0 Captive Screw	8	10,01	80,08
Optical and Optomechanical Hardware	Mechanical support	Posts	RS05P/M - Ø25.0 mm Pedestal Pillar Post, M6 Taps, L = 12.5 mm	5	18,17	90,85
Optical and Optomechanical Hardware	Mechanical support	Posts	RS1P/M - Ø25.0 mm Pedestal Pillar Post, M6 Taps, L = 25 mm	3	20,86	62,58
Optical and Optomechanical Hardware	Mechanical support	Posts	RS2P/M - Ø25.0 mm Pedestal Pillar Post, M6 Taps, L = 50 mm	1	24,8	24,8
Optical and Optomechanical Hardware	Mechanical support	Posts	RS2.5P4M - Ø25.0 mm Pedestal Pillar Post, M4 Taps, L = 65 mm	4	23,18	92,72
Optical and Optomechanical Hardware	Mechanical support	Posts	RS4P4M - Ø25.0 mm Pedestal Pillar Post, M4 Taps, L = 100 mm	1	29,44	29,44
Optical and Optomechanical Hardware	Mechanical support	Posts	RS10/M - Ø25 mm Post, M6 Tap, L = 10 mm	2	10,76	21,52
Optical and Optomechanical Hardware	Mechanical support	Posts	RS50/M - Ø25.0 mm Pillar Post, M6 Taps, L = 50 mm, M4 Adapter Included	2	20,4	40,8
Optical and Optomechanical Hardware	Mechanical support	Posts	RS2M - Ø25 mm Post Spacer, Thickness = 2 mm	1	6,21	6,21
Optical and Optomechanical Hardware	Mechanical support	Posts	RS3M - Ø25 mm Post Spacer, Thickness = 3 mm	3	6,77	20,31
Optical and Optomechanical Hardware	Mechanical support	Posts	RS10M - Ø25 mm Post Spacer, Thickness = 10 mm	1	7,83	7,83
Optical and Optomechanical Hardware	Mechanical support	Posts	TR30/M - Ø12.7 mm Optical Post, SS, M4 Setscrew, M6 Tap, L = 30 mm	1	4,31	4,31

Group	Subgroup1	Subgroup2	Item (CTRL + click for Link)	Quantity	Price (w/o VAT)	Total
Optical and Optomechanical Hardware	Mechanical support	Posts	TR40/M - Ø12.7 mm Optical Post, SS, M4 Setscrew, M6 Tap, L = 40 mm	1	4,52	4,52
Optical and Optomechanical Hardware	Mechanical support	Posts	TR50/M - Ø12.7 mm Optical Post, SS, M4 Setscrew, M6 Tap, L = 50 mm	3	4,72	14,16
Optical and Optomechanical Hardware	Mechanical support	Posts	TR75/M - Ø12.7 mm Optical Post, SS, M4 Setscrew, M6 Tap, L = 75 mm	1	4,93	4,93
Optical and Optomechanical Hardware	Mechanical support	Posts	RA90/M - Right-Angle Clamp for Ø1/2" Posts, 5 mm Hex	1	8,87	8,87
Optical and Optomechanical Hardware	Mechanical support	Objective Wheel	OT1 - Objective Lens Turret, 4 RMS-Threaded Objective Ports	1	292,06	292,06
Optical and Optomechanical Hardware	Mechanical support	Adapter	SM1A9 - Adapter with External C-Mount Threads and Internal SM1 Threads	1	17,1	17,1
Optical and Optomechanical Hardware	Mechanical support	Adapter	SM1A10 - Adapter with External SM1 Threads and Internal C-Mount Threads	2	17,8	35,6
Optical and Optomechanical Hardware	Mechanical support	Adapter	SM1A39 - Adapter with External C-Mount Threads and External SM1 Thread	1	18,17	18,17
Optical and Optomechanical Hardware	Mechanical support	Adapter	SM1A2 - Adapter with External SM1 Threads and Internal SM2 Thread	1	22,72	22,72
Optical and Optomechanical Hardware	Mechanical support	Adapter	SM2A6 - Adapter with External SM2 Threads and Internal SM1 Threads	1	22,72	22,72
Optical and Optomechanical Hardware	Mechanical support	Adapter	SM1A4 - Adapter with External RMS Threads and Internal SM1 Threads	4	20,93	83,72
Optical and Optomechanical Hardware	Mechanical support	Adapter	SM1A3 - Adapter with External SM1 Threads and Internal RMS Threads	1	15,85	15,85
Optical and Optomechanical Hardware	Camera	Camera	ORCA-Flash4.0 V3 Digital CMOS camera C13440-22CU	1	13158,75	13158,75
Optical and Optomechanical Hardware	Camera	Camera	CAM1/M - Right-Angle Bracket for SM1 Lens Tubes, Metric Tap	1	95,5	95,5
Optical and Optomechanical Hardware	Camera	Camera	Camera link 3m with MDR-SDR connector	2	N/A	N/A
Optical and Optomechanical Hardware	Camera	Camera	USB 3.0 9-9 A-B Cable 3.0m (for Flash 4.0) US2-2003	1	N/A	N/A

Group	Subgroup1	Subgroup2	Item (CTRL + click for Link)	Quantity	Price (w/o VAT)	Total
Optical and Optomechanical Hardware	Camera	Camera	HC Image Live Software	1	N/A	N/A
Optical and Optomechanical Hardware	Camera	Camera	Phoenix Camera Link Frame Grabber (ORCA Flash 4.0)	1	N/A	N/A
Optical and Optomechanical Hardware	Laser	Laser	Ultra Compact Diode Laser, 488nm, 100mW	1	5824	5824
Optical and Optomechanical Hardware	Laser	Laser	Ultra Compact Diode Laser, 633nm, 100mW	1	2844	2844
Optical and Optomechanical Hardware	Laser	Laser	Power Supply for IBeam smart	2	90	180
Optical and Optomechanical Hardware	Laser	Laser	Breadboard adapter for IBeam smart	2	57	114
Optical and Optomechanical Hardware	Motors	Linear Stages	T-LSM050A: Motorized stage, 50 mm travel, RS-232 plus manual control	1	1510	1510
Optical and Optomechanical Hardware	Motors	Linear Stages	T-LS28M: Motorized linear stage, 28 mm travel, M6 thread, RS-232 plus manual control	2	1016	2032
Optical and Optomechanical Hardware	Motors	Linear Stages	AP102B: X-LSM and X-LHM Top Adaptor Plate	1	34	34
Optical and Optomechanical Hardware	Motors	Linear Stages	T-DC06: Data cable, 6 ft, 6 pin mini-din male to female PS/2 extension cable	1	8	8
Optical and Optomechanical Hardware	Motors	Linear Stages	PS01-15V04: regulated 110-120 V AC input power supply. Output: 15V DC, max 400mA	1	15	15
Optical and Optomechanical Hardware	Motors	Linear Stages	T-DSUB9: Serial adaptor - 9 pin D-sub male RS-232 serial port	1	10	10
Optical and Optomechanical Hardware	Motors	Linear Stages	MSAP90/M - Mini-Series Right-Angle Bracket, M3 Holes	1	40,73	40,73
Optical and Optomechanical Hardware	Filters	Filter	77 & 690nm, 25mm Dia., Dual-Band Filter	1	335	335
Optical and Optomechanical Hardware	Filters	Filter	552nm, 25.0mm Diameter, Dichroic Filter	1	185	185
Electronic and Computer Hardware	Electronic and	Electronic and	Desktop computer and screen	1	1865,74	1865,74

Group	Subgroup1	Subgroup2	Item (CTRL + click for Link)	Quantity	Price (w/o VAT)	Total
	Computer Hardware	Computer Hardware				
Electronic and Computer Hardware	Electronic and Computer Hardware	Electronic and Computer Hardware	Graphics card	1	167	167
Electronic and Computer Hardware	Electronic and Computer Hardware	Electronic and Computer Hardware	Logitech Wireless Keyboard K400	1	51,98	51,98
Electronic and Computer Hardware	Electronic and Computer Hardware	Electronic and Computer Hardware	HDMI Cable 1.8m	1	5	5
Electronic and Computer Hardware	Electronic and Computer Hardware	Electronic and Computer Hardware	USB 2.0 Type-A male / RS-232 DB9 male adapter	3	19,5	58,5
Electronic and Computer Hardware	Electronic and Computer Hardware	Electronic and Computer Hardware	NI DAQ Model USB-6363 Part Number 781443-01	1	2946	2946
Electronic and Computer Hardware	Electronic and Computer Hardware	Electronic and Computer Hardware	LED Components (resistors, breadboard, transistor, case,...)	1	35	35
Software	Software	Software	4D Nature Opt3D Software	1	17000	17000
Other	Other	Other	Twister Evolution | Vacuum mixer and base	1	1335	1335
Other	Other	Other	Microdevice Silicon Mold	1	843,37	843,37
Other	Other	Other	Microdevice Methacrylate Mold	1	75,75	75,75
Other	Other	Other	Cover glass (37,63 / 1000 units)	20	0,03763	0,75
Other	Other	Other	Kit PDMS + curing agent (171,54 / 100 units)	20	0,17154	3,43
Other	Other	Other	Methacrylate Cover Box	1	200	200

Group	Subgroup1	Subgroup2	Item (CTRL + click for Link)	Quantity	Price (w/o VAT)	Total
Human Resources	Human Resources	Human Resources	Project Manager	80	70	5600
Human Resources	Human Resources	Human Resources	Optics Expert	80	70	5600
Human Resources	Human Resources	Human Resources	Research Assistant (chemist)	60	25	1500
Human Resources	Human Resources	Human Resources	Undergraduate Researcher	800	15	12000
Human Resources	Human Resources	Human Resources	Laboratory technician (IT)	20	20	400
Human Resources	Human Resources	Human Resources	Laboratory technician (electronics)	60	20	1200
Human Resources	Human Resources	Human Resources	Laboratory technician (biology)	10	20	200